DESIGN, FABRICATION AND ASSESSMENT OF A SHORT TANK INTERNALLY-ILLUMINATED CONCENTRIC-TUBE AIRLIFT PHOTOBIOREACTOR FOR THE CULTIVATION OF *Spirulina platensis*

A Dissertation

by

BUTCH GALICIA BATALLER

Submitted to the Office of Graduate and Professional Studies of
Texas A&M University
in partial fulfillment of the requirements for the degree of

DOCTOR OF PHILOSOPHY

Chair of Committee,	Sergio C. Capareda
Committee Members,	Mahmoud M. El-Halwagi
	Zivko L. Nikolov
	Gerald L. Riskowski
Head of Department,	Stephen W. Searcy

December 2018

Major Subject: Biological and Agricultural Engineering

ABSTRACT

A comprehensive study on the bench-scale cultivation of *Spirulina* in a short-tank concentric-tube internally-illuminated airlift photobioreactor was presented. This study includes: (a) the development of a rapid and non-destructive analytical method for biochemical analysis of the *Spirulina* biomass via FTIR spectroscopy and PLS regression*;* (b) design, construction and hydrodynamic and mass transfer characterization of a 3-L photobioreactor; and (c) performance assessment of the reactor in cultivating *Spirulina.* A preliminary techno-economic analysis was also performed.

The use of FTIR-ATR spectroscopy and PLS-regression for biochemical analysis was successfully demonstrated. PLS-regression was found to have better predictive power than multipoint regression. While, comparison of the new method with conventional biochemical methods revealed statistically similar results. This new method reduced the time for sample preparation and eliminated the extraction of target biomolecule for analysis. It has also been valuable in monitoring the growth and biochemical changes in *Spirulina* biomass during growth.

For the second part, a 3-L internally-illuminated concentric-tube airlift photobioreactor with a H/D of approximately 2.0 and A_r/A_d of less than 1.0 was designed. From the hydrodynamic and mass transfer characteristics, it was hypothesized that at 0.3 vvm air flow rate would result to better growth performance due to better liquid circulation (shorter light/dark cycle) and lesser accumulation of dissolved oxygen. This hypothesis was proven to be correct.

The third part was to assess the reactor's performance in cultivating *Spirulina*. The effects of light intensity, air flow rate, and initial biomass concentration on growth parameters such as specific growth rate, overall and daily biomass and product productivity, and

photosynthetic efficiency were tested. From the results, it was recommended that the right combination of light intensity, air flow rate, and initial biomass concentration must be selected to produce the highest biomass throughput. A smart control of these factors with respect to the instantaneous population density must also be developed to attain better growth performance. On the other hand, preliminary techno-economic analysis revealed that producing *Spirulina* powder from 80-m^3 short tank internally-illuminated airlift photobioreactor is feasible. A few ways to further reduce the production cost were also presented.

ACKNOWLEDGEMENTS

It has always been my plan to pursue a graduate degree outside of the Philippines. But I have never considered that adjusting to a foreign country let alone do research work independently will be difficult. I owe the success of pursuit for a PhD degree to the following people and institutions.

I would like to express my gratitude to my professor, Dr. Sergio Capareda, for accepting me as his graduate student and for his guidance, encouragements, and ideas. I would also like to thank my committee members, Dr. Zivko Nikolov, Dr. Gerald Riskowski, and Dr. Mahmoud El-Halwagi for sharing their valuable insights and expertise towards improving my work.

Special thanks to the people that I have worked with throughout the course of my research. To my fellow grad students – Julius, Nam, Jinny, Tyler, Walter, and Seaborn – for being kind, supportive, and friendly lab mates. You have made working in the lab a warm environment. To Amado Maglinao, for answering all my questions and helping me with whatever I need. Everyone who has worked in the lab owe their successes to you. You are always eager to help even if it is not part of your job description. To Dr. Raghupathy Karthikeyan, for allowing me to use his lab. To Susana Cabrera of the Bioseparations Laboratory supervised by Dr. Nikolov, for giving me the *Spirulina* inoculant. To Ayswarya Ravi for lending me centrifuge bottles. And, to Daniela Oliveira, for teaching me to use and maintain the freeze dryer.

I am also grateful for the support given by the Department of Biological and Agricultural Engineering staff. To Amy Santoy for her assistance in obtaining purchase orders. To Stormy Kretzschmar for her assistance in completing my degree plan and other requirements in my

degree. To Susan Corgiat, for all the encouraging words especially when I was about to take my preliminary and final examinations.

Thank you, also, to the Engineering Research and Development for Technology – Faculty Development Program, headed by Dr. Arnold Elepaño in UPLB, for awarding me the ERDT Scholarship. To Pau Micor and the previous ERDT RAs, for your administrative assistance. It would not have been possible for me to study abroad without your support. To the Chemical Engineering Department, University of the Philippines Los Baños, for approving my study leave and its extension. Thank you also to Tita Otie and Lisa Dizon, for being my link to UPLB and ERDT while I was here in the US. Thank you for processing documents on my behalf.

I also like to thank the Filipino community in College Station, Texas. College Station will never feel like home if not for you. To Kat and Aldrin and Joan and Amado, for letting me stay in your homes during my first nights in College Station and for helping me move in to my dormitory. To Abby, Troy, KC, and Tess, for the friendship, road trips, and fun. Thank you, too, for being the vent of my frustrations and disappointments about my research. To Samae and JC, for your hospitality whenever we crash at your house. To my colleague, Jerico Alcantara, for visiting me in Texas and for being my company during the Christmas breaks. Thank you, also, for the emotional and professional support.

To my mom, Lilia Bataller, and my siblings, who have always been supportive and proud of me, I can't wait to see you. To my dad, Santiago Bataller Sr.†, may you always guide me from heaven. I offer my success to you.

CONTRIBUTORS AND FUNDING SOURCES

This work was supervised by a dissertation committee consisting of Professor Sergio C. Capareda (advisor) and Professor(s) Zivko L. Nikolov and Gerald L. Riskowski of the Department of Biological and Agricultural Engineering and Professor Mahmoud M. El-Halwagi of the Artie McFerrin Department of Chemical Engineering.

All work conducted for the dissertation was completed by the student independently.

Graduate study was supported by the Engineering Research and Development for Technology (ERDT) – Faculty Development Program (FDP), Department of Science and Technology (DOST), Philippines. This work was also partly funded by the Biomass Testing and Analysis Laboratory (BETALab), Department of Biological and Agricultural Engineering, Texas A&M University. A dissertation allowance was also provided by the ERDT-FDP, DOST, Philippines.

NOMENCLATURE

A_i	Inside cross-sectional area
A_o	Outside cross-sectional area
A_r/A_d	Riser area-to-downcomer area ratio
CA	Corrosion allowance
D	Main chamber diameter of the PBR
d	Light chamber diameter of the PBR
D_d	Draft tube diameter of the PBR
D_i	Inside diameter
D_o	Outside diameter
ε	Gas Holdup
G	Specific gravity
H	Tank height
h	Light chamber height
h_d	Draft tube height
H/D	Height-to-diameter ratio
k_La	Overall volumetric mass transfer coefficient
N	Impeller speed
n_d	Number of light chambers in the downcomer
n_r	Number of light chambers in the riser
PAR	Photosynthetically active radiation
PBR	Photobioreactor

PE	Photosynthetic efficiency
PLS	Partial least square
PPFD	Photosynthetic photon flux density
P/V	Power-to-volume ratio
R^2	Coefficient of determination
RMSECV	Root mean square error of cross-validation
RMSEP	Root mean square error of prediction
RPD	Residual prediction deviation
S/V	Illuminated surface-to-volume ratio
σ	Conductivity
t	Thickness
t_c	Circulation time
t_m	Mixing time
μ	Specific growth rate
U_{GR}	Superficial gas velocity
V_L	Effective reactor capacity
V_p	Blade tip speed
vvm	air volumetric flow rate per reactor volume capacity (L L^{-1} min^{-1})

TABLE OF CONTENTS

Page

LIST OF FIGURES

FIGURE Page

FIGURE Page

LIST OF TABLES

CHAPTER I

INTRODUCTION

Spirulina has been used for human consumption for centuries. In the 16th century, the Aztecs living in the valley of Mexico consumed a blue-green cake gathered from a lake as food [1]. This food was speculated to contain blue-green alga. In the mid-1960s, Jean Léonard from a French-Belgian expedition to Africa described a blue-green cake sold in the food market of Fort Lamy, Chad and consumed by the Kanembu tribe living along the alkaline lakes of Chad and Niger [1]. This cake was found to contain *Spirulina.* About the same time in Mexico, Zarrouk performed a systematic and detailed study on the growth requirements and physiology of *Spirulina* from an algal bloom in the evaporation ponds of Sosa Texcoco's sodium bicarbonate production facility [1], [2].

Spirulina platensis is a planktonic cyanobacteria that form massive populations in tropical and subtropical bodies of water characterized by high pH (up to 11) and high levels of carbonate and bicarbonate. It is widely distributed in Africa, Asia and South America. It is included in the Genus *Arthrospira* Stizenberger 1852, Subsection III, Order *Oscillatoriales* under the respective designation *A. platensis* (Nordst.) Gomont 1892 [1].

Spirulina is exploited as a source of food, feed, and fine chemicals. It is relatively rich in γ-linolenic acid (GLA) that is claimed to lower low-density lipoprotein in hypercholesterolemic patients, treat atopic eczema, and alleviate the symptoms of premenstrual syndrome. Due to its pigment composition, *Spirulina* is used as a feed ingredient for pigmentation of ornamental fishes as well as for improvement of the integumentary color of cultured fishes. In the poultry industry, *Spirulina*-fortified diet incorporates xanthophylls in the egg yolk improving its color.

Phycocyanin from *Spirulina* is mainly used as a natural pigment in the food, drug and cosmetics industries to replace the current synthetic pigments that are allegedly carcinogenic. Phycocyanin is also used as a biochemical tracer in immunoassays, microscopy and cytometry. *Spirulina* is also especially rich in proteins, which is unusual for a microorganism. Polyhydroxybutyric acid (PHB), a carbohydrate, in *Spirulina* can also be used as a biodegradable thermoplastic polymer. Cyanocobalamin (Vitamin B_{12}) has also been found in *Spirulina* at relatively high amount (11 mg kg^{-1}). Phosphoglycerate kinase (PGK) that may be used for enzymatic determination of ATP and superoxide dismutase that is used as a health food and as a therapeutic agent for cancer and other diseases are also found in *Spirulina*.

Traditional cultivation of algal cultures are in open ponds, either in natural waters (such as lakes, lagoons, and ponds) or in artificial ponds or containers, due to their simplicity and inexpensiveness [3], [4]. However, these systems suffer from poor light utilization [3], uneven light intensity, evaporative losses, CO_2 diffusion to the atmosphere, difficult control of environmental conditions, contamination [4], [5], and requirement of large areas of land [6]. Cultures from open ponds also have low cell densities resulting in expensive harvesting procedures and unfavorable economics [5]. Poor mixing in ponds results to settling of the cells that would in turn cause low yields, unstable algal populations, and difficulty in distributing nutrients [5].

To overcome these limitations, much attention has been given to closed systems, also known as photobioreactors, in propagating algae. These systems minimize contamination and allow axenic algal cultivation of monocultures [4]. Better control of growth conditions such as pH, temperature, light, CO_2 level, and cell concentration can also be achieved [3], [4]. There is

less CO_2 loss and water evaporation [4] and can support much higher photosynthetic efficiency and biomass productivity [7].

From the wide range of possible photobioreactor configurations, airlift column was selected in this study to grow *Spirulina* due to its simplicity and cost-effectiveness. This type of photobioreactor does not contain moving parts that can potentially damage the cells. It also offers high mass transfer rate, large surface area to volume ratio, ease of control, and safe sterile operation that can lead to high biomass productivity [8]. Airlift columns can also achieve better CO_2 and O_2 gas exchange between the liquid medium and aeration gas [9]. Flashing light effect that results from the continuous passage of liquid through the light and dark zones of the reactor leads to better photosynthetic efficiency [10].

In this study, a 3-L concentric-tube airlift photobioreactor with internal lighting was fabricated. This reactor has a height-to-diameter ratio (H/D) equal to 2.0 and a riser-to-downcomer area ratio (A_r/A_d) less than 1.0. Such specifications were adopted so that for bench-scale cultivation, we can use our laboratory's old fermenters and reconfigure them into airlift photobioreactor. Also from the results of Hwang and Cheng [11], it was expected that shorter tube length and smaller A_r/A_d can lead to lesser gas entrainment in the downcomer region of the airlift column resulting to better liquid circulation, and thus growth.

This study has three main chapters. In Chapter II, a rapid and non-destructive method to quantify total proteins, carbohydrates, and lipids in the *Spirulina* biomass was developed. This new analytical method enabled us to monitor the growth and biochemical composition of *Spirulina* on a daily basis using biomass samples gathered directly from the culture and without requiring sample storage. This new method can also analyze composition from whole cell biomass without the need for tedious sample preparation and analyte extraction.

In Chapter III, the hydrodynamic and mass transfer characteristics of the reactor were determined at various superficial gas velocities (U_{GR})within air flow rate range of 0.13 and 1.0 vvm. Mixing time (t_m), circulation time (t_c), gas holdup (ε), and overall volumetric mass transfer coefficient ($k_L a$) were obtained. From the results, a U_{GR} that can possibly result to better growth can be selected. Also, information gathered from the reactor characterization studies can be used to explain results of the growth assessment studies.

In Chapter IV, the photobioreactor's performance on the growth of *Spirulina* was assessed at various levels of environmental and operating conditions. The effects of light intensity, air flow rate, and initial biomass concentration on specific growth rate (μ), overall and maximum daily biomass productivity, overall and maximum daily product productivity, and photosynthetic efficiency (PE) were determined. The total proteins, total carbohydrates, and total lipids content were also monitored using the novel analytical method developed in Chapter II. The results in Chapter III were also essential in explaining the effect of air flow rate on the growth of *Spirulina*. Moreover, a preliminary techno-economic and sensitivity analyses were performed on a scaled-up 20-m^3 short-tank concentric-tube internally-illuminated airlift photobioreactor.

In summary, this research provides a comprehensive study on the growth of *Spirulina* in a short-tank concentric-tube internally-illuminated airlift photobioreactor where the H/D is approximately 2.0 and the A_r/A_d is less than 1.0 as opposed to typical airlift reactors with higher H/D and A_r/A_d. A new analytical method was developed for the rapid analysis of the biomass' biochemical composition; hydrodynamic and mass transfer characterization was performed, and; the reactor's performance was tested on the growth of *Spirulina*.

CHAPTER II

DEVELOPING A RAPID AND NON-DESTRUCTIVE METHOD IN QUANTIFYING BIOMOLECULES IN *SPIRULINA PLATENSIS* VIA CHEMOMETRICS AND FTIR-ATR SPECTROSCOPY*

II.1. INTRODUCTION

Proteins, carbohydrates, and lipids compose more than 90% of algal dry weight [12]. They are typically quantified by conventional biochemical methods that are usually time-consuming and often require high temperature. Proteins are commonly analyzed by colorimetric methods such as Lowry, bicinchoninic acid (BCA), and Bradford assays. The Lowry assay is highly sensitive to specific amino acids, such as tyrosine and tryptophan, and some other interfering substances like carbohydrate, glycerol, and EDTA that are typically present in algal extracts or in extraction buffer [13]. On the other hand, BCA can tolerate the detergents known to interfere with the Lowry reagent but not substances like glucose, mercaptoethanol, dithiothreitol, and certain reagents such as ammonium sulfate and ampholytes [13]. Detergents like sodium dodecyl sulfate and Triton X-100 may also interfere with color development in Bradford assay. The presence of high arginine and/or phenylalanine that bind disproportionately with the Coomassie Brilliant Blue G250 dye may also lead to overestimation of protein content [13].

---

* Reprinted with permission from "A rapid and non-destructive method for quantifying biomolecules in *Spirulina platensis* via Fourier transform infrared – Attenuated total reflectance spectroscopy" by B.G. Bataller and S.C. Capareda, 2018. Algal Research, Vol. 32, pp. 341-352, Copyright 2018 by Elsevier.

Before any analysis can be done, the proteins are extracted from the biomass at high temperature using alkaline solution or a detergent-containing buffer. To prevent underestimation of protein content, several extraction steps are necessary to ensure maximum extraction of protein. This makes the method laborious. Also, the presence of pigments such as chlorophylls and carotenoids in the protein extracts can interfere with the protein assays. The presence of *Chlorophyll a* (*Chl a*) can lead to overestimation of protein content by Lowry method by as much as 50% if the protein to *Chl a* ratio is less than 5 and 10-120% overestimation when the protein to *Chl a* ratio ranges from 5 to 80 in BCA method [13]. *Chl b* can also interfere with both methods. On the other hand, Bradford assay is less sensitive to presence of chlorophylls [13].

The most common method in determining total carbohydrates is the colorimetric phenol-sulfuric acid method. This method is highly sensitive, simple, and applicable to a wide variety of biological samples. In this method, polysaccharides and oligosaccharides are hydrolyzed by a strong acid to break them down to their constituent monosaccharides such as glucose. In the presence of phenol and sulfuric acid, these monosaccharides are dehydrated to hydroxymethyl furfurals that are orange-colored products with an absorption maximum at 490 nm [13]. Quantification of these colored products can be done using a spectrophotometer and a calibration curve on glucose standard. Complete hydrolysis of carbohydrates to their component monosaccharides, that typically takes four hours in boiling water baths, must be achieved for accurate estimation of carbohydrate content. The presence of pigments may also interfere with this method leading to overestimation. A decolorization step is needed before hydrolyzing algae samples to overcome this problem. Careful handling of the reagent is also needed since phenol is toxic and sulfuric acid is highly corrosive.

Lipids can be quantified by several methods. These include Floch method, Bligh-Dryer method, Bigogno method, and soxhlet extraction method. What is common about these methods is the use of toxic solvents such as chloroform, hexane, and ethers as well as high temperature to extract the lipids. Several extraction steps are also needed.

Aside from these limitations, conventional biochemical methods are limited to detecting whole communities of algae due to the large quantity of materials needed [14], [15]. Analysis at a single-cell level will be difficult. Moreover, results from such methods are only accurate to a certain degree [16]. Characterization of algal composition and monitoring algal growth, therefore, need a fast and sensitive method, preferably at the scale of single cells [17].

Fourier-Transform Infrared (FTIR) spectroscopy coupled with chemometric techniques can be used to develop a method alternative to the conventional. FTIR spectroscopy in algal characterization can overcome the limitations of conventional methods [18]. It has the potential for determining single-cell biomass composition [16]. It is highly reliable, fast, and sensitive to species-specific changes in molecular composition [14], [15], [19]–[21].

FTIR characterizes biomass using band intensities at characteristic wavenumbers of the vibrational motion of functional groups in molecules upon absorption of infrared ray. Interpretation of the infrared spectrum by identifying the presence of these functional groups indicate the identity of a molecule. The presence of proteins, carbohydrates, and lipids in algal biomass can be determined by identifying band intensities related to their characteristic bonds such as the amide bond in proteins, C-C and C-O bonds in carbohydrates, and C=O ester bond in lipids. Furthermore, quantification can be done by relating the absorbance and the spectral structure of these functional groups to known concentrations of standards.

The simplest model that linearly relates absorbance to concentration is the Beer-Lambert's law. Linear regression can be done on the spectral peak absorbance or peak area against concentration. However, linear regression on spectral data may not be highly reliable since such data often contain numerous, noisy, and strongly correlated predictor variables [22]. Partial least squares (PLS) regression is good in this situation especially where there are many variables but not necessarily many samples or observations. It also gives the maximal reduction in covariance of the data in order to give the minimum number of variables necessary to build a reliable prediction model [22].

This study will employ FTIR spectroscopy and chemometrics to quantify the total protein, carbohydrate, and lipid content of *Spirulina platensis*. If successful, the results can be used to rapidly determine algal composition. No storage of samples is required is samples can be analyzed right away. Extraction of the analyte is also not needed since algal composition can be determined from whole cells. The results of this study can also be used for process monitoring. Since all analysis can be done at room temperature and solvents are not required, the method is deemed to be non-destructive.

II.2. HYPOTHESIS AND OBJECTIVES

This study hypothesized that Fourier Transform Infrared – Attenuated Total Reflectance (FTIR-ATR) coupled with chemometric techniques, such as multipoint and partial least squares (PLS) regression, can be used to develop a rapid and non-destructive analytical method to determine total protein, carbohydrate, and lipid content in *Spirulina platensis.*

To prove this hypothesis, the following objectives were undertaken:

Objective 1. To create a cell spectra model of *Spirulina* at different proportions of protein, carbohydrate, and lipid via iterative subtraction and addition method from individual spectra of biomolecule standards;

Objective 2. To develop regression models using multipoint and PLS regression techniques on model cell spectra of *Spirulina*;

Objective 3. To compare the robustness of multipoint and PLS regression in terms of coefficient of determination (R^2), root mean square error of prediction (RMSEP), residual prediction deviation (RPD), and percent relative error; and

Objective 4. To validate the algal composition of *Spirulina* predicted by the regression models by statistically comparing with the results of conventional biochemical methods.

II.3. LITERATURE REVIEW

FTIR spectroscopy has been used in the characterization of *Chromochloris zofingiensis*, *Acutodesmus obliquus*, *Chlorella sorokiniana* [20], *Chlorella vulgaris*, and *Scenedesmus obliquus* [16], [19]. These studies have only identified the presence of macro-constituents that are indicated by their band intensities at distinct wavenumbers.

Attempts have also been made to quantify biomolecules from spectral scans. Meng *et al.* [23] semi-quantified microalgal cell composition by correlating by linear regression the lipid and carbohydrate contents obtained from conventional methods to the ratios of peak area of lipid/amide I band and of carbohydrate/amide I band, respectively, of FTIR spectra of seven algal strains. They found good linear correlation for both lipid content versus lipid/amide I ($R^2 = 0.951$) and carbohydrate versus carbohydrate/amide I ($R^2 = 0.962$) when two algal species (*Porphyridium cruentum* and *Chaetoceros* sp.) were excluded in the calibration. They did not,

however, tested the reliability of the regression equations by statistically comparing them with results of conventional biochemical methods. The exclusion of the two species means that this method is not applicable to a wide variety of microalgae.

Mayers, Flynn and Shields (2013) [24] used least square polynomial regression analysis, which is a univariate method, to create a single-species model from FTIR spectra of *Nannochloropsis* sp. The regression analysis was done on reference microalgal spectra of known composition and infrared peak integrals. Cross-validation of the models show good predictive power with root mean square error of cross validation (RMSECV) values approximately 1%, R^2 more than 0.95, relative prediction deviation more than 3, and relative error less than 5%.

PLS-regression has been used in quantifying dry matter, proteins, lipids, and carbohydrates from near-infrared spectra (NIR) of various microalgae. Laurens and Wolfrum [25] determined the algal composition of *Chlorella* sp., *Nannochloropsis* sp., and *Scenedesmus* sp. via NIR spectroscopy and multiple linear regression (MLR) and PLS-regression. PLS-regression on lipid, protein, and carbohydrate resulted to correlation coefficient approximately 0.90, except for carbohydrate where the correlation coefficient is closer to 0.80. RMSECVs for lipid, protein, and carbohydrate are less than 4%, 2.1%, and 6%, respectively. The authors also investigated the use of single and multiple linear regression for lipid quantification because they observed distinct increases in lipid-specific NIR spectra. They found good correlation at 1725 or 2305 nm spectra (R^2 = 0.86 and 0.77, respectively); but unsatisfactory at 1215 nm spectra alone (R^2 = 0.66). It was also shown that the predicted lipid contents are within 4% relative deviation for four independent test samples.

Challagulla, Walsh, and Subedi (2014) [26] assessed the dry matter and total lipid content in combined culture of *Chlorella vulgaris*, *Navicula* sp. 1 and 2, and *Nitzschia pusilla* using near

and short wave infrared spectroscopy and PLS-regression. Their results showed poor cross-validation results indicating that the regression models for dry matter and lipid contents were not robust across species. However, the single-species model on the lipid content of *C. vulgaris* dry filtrates showed better statistics (RMSECV = 0.29 g L^{-1}, R_{CV} = 0.96, and RPD = 3.83). This shows that species-specific regression models have better predictive power for lipid content. On the other hand, regression models for dry matter content of the combined culture and single species showed better statistics than the models for lipid content. In another study, they also determined the dry matter and total lipid content and fatty acid composition in *Rhopalosolen saccatus* [27]. They found that PLS models are acceptable for the transmission spectra of liquid culture and reflectance spectra of wet and dry filtrates of cultures for both dry matter (R_{CV} > 0.87) and lipid content (R_{CV} > 0.68). But models on dry filtrates are more robust and thus recommended. Models for fatty acids on transmittance spectra of liquid spectra, reflectance spectra of wet and dry filtrates, or reflectance spectra of fatty acid methyl esters in solvent were not acceptable; while models on dry extracts of methyl esters are adequate. This shows that PLS models on dry samples gave better prediction than models on wet samples.

In FTIR spectroscopy at the mid-infrared (MIR) range , PLS has also been used in determining the composition of water-soluble cell wall polysaccharides from *Ulva* spp. as well as protein and sulfate contents [28]. PLS gave good predictions for rhamnose, xylose, glucuronic acid, and sulfate contents but not for minor constituents such as galactose, iduronic acid and protein. PLS was also used to determine the composition (total phosphorous, total nitrogen, total sugar, mono-sugar, ash, total lipid, and total fatty acid) of NIR and MIR spectra of a set of samples from algal turf scrubber (ATS) [29]. It was shown that both NIR and MIR spectroscopy accurately determined ash and total nitrogen but not phosphorous, total sugar, mono-sugar, lipid

and fatty acids. Detection of specific peaks in the MIR related to specific components is difficult due to the overlap in spectral bands of organic constituents. In this study, spectral pretreatments were performed to deconvolve the overlapping peaks and correct for baseline differences. These pretreatments may not be enough to identify distinct bands for each component. Spectral pretreatment at the fingerprint region of the spectra may be more effective.

The changes in algal composition of *Micrasterias hardyi* in the presence of active pharmaceutical ingredients (API) was also investigated [30]. This study has shown the power of spatial metabolic fingerprinting in investigating the effect of abiotic stresses on complex biological species. *M. hardyi* was exposed to propranolol, metoprolol, and mefenamic acid at 0.002 – 0.2 mM concentrations. FTIR spectroscopy revealed that the APIs have quantitative effect on the metabolism of the organism. PLS on the FTIR fingerprints can also can also estimate the level of API exposure. The authors found that all drugs influenced protein and lipid levels. Specifically, propranolol caused reduction in the lipid complement in the lipid storage areas in the processes of *M. hardyi*.

FTIR spectra was also used as physiological fingerprints to assess the growth rates of *Microcystis aeruginosa* and *Protoceratium reticulatum* as affected by the availability of nutrients or light [31]. Species-specific PLS models developed on the whole cell spectra gave a very high correlation between predicted and measured growth rates regardless of growth conditions. With this finding, the success of the proposed study can also be used to assess the growth potential of *S. platensis* at different growth conditions.

PLS and FTIR spectroscopy have even been used to quantify exogenous lipids in *Nanochloropsis* sp., *Chlorococcum* sp., and *Spirulina* sp. cultures [32] and sugars in complex microalgal media [33]. It was shown that PLS models on NIR and FTIR spectra of

Nanochloropsis sp., *Chlorococcum* sp., and *Spirulina* sp. can adequately predict the levels of exogenously added lipids. But models on NIR spectra are more accurate than models on FTIR spectra. Sugars that represent more than 20% of the total in complex microalgal media are also accurately predicted (predictive accuracy > 90%) with FTIR and PLS. This method presents an alternative to conventional substrate monitoring in microalgal cultures.

II.4. METHODOLOGY

II.4.1. Growth conditions in growing *Spirulina*

A stock culture of *Spirulina platensis* was obtained from the Bioseparations Laboratory, Texas A&M University. Ten percent by volume of 1.21 g L^{-1} was inoculated in 300 mL Zarrouk's medium [34] in a 500-mL Erlenmeyer flask. The culture was grown in a shaker-incubator at 60 μmol photons m^{-2} s^{-1} light intensity, 30 °C, initial pH = 9.20, and 200 RPM. The culture was harvested after 14 days and the final volume was noted. Three samples were then taken for FTIR scanning (see Section II.4.3 for methods). It was then centrifuged (Beckman-Coulter Allegra™ 25R Centrifuge) and washed twice with deionized water at 5 °C and 4633 × g in the dark, and freeze-dried (Labconco 6L Benchtop 115 Freeze Dryer). The total mass of the freeze-dried algal sample was determined. The dry *Spirulina* biomass was used for protein and carbohydrate analysis.

Since the harvested biomass from the 300-mL culture was not enough for lipid analysis, another *Spirulina* culture was grown in a larger reactor. Ten percent by volume of 1.64 g L^{-1} stock culture was inoculated in three liters Zarrouk's medium [34]. The culture was grown in 4-L airlift photobioreactor at 166 μmol photons m^{-2} s^{-1} light intensity, 30-32 °C, initial pH = 9.0 to 9.5, and 0.167 vvm air flow rate. *Spirulina* was harvested after 17 days at its stationary phase and

the final volume was noted. Three samples were then taken for FTIR scanning (see Section II.4.3). The culture was centrifuged (Beckman-Coulter Allegra^{TM} 25R Centrifuge) and washed twice with deionized water at 5 °C and 4633 × g in the dark, and freeze-dried (Labconco 6L Benchtop 115 Freeze Dryer). Total mass of the freeze-dried algal sample was determined. Biomass from the 3-L culture was used for lipid analysis.

II.4.2. Conventional biochemical methods

For total carbohydrates and protein, cell disruption and pigment extraction were conducted first before hydrolysis of carbohydrates and protein extraction. Cell disruption was achieved by incubating nine 10-mg dry algal samples in 0.5 mL concentrated acetic acid in 85 °C water bath for 15 min. Pigments were removed by adding 10 mL acetone to the sample, centrifuging at 1717 × g for 10 min and then decanting the supernatant.

Total carbohydrates was measured using the phenol-sulfuric acid method as presented in Quiang and Richmond [13]. Spectrophotometric measurements were done using VWR spectrophotometer (UV-Vis Scanning UV-3100) at 490 nm. Total carbohydrates was calculated from a standard curve that was made using standard grade D-(+)-glucose. The percent total carbohydrate was computed using Eq. (II.1):

$$\%\, Total\ carbohydrate = \frac{(Absorbance\ -\ Intercept)\ \times\ Total\ hydrolyzate\ (mL)}{Sample\ weight\ (mg)\ \times\ Slope} \times 100\% \qquad \text{Eq. (II.1)}$$

Proteins were extracted using the method of Rausch (1981) [35] and total proteins were measured using Macro-Bradford Assay (1976) [36]. Spectrophotometric measurements were

done at 595 nm using VWR spectrophotometer (UV-Vis Scanning UV-3100). The percent of total proteins was calculated from a calibration curve made in the range of 0.2 to 0.8 mg/mL standard grade bovine serum albumin (BSA). Percent total protein was calculated using Eq. (II.2):

$$\%\, Total\ protein = \frac{(Absorbance\ -\ Intercept)\ \times\ Total\ extract\ (mL)}{Sample\ weight\ (mg)\ \times\ Slope} \times 100\% \qquad \text{Eq. (II.2)}$$

Nine 100-mg dry algal biomass samples were used for lipid extraction. Pigments were removed prior to lipid extraction. Pigments were removed with 90% methanol for one hour in the dark at room temperature and the procedure was repeated until the extract phase became colorless. Lipid extraction and total lipids determination were done using a method proposed by Bigogno (2002) [13], [37]. Lipid content was expressed as percent by weight of dry algal sample.

II.4.3. FTIR spectroscopy

FTIR spectroscopy analysis of macromolecule standards. Three replicates of 0.05 – 1.00 mg ml^{-1} solutions of BSA and D-(+)-glucose were prepared in deionized water; while, three replicates of 0.05 – 0.50 mg ml^{-1} solutions of standard grade glycerol tripalmitate were prepared in chloroform. Lipid solutions were carefully prepared to prevent significant evaporation of the solvent. Spectral measurements were done using FTIR (Shimadzu IRAffinity-1) equipped with MIRacle™ Single Reflectance Attenuated Total Reflectance (ATR) and with deuterated triglycine sulfate (DTGS) detector. A background scan on atmospheric air was made before scanning the protein, glucose and lipid standards. Five microliters were pipetted to the ATR

sample cells and dried with nitrogen purge gas at 2.5 LPM for 4.5-5.0 mins. FTIR scans were done using Happ-Genzel apodization at 4000-600 cm^{-1} wavenumber range, 4 cm^{-1} resolution and 45 scans. Three FTIR measurements per sample were made. The resulting spectra of the standards were used to model the *Spirulina* cell spectra (see section 2.4). For all scans, atmospheric correction for CO_2 and H_2O were done.

FTIR spectroscopy analysis of Spirulina cells. Right before harvesting, three 10-ml *Spirulina* samples were taken for FTIR scanning. The samples were centrifuged, washed twice with deionized water, and resuspended in deionized water to make 10-ml sample before scanning in FTIR. This was done to avoid interference by the medium in FTIR readings. Five microliters were pipetted to the ATR sample cell and dried with nitrogen purge gas at 2.0 LPM for 6.0 mins. FTIR scans were made using Happ-Genzel apodization at 4000-600 cm^{-1} wavenumber range, 45 scans, and 4 cm^{-1} resolution. Three FTIR measurements were made per sample. For all scans, atmospheric correction for CO_2 and H_2O were done.

II.4.4. Building regression models from model cell spectra

Approximated least squares smoothing with 15 points and multipoint baseline correction were performed on all spectra prior to model development. The model *Spirulina* cell spectra were built from the corrected spectra of protein, carbohydrate and lipid spectra by iterative spectral subtraction and addition. According to Beer-Lambert's Law, the optical density of a cell spectrum $Y_c(v_1 \dots v_n)$ at the frequency region $v_1$to v_n is equal to the sum of the partial optical density of infrared radiation absorbing cellular components $S_n(v_1 \dots v_n)$, as described by the Eq. (II.3):

$$Y_c(v_1 \dots v_n, f_1 \dots f_n) = \sum_{1}^{n} f_n \cdot S_n(v_1 \dots v_n) \quad \text{Eq. (II.3)}$$

where, f_n is the wavenumber-specific spectral proportion of each reference spectra. Spectral subtraction method provided in Shimadzu IRSolution 1.60 software package (Shimadzu IRAffinity-1) was used to determine f_n. Spectral addition in IRSolution was then performed to model the cell spectra. A total of 54 cell spectra models were made with different concentrations of protein, carbohydrate, and lipid.

For quantification, PLS-regression was conducted within the spectral range of 1750 to 950 cm^{-1} [12]. The 3100- 2800 cm^{-1} spectral range (C-H stretching bands) was not included due to overlapping OH band absorption that may lead to misinterpretations. Nonlinear iterative partial least squares (NIPALS) algorithm and leave-one-out cross-validation were used for model development. Spectral data were also centered, scaled, and standardized. PLS-regression was done in JMP® Pro 12.2. Multipoint regression, which is included in IRSolution's quantification package, was also performed. Peak absorbance within characteristic wavenumbers and sample mass were used in multipoint regression. The regression models are compared in terms of coefficient of determination (R^2), root mean square error of prediction (RMSEP), residual prediction deviation (RPD), and percent relative error. These statistics will be computed using the following equation:

$$RMSEP = \sqrt{\frac{\sum_{i=1}^{n}(\hat{y} - y_i)^2}{n}} \quad \text{Eq. (II.4)}$$

$$RPD = \frac{SD}{RMSEP} \quad \text{Eq. (II.5)}$$

$$\%\ relative\ error = \frac{RMSEP}{mean} \quad \text{Eq. (II.6)}$$

II.4.5. Confirmation of regression models

To test the reliability of the PLS and multipoint regression models, predicted values were compared with results of conventional biochemical method by appropriate mean comparison and pairwise comparison methods. Normality (normal plot of residuals) and homoscedasticity (Levene test) were determined first. For dataset that are non-parametric, Wilcoxon/Kruskal-Wallis test for mean comparison and Wilcoxon Each Pair test for pairwise comparison were used. For dataset that have normal distribution, one-way ANOVA and Tukey HSD pairwise comparison methods were used. All tests were performed in JMP® Pro 12.2. In the ANOVA and Wilcoxon/Kruskal-Wallis tests, the null hypothesis is tested at 95% level of confidence. The null hypothesis is that the mean macromolecule content determined via conventional, multipoint regression and PLS regression are the same. If the p-value is less than 0.05, we reject the null hypothesis and we conclude that at least one of the mean macromolecules is different. If this is the case, pairwise comparison was performed to determine which of the mean macromolecule content is different. A p-value less than 0.05 would mean that results from two methods being compared are different.

II.5. RESULTS AND DISCUSSION

II.5.1. Growth of *Spirulina*

Since algal composition was reported in per weight basis, it is important to know the mass of dried sample placed in the ATR sample cell. The sample mass can be computed from the final biomass concentration at known sample volume. The final volume from the 300-mL culture was 284 mL and the mass of freeze-dried *Spirulina* biomass was 330 mg (1.162 g L^{-1}). At 5 µL sample size, the mass of the sample placed in the ATR sample cell is 5.81 µg. For the 3-L culture, the final biomass concentration was found to be 3.11 g L^{-1} (15.54 µg biomass at 5 µL sample size).

II.5.2. Modeling cell spectra via FTIR-ATR

Wagner *et al.* [12] showed that a pool of different substances can be quantified by an individual molecule. In this study, glucose standard was used to quantify all the carbohydrates in *Spirulina* cells. Also, BSA and glycerol tripalmitate standards were used to quantify all the proteins and lipids in the biomass, respectively. Model cell spectra were built from these standards.

Iterative spectral subtraction was conducted to determine f_n. The model spectra were built by spectral addition according to the Beer-Lambert's law. The wavenumber-specific spectral proportion, f_n, was determined to be equal to 1.0 for both spectra of carbohydrate and lipid standards (reference spectra) relative to spectra of protein standard (source spectra). Since each biomolecule standard have distinct absorption bands at their characteristic wavenumbers and that different concentrations have different absorbance levels, a value of $f_n = 1.0$ is considered logical.

Beer–Lambert's law can be limited in FTIR spectroscopy [38] due to non-homogeneous distribution of cells on the instrument sample cell [12]. But this limitation can be minimized by forming a thin cell layer on the sampler such that the path length of infrared light is uniform throughout the sample spot [12]. Using 5 µL sample only and then drying the solvent by a nitrogen purge at low flow rate formed a thin layer of sample on the ATR sample cell. The high linearity of the multipoint and PLS-regression confirms that Beer-Lambert's law is applicable on the data set.

The similarity between the model cell spectra and the spectra of *Spirulina* cells, as shown in Figure II-1, shows that regression on the model cell spectra is applicable in predicting biomass composition. For both the model cell and biomass spectra, the amide I band that results from the C=O stretching vibrations of peptide bonds can be observed at wavenumbers 1,774 – 1,583 cm^{-1}. The amide II band, which results from N-H bending and C-N stretching vibrations, are observed at 1,583 – 1,484 cm^{-1}. At 1,426 – 1,377 cm^{-1} and 1,329 – 1,290 cm^{-1}, the protein COO– side chain and amide III band are present, respectively. The amide III band is a complex band that results from several coordinate displacements.

At the wavenumber range 3,960 – 3,340 cm^{-1}, O–H vibrational stretching can be observed; while, C–H vibration is present at 2,981 – 2,767 cm^{-1}. C=O stretching is present at 1,762 – 1,719 cm^{-1} and a combination band of OCH and COH deformation exist in 1,560 – 1,350 cm^{-1}. At 1,186 – 1,350 cm^{-1}, C-H and O-H deformations are present. The carbohydrate characteristic bands, C–O and C–C stretching, were observed at 955 – 1,186 cm^{-1}. CH_3 and CH_2 absorption bands are at 2,998 – 2,829 cm^{-1}. The lipid characteristic band, C=O ester absorption band, can be observed at 1,771 – 1,688 cm^{-1}, although very indistinct due to low

absorbance (low lipid content) and overlap with the tail amide I band. C–O stretching is present at 1,211 – 1,139 cm^{-1} and CH_2 absorption bands at 1,482 – 1,456 cm^{-1}.

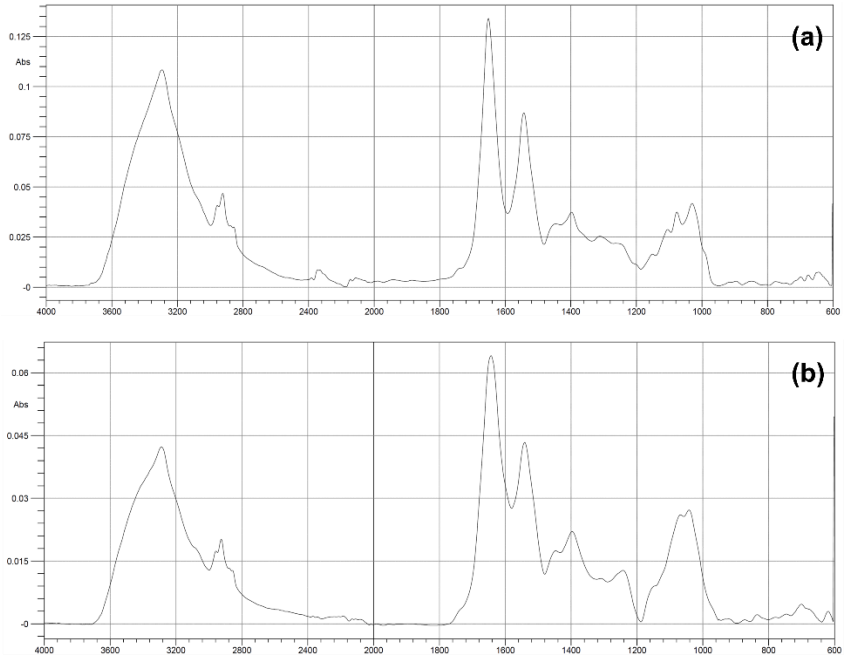

Figure II-1. Samples of (a) model cell spectra (result from spectral addition of spectra from 5.0 µg protein, 5.0 µg carbohydrate and 0.5 µg lipid standards) and (b) *Spirulina* cell spectra (from 5.8 µg cells) gathered from 45 spectral scans using Happ-Genzel apodization at 4 cm^{-1} resolution.

In developing the regression model, one of the considerations in this study was whether to work with a wet or dry sample. Working with a wet sample would be more advantageous if the sample from the culture can be directly scanned by FTIR thereby eliminating sample preparation step. Multipoint regression on characteristic wavenumbers of aqueous solution of protein and carbohydrate standards, at 0.45 – 33.73 mg ml^{-1}, revealed a linear relationship between peak height and concentration (see Appendix A-1). However, the spectra have low resolution compared to spectra of dry samples (see Appendix A-2). Also, we found that in FTIR

scans of wet algal samples, the absorption bands of the medium masked the absorption bands of the biomass (see Appendix A-3). Sample preparation to remove the salts in the medium is, therefore, needed.

In working with dry samples, the next consideration would be to find a range of concentration that would give high regression coefficient. We first worked with concentration 0.25 – 10.0 mg ml^{-1} (equivalent to 1.25 – 50.0 µg for 5.0 µL sample size). We found that for the protein standard, a linear relationship between peak height at characteristic wavenumber and concentration is found until 6.0 mg ml^{-1} (30 µg at 5 µL sample size) where the maximum absorbance at the amide I band is 0.30 (see Appendix A-4(a)). For the glucose standard, there is high variability of absorbance readings at higher concentration starting from 2.0 mg ml^{-1} (see Appendix A-4(b)). Thus, the limit of quantification was set until 1.0 mg ml^{-1} (5 µg at 5 µL sample size) where the maximum absorbance at the characteristic wavenumber is 0.06. The lipid standard has a linear relationship up to 2 mg ml^{-1} (10 µg at 5 µL sample size) as shown in Appendix A-4(c). We therefore recommend that in scanning *Spirulina* samples using FTIR-ATR, sample dilution is needed if the maximum absorbance at the amide I band is more than 0.30 to get reliable results.

PLS-regression models were made over the infrared spectra of 0.25 – 1.00 mg ml^{-1} carbohydrate standard, 0.25 – 6.00 mg ml^{-1} protein standard, and 0.5 – 2.00 mg ml^{-1} lipid standard. The models predicted negative values of protein and lipid content (see Appendix B-1). The models, therefore were not able to capture the actual concentration of biomolecules in *Spirulina*. With this, new PLS models were made at lower concentrations (0.05 – 1.0 mg ml^{-1} for protein and carbohydrate and 0.05 to 0.5 for lipid).

Another consideration was to select the appropriate wavenumber range that would result to high quality PLS model [33] since too few factors lead to insufficient recognition of spectral structure and too many factors lead to inclusion of spectral noise [26]. Quantification also requires different calibration curves for each macromolecule due to diverse extinction coefficients [12]. Thus, separate regression models were made for each biomolecule, which were made at the characteristic wavenumbers of the target biomolecule. Multipoint and PLS-regression models for protein was made at the amide I band (1,680 – 1,605 cm^{-1}), for carbohydrate at the C–O and C–C absorption bands (1,200 – 950 cm^{-1}), and for lipid at the C=O ester band (1,750 – 1,700 cm^{-1}).

II.5.3. Building regression models from model cell spectra

Two regression methods were considered in this study. They were multipoint regression, which is included in IRSolution's software package, and PLS-regression, which was done in JMP Pro 12.2.

Table II-1 shows the results of multipoint regression on model cell spectra. High regression coefficients, that is at least 0.90, were obtained for all models. The high regression coefficient indicates the applicability of the Beer-Lambert's law on the model cell spectra. Lipid has lower regression coefficient since the C=O ester band has a weaker resolution due to its overlap with the tail of the amide I band. This is further weakened by its relatively low concentration compared with carbohydrate and protein.

Table II-1. Results of multipoint regression on the model cell spectra at the characteristic wavenumbers of the target components.

Target Component	Multipoint Regression Equation	R^2
Protein	Corr. Height = 5.217E-3 + 1.518E-2 * c	0.984
Carbohydrate	Corr. Height = 9.362E-4 + 7.289E-3 * c	0.970
Lipid	Corr. Height = -1.459E-3 + 3.559E-3 * c	0.935

Where, "Corr. Height" is the peak height and "c" is the amount of analyte expressed in µg

PLS, on the other hand, assumes that the investigated system is influenced by just a few underlying or latent variables (LV's) [39] that are linear combinations of the original predictors. The number of LV's is usually unknown and one aim of the PLS is to estimate this number. The LV's are indirectly estimated by the **X**-scores, which are predictors of **Y** (response variables) and are used to model **X** (independent variables). The optimum number of LV's is the number of variables with the lowest RMSEP. In the PLS model for proteins, NIPALS algorithm with leave-out-one cross validation reduced 41 predictors (wavenumbers from 1,680 – 1,605 cm^{-1}) to 7 latent variables (RMSEP = 0.127). These 7 latent variables account for 100.00% variation in **X** and 98.93% variation in **Y**. In the carbohydrate PLS model, 132 predictors (wavenumbers from 1,200 – 950 cm^{-1}) were reduced to 15 latent variables (RMSEP = 0.090) that account for 100.00% variation in **X** and 99.78% variation in **Y**. For lipids, 53 predictors (wavenumbers from 1,750 – 1,700 cm^{-1}) were reduced to 11 latent variables (RMSEP = 0.219) that account for 99.99% variation in **X** and 97.93% variation in **Y**.

The model's goodness of fit is illustrated by the actual vs. predicted plot in Figure II-2. The predicted values are well within the 45-degree line for all target biomolecules. The PLS model for carbohydrate exhibited the best fit since there is less variability in predicted results. The PLS model for lipids gave the largest variability in predicted results.

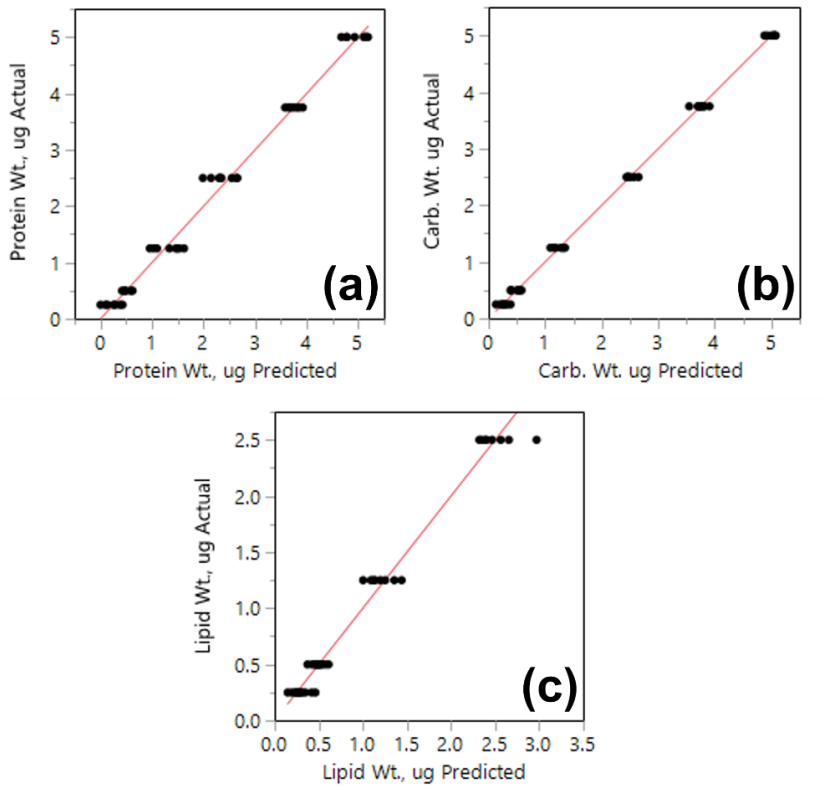

Figure II-2. Actual vs. predicted plot of partial least square-regression model for (a) protein, (b) carbohydrate, and (c) lipid on model cell spectra for *Spirulina* using NIPALS algorithm and leave-one-out cross validation method.

The regions in the spectra that have the greatest influence in the model can be illustrated by the variable importance plot and coefficients plot. Predictors with variable importance in projection (VIP) greater than 0.8 and with non-zero coefficients are considered important. Figure II-3 shows the variable importance in projection plot. It can be observed that all 41 predictors in the protein PLS model and all 53 predictors in the lipid PLS model are influential in determining 7 and 11 latent variables, respectively. For carbohydrates, wavenumbers ranging from 972.12 – 1,201.65 cm^{-1} (120 predictors) are important in determining 15 latent variables. Furthermore, VIP > 1.0 are obtained in wavenumbers 1,745.58 – 1,724.36 cm^{-1} for lipids where the C=O ester

bond exists. As expected, most if not all predictors are found important since PLS models were made at the characteristic wavenumbers of each biomolecule.

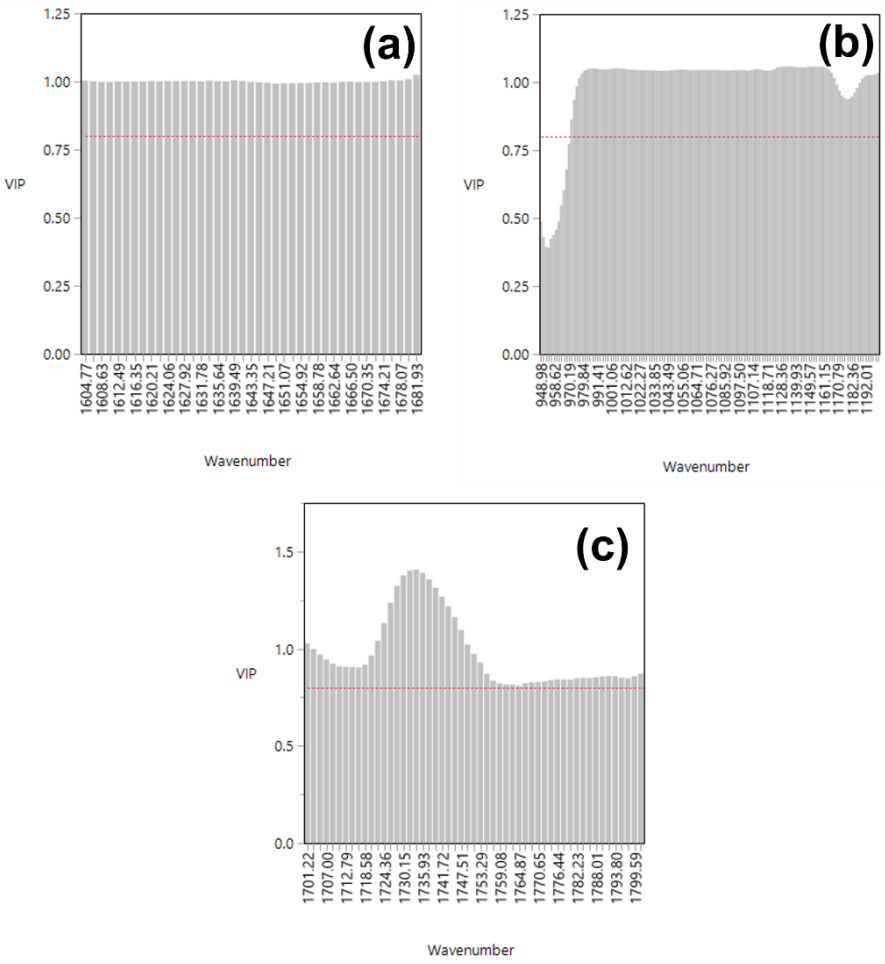

Figure II-3. Variable importance in projection plot of partial least square-regression model for (a) protein, (b) carbohydrate, and (c) lipid on model cell spectra for *Spirulina* using NIPALS algorithm and leave-one-out cross validation method.

The extrema in the coefficient plot in Figure II-4 were identified. The extrema determine which predictor has the greatest contribution to the model. If the absorbance at the maxima increases, the predicted value of the response variable will also increase. While, if the

absorbance at the minima increases, the predicted value will decrease. The minima were found at 1620.21 cm^{-1} (coefficient = -7.61), 1111.00 cm^{-1} (coefficient = -1.6497), and 1741.72 cm^{-1} (coefficient = -1.03) for the protein, carbohydrate and lipid PLS models, respectively. On the other hand, the maxima were found at 1633.71 cm^{-1} (coefficient = 6.80), 1128.36 cm^{-1} (coefficient = 2.12), and 1753.29 cm^{-1} (coefficient = 1.09) for the protein, carbohydrate and lipid PLS models, respectively. It is interesting to note that the extrema did not correspond to the peak heights at the characteristic bands of protein, carbohydrate and lipid spectra. Peak heights were determined at 1651.1 cm^{-1} (absorbance = 0.134), 1029.99 cm^{-1} (absorbance = 0.04), 1738.84 cm^{-1} (absorbance = 0.01). However, the extrema are within the range of wavenumbers that have VIP>1.0. It can be further observed that all predictors (wavenumbers) have non-zero coefficients. Thus, all predictors are useful in developing the PLS model.

Results of cross-validation illustrate the quality and robustness of the model. In this study, the quality of the calibration was measured by R^2, RMSEP, RPD and relative error. R^2 represents the proportion of the variance in response variables (in this case, the algal composition) that is explained by the independent variable (absorbance at the characteristic wavelength). RMSEP, which approximates prediction error between true and calculated value, represents the uncertainty that can be expected from predictions of future samples [40]. Whereas, RPD is the ratio of standard deviation of the response variable to the RMSEP. An RPD less than 1.5 means that the model is insufficient or poor. A value between 1.5 and 2 means that the model can discriminate low from high values of the response variable; a value between 2 and 2.5 indicates that the model has coarse predictive capacity, and; a value between 2.5 and 3 or above means that the model is good and excellent, respectively [40]. Finally, relative error is defined as

the ratio of RMSEP to the mean of the response variable [24]. A low relative error value is desired. Table II-2 summarizes these statistics.

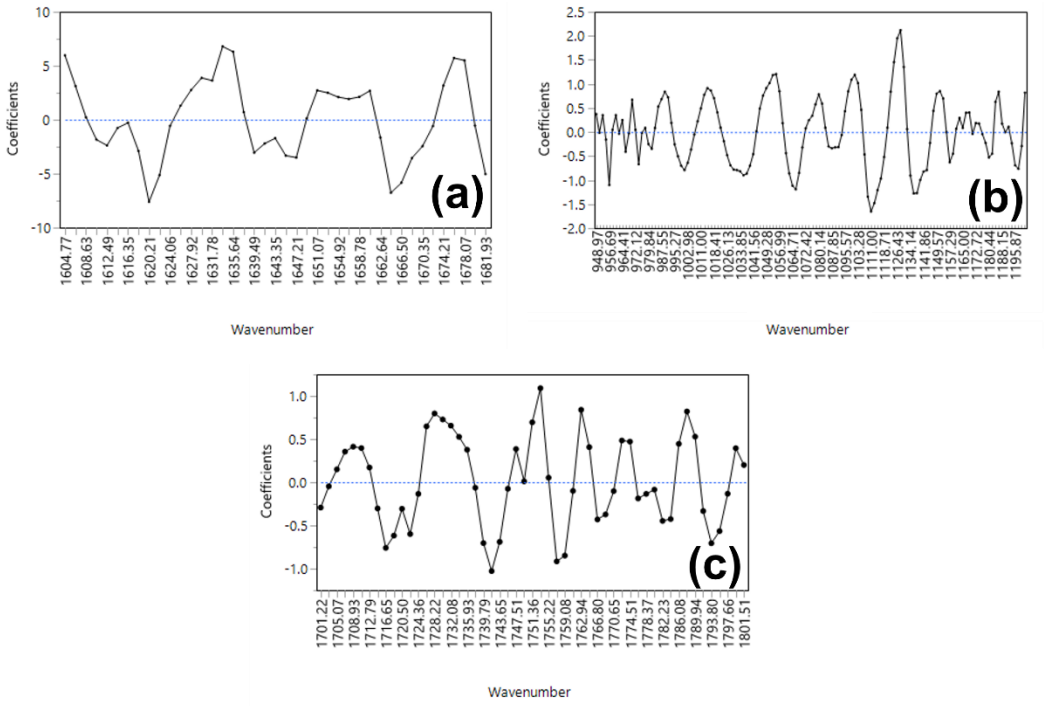

Figure II-4. Coefficients plot of partial least square-regression model for (a) protein, (b) carbohydrate, and (c) lipid on model cell spectra for *Spirulina* using NIPALS algorithm and leave-one-out cross validation method.

Comparison between the correlation coefficients, in Table II-2, of the PLS-regression and multipoint regression shows that PLS- regression is a better model for the FTIR spectra. This is further demonstrated by the PLS-regression models' lower RMSEP and relative error, and higher RPD than multipoint regression models. The PLS model for carbohydrate can excellently predict (RPD = 3.553) carbohydrate content in *Spirulina* biomass, and; the predicted values are only 2.55% away from the mean. The PLS model for protein has good predictive quality since the

RPD is high at 2.936 and the predicted values only have 1.98% error from the mean. However, PLS-regression and multipoint regression models are insufficient in predicting lipid content in *Spirulina*. One possible reason is that the tail of the amide I band masks the characteristic band of C=O ester bond that are present in lipids. Another possible reason is that lipid content in *Spirulina* is very low, such that the peak absorbance and spectral structure of the C=O ester bond are almost negligible. Therefore, PLS-regression and FTIR spectroscopy can only be used on major components of *Spirulina*.

Table II-2. Summary statistics of PLS-regression and multipoint regression models for predicting protein, carbohydrates, and lipids in *Spirulina* biomass.

Component/Statistics	**Regression Models**	
	PLS	**Multipoint**
Protein		
R^{2*}	0.989	0.984
RMSEP*	0.128	0.314
RPD*	2.936	0.400
Relative Error	1.98%	16.42%
Carbohydrate		
R^2	0.998	0.970
RMSEP	0.090	0.434
RPD	3.553	0.600
Relative Error	2.55%	11.66%
Lipid		
R^2	0.979	0.935
RMSEP	0.219	0.303
RPD	0.343	0.000**
Relative Error	78.37%	73.92%

*R^2 = coefficient of determination; RMSEP = root mean square of prediction; RPD = residual prediction deviation
**RPD for multipoint regression is zero since standard deviation of the validation set is zero.

II.5.4. Confirmation of regression models

A high regression coefficient does not always guarantee applicability and robustness of the model. Experimental confirmation and validation are a better way to test model reliability.

The PLS- and multipoint regression models are validated by comparing predicted biomolecule content with the results of conventional biochemical methods. Figure II-5 presents the scatter plot of the results from the regression models and conventional methods of analysis. Means and standard deviation are also shown. From visual examination of the scatter plots, we can see that the multipoint regression's predicted result is different from the result of PLS-regression and Bradford assay for protein and Bigogno method for lipids. Meanwhile, results from all methods are similar for carbohydrate content. Analysis of variance and pairwise comparison were done to support this observation.

For proteins, non-parametric ANOVA and pairwise comparison methodology were used since Levene test revealed that variances are unequal (p-value < 0.0001). It was found, by Wilcoxon/Kruskal-Wallis test, that at least one of the mean protein contents predicted by each method is different (p-value < 0.0001). Non-parametric comparison for each pair using the Wilcoxon method revealed that results from Macro-Bradford assay (95% confidence interval = 55.28±9.47% w/w) and PLS-regression (55.46±2.48% w/w) are statistically the same (p-value = 0.6587); while, predicted protein content from multipoint regression (16.47±0.82% w/w) is different from both PLS and Bradford assay (p-value = 0.0004). It is interesting to note, however, that the results from the Bradford assay have large standard deviation (12.3%). This shows that FTIR spectroscopy coupled with PLS-regression have better precision.

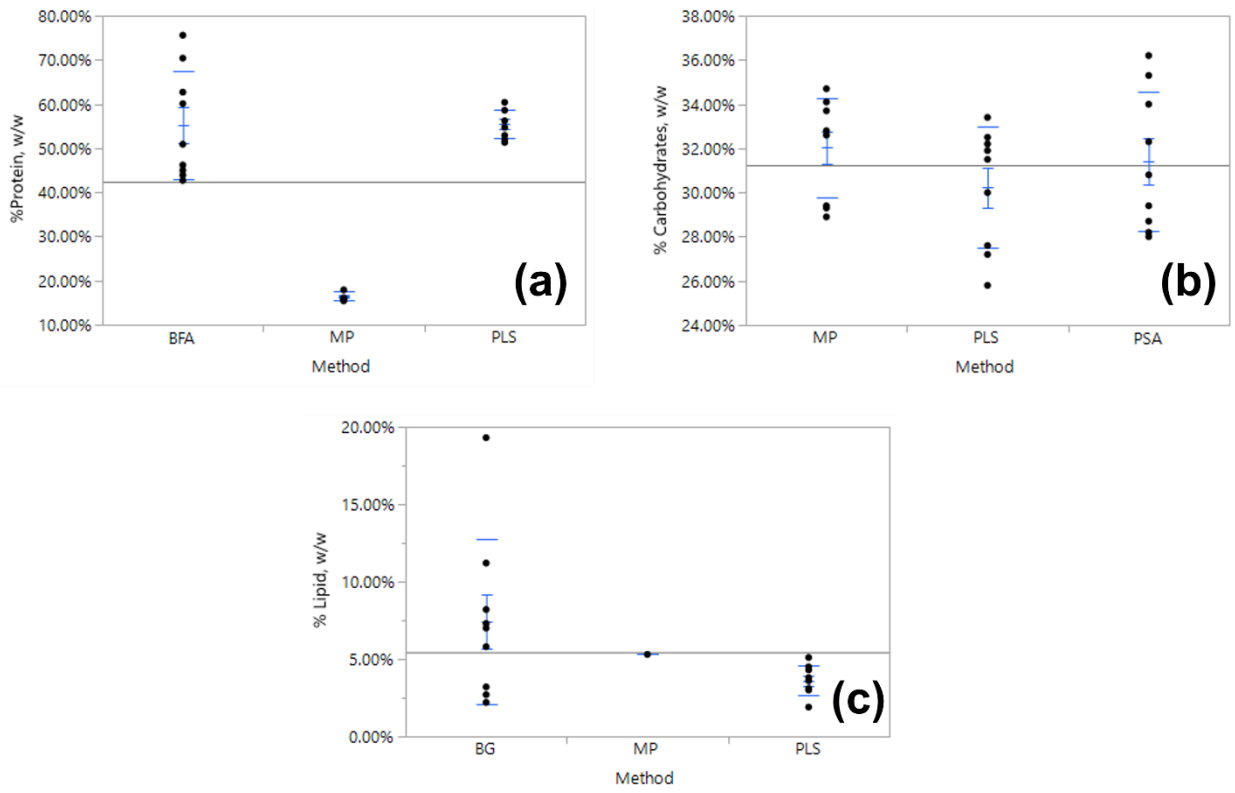

Figure II-5. Scatter plot showing mean and standard deviation of algal composition determined by conventional biochemical methods, multipoint regression and partial least square-regression for (a) protein content, (b) carbohydrate content, and (c) lipid content determination. Where, BFA = Macro-Bradford Assay, PSA = Phenol-sulfuric acid method, BG = Bigogno method, MP = Multipoint regression, and PLS = PLS-regression.

For carbohydrates, results from all methods are statistically similar (p-value = 0.3767). The total carbohydrate content determined by phenol-sulfuric acid method is 31.43±2.42% w/w. While, the predicted total carbohydrate content by multipoint and PLS-regression are 32.03±1.72% w/w and 30.23±2.09% w/w, respectively. As for the lipids, Wilcoxon/Kruskal-Wallis test revealed that at least one of the methods predicted a different lipid content. By Wilcoxon pairwise comparison, it was found that results from multipoint (5.30±0.00% w/w) and PLS-regression (3.60±0.74% w/w) are different (p-value<0.0002). However, it was found that results of the multipoint and PLS-regression are statistically similar (p-value = 0.2201 and

p-value = 0.0932, respectively) to lipid content measured by the Bigogno method (5.32±1.67% w/w). Since it was previously concluded that PLS-regression and multipoint regression models are insufficient in predicting lipid content in *Spirulina*, the applicability of Bigogno method to *Spirulina* is placed into question. The standard deviation of measurements using this method is also large. The Bigogno method may need larger sample size to give better statistics.

We tried to create regression models for lipid using different wavenumber ranges. Meng *et al.* (2014) characterized lipid at 3,000 – 2,800 cm^{-1} (C-H stretching bands) [23]. In this study, we did not consider this wavenumber range due to the possible interference from the overlapping O-H band absorption. Also, C-H stretching from carbohydrates may also contribute to this band. Nevertheless, regression models for lipid at this wavenumber range were still made to demonstrate the results of doing so. We found that a highly linear model was obtained via PLS-regression (R^2 = 0.989) and less linear using multipoint regression (R^2 = 0.884). However, using the model on an independent validation set resulted in very low RPD (0.247 and 0.192 for PLS and MP, respectively) and very high relative error (441.39% and 549.48%, respectively). Interferences at the wavenumber range considered, therefore, have a large effect on the applicability of the model. In the study by Meng *et al.* (2014) [23], RMSEP, RPD and relative error were not presented. They also used different algal species and used band ratios for quantification instead of band intensities. Thus, a comparison of our results to theirs is not possible.

Mulbry *et al.* (2012) [29] also used PLS to determine the composition of near-infrared (NIR) and mid-infrared (MIR) spectra of a set of samples from algal turf scrubber (ATS). It was shown that both NIR and MIR spectroscopy accurately determined ash and total nitrogen, but not phosphorous, total sugar, mono-sugar, lipid and fatty acids. Detection of specific peaks in the

MIR related to specific components is difficult due to the overlap in spectral bands of organic constituents. In their study, spectral pretreatments were performed to deconvolve the overlapping peaks and correct for baseline differences. The authors concluded that these pretreatments may not be enough to identify distinct bands for each component. Unless two components have distinct bands or the band intensity of one component is not masked by another, analysis of overlapping bands may be difficult.

II.5.5. Overall benefits of FTIR-ATR

Through the use of an ATR, this paper presents a method that eliminates the need for rigorous sample preparation, such as those involved in KBr method and other transmission sampling techniques. Pressing, grinding, dissolving, and diluting of samples are avoided and samples can be analyzed as is. These make the ATR technique non-destructive, fast and easy. In this study, separation of the biomass from the culture media and drying of the sample in the ATR crystal are the only sample preparation steps required. In the KBr technique, besides the sample preparation steps mentioned, dry biomass should be ground and embedded in a KBr pellet prior to FTIR scanning. If the pellet is not properly prepared and unworkable spectra is obtained, the operator may need to repeat these steps over and over until a usable spectrum is obtained. Unfortunately, the quality of the pellet can only be determined by measuring its spectrum.

FTIR-ATR is also probably the best technique to use for quantification, since it does not suffer from opacity problems [41]. The ATR technique only depends on the penetration depth of the evanescent wave, such that the sample thickness will have negligible effect on the absorbance intensity. As long as the difference in the refractive indices of the standards and of the sample are minimal and there is proper contact between the sample and the ATR crystal, the

penetration depth will be effectively constant across all measurements. In contrast to transmission sampling techniques, sample thickness highly affects absorbance intensity. Too thin a sample will not absorb enough light and too thick a sample will absorb all light. Since the spectra are developed from transmitted light, the sample thickness and its optical properties must be kept constant to obtain reliable spectra for quantification. Due to this limitation, quantification from transmission spectra are often performed using band ratios rather than absolute band intensities.

However, penetration depth of the evanescent wave is usually shallow – not greater than 10 microns [41]. A loss of sensitivity may result since relatively small absorbances are measured. ATR can generally detect samples with more than 0.1% analyte concentration [41]. In this study, the individual concentrations of the major components of the *Spirulina* biomass measured by the FTIR-ATR are greater than this threshold. Another disadvantage of the ATR technique is that ATR accessories are more expensive than transmission sampling accessories. But the faster and easier way to get results balances this drawback.

II.6. SUMMARY AND CONCLUSION

This study has successfully demonstrated the use of FTIR-ATR spectroscopy and regression techniques, such as PLS-regression and multipoint regression, in quantifying protein, carbohydrate and lipid content of *Spirulina platensis.* PLS-regression was found to have better predictive power than multipoint regression as confirmed by higher R^2 and RPD and lower RMSEP and relative error. By PLS-regression, *Spirulina* was found to contain 55.46±2.48% w/w proteins, 30.23±2.09% w/w carbohydrates, and 3.60±0.74% w/w lipids. The predicted total protein and carbohydrate contents were confirmed by conventional biochemical methods. By

Macro-Bradford assay, protein content was determined to be 55.28±9.47% w/w and was found to be statistically similar the PLS-regression result. The carbohydrate content (31.43±2.42% w/w) determined using phenol-sulfuric acid method was also found to be statistically the same with PLS-regression result. Only the multipoint regression's predicted value on carbohydrate content (32.03±1.72% w/w) coincided with the conventional method. Both multipoint regression and PLS-regression were found to be inadequate in predicting lipid content in *Spirulina* possibly due to its low lipid content, small sample size and overlapping bands of amide I and C=O ester bond. Nevertheless, FTIR spectroscopy and PLS-regression reduced the time for sample preparation. Extraction of the target biomolecule, which usually requires long time and high temperature, was not needed since infrared spectroscopy detects distinct absorption bands of the target biomolecule in whole cells. FTIR spectroscopy coupled with PLS-regression was proven to be a rapid and non-destructive method in determining algal composition.

CHAPTER III

DESIGN AND CHARACTERIZATION OF THE SHORT TANK INTERNALLY-ILLUMINATED CONCENTRIC-TUBE AIRLIFT PHOTOBIOREACTOR

III.1. INTRODUCTION

Algal cultures have been traditionally grown in open ponds, either in natural waters (such as lakes, lagoons, and ponds) or in artificial ponds or containers due to their simplicity and inexpensiveness [3], [4]. Open pond systems are still cheaper than closed photobioreactors (PBRs) even if mixing systems (such as paddle-wheels, propellers, rotating arms, and pumps) that increases capital and operating cost are added [5]. In open pond systems, light is essentially free as the main source of light is the sun. Larger production capacity can also be achieved in open pond systems relative to PBRs of comparable cost [4].

However, open pond systems suffer from poor light utilization [3],uneven light intensity, evaporative losses, diffusion of CO_2 to the atmosphere, and requirement of large land areas [6]. In order for sunlight to penetrate the bottom of the pond water, pond systems are usually kept shallow [4], which necessitates large tracks of land to attain large production capacity. Environmental conditions, such as temperature and lighting, are hard to control and cultures are highly prone to contamination [4], [5]. Axenic culturing is also almost impossible except for strains that grow on extremely harsh conditions. Growing season is highly weather- and location-dependent and is limited to warmer months, except in tropical regions. Cultures from open ponds also have low cell densities resulting in expensive harvesting procedures and unfavorable economics [5]. Poor mixing results to settling of the cells that would in turn cause low yields, unstable algal populations, and difficulty in distributing nutrients [5].

Much attention has been given to closed systems, also known as photobioreactors, in propagating algae to overcome the limitations of open pond systems. These systems minimize contamination and allow axenic algal cultivation of monocultures [4]. Better control of growth conditions such as pH, temperature, light, CO_2 level, and biomass concentration can be achieved [3], [4]. There is also less CO_2 loss and water evaporation [4]. Photobioreactors can also support much higher photosynthetic efficiency and biomass productivity [7].

Due to closed systems' advantages over open ponds systems, this study designed and constructed a photobioreactor that was used in growing *Spirulina*. Several design considerations were considered in the design. These included light capture, distribution and utilization, CO_2/O_2 balance and gas exchange, mixing and mass transfer, and sterility and cleanability. Due to the photosynthetic nature of *Spirulina*, light plays an important role. Therefore, its supply, distribution, and utilization were the major focus in the design. High CO_2 and O_2 mass transfer rate in means that do not damage the cells or suppress algal growth is also necessary [42]. A design that have high surface area to volume ratio must also be selected to increase productivities [5]. Fouling particularly on its light transmitting surfaces should be prevented or minimized [42]. Design should have minimum non-illuminated part and must work under intense foaming [42].

Several design configurations were considered. These can be categorized into tubular, flat plate, and column reactors. Tubular reactors are considered to be the most suitable design for commercial large-scale cultures [43]. They are usually constructed with either glass or transparent plastic tubes [3] where the culture is pumped through. They can be oriented horizontally, vertically, or inclined and tubes can be arranged as serpentine or as a helix [9]. Tubular reactors are strategic in outdoor cultivation since it can be oriented towards the sunlight for better light conversion efficiency [4]. Even if tubular reactors are characterized by high

illumination area, scaling them up by increasing tube diameter would decrease the surface area to volume ratio [3]. Scaling up by increasing the tube length is also limited by CO_2 depletion, pH variation, and oxygen accumulation [9] that may result to photo-bleaching and reduction in photosynthetic efficiency [3], [44]. Another drawback is temperature control [3]. The systems can be cooled by spraying water on the tube surface, placing them in a pool of temperature controlled water, or controlling the temperature of feed or recirculation stream [4]. Tubular reactors also have high energy consumption of about 2000 W m^{-3} compared with 50 W m^{-3} for bubble column and flat plate PBRs [4]. High energy is needed to maintain linear velocity of 20-50 m s^{-1} to achieve turbulent conditions, which is in turn needed to achieve short light/dark cycles [45].

Another type of photobioreactor is the flat plate PBR. Here, a thin layer of very dense culture is pumped through a shallow flat plate [9]. Mixing is provided either pneumatically by air bubbling through perforated tubes or mechanically by a motor [4]. This type of PBR is characterized by high surface area to volume ratio and open gas disengagement systems [4]. One advantage of flat plat reactors over tubular reactors is the low dissolved oxygen accumulation [3]. It also supports high cell densities exceeding 80 g L^{-1} [46]. In scaling up flat-plate reactors, several plates can be arranged over an area. Lengthening the reactor is not advisable but the liquid height and the width of light path can be increased instead [4]. Difficulty in controlling culture temperature, like in tubular reactors, is one of the limitations of flat plate reactors. There is also some degree of wall growth and the possibility of hydrodynamic stress to some algal strains [3].

Cylindrical photobioreactors (column PBRs), on the other hand, can reach radius and height up to 0.2 m and 4 m, respectively [7]. They are occasionally stirred tank reactors but often

bubble columns or airlifts. The columns are vertically oriented, aerated from below, and illuminated through transparent walls [9]. Sparging with gas mixture provides overall mixing, and mass transfer of CO_2 and O_2 [4] with very little shear stress [7].

Column PBRs have the most efficient mixing, highest volumetric gas transfer rates, and most controllable growth conditions [9]. It is compact, low-cost, and easy to operate monoseptically [47]. However in scaling up, the radius is limited by illuminated surface area to volume ratio and height is limited by gas mass transfer rates [7]. Scale-up can be achieved by employing multiple vertical column reactors [44], [48]. Outdoor application is also limited due to low illumination area [3]. Most column reactors are externally illuminated by fluorescent lamps or any other artificial light source.

The most conventional type of column reactor is the stirred tank reactor where agitation is provided by impellers and CO_2-enriched air can be bubbled through at the bottom to provide carbon source [4]. Lighting in stirred tanks is provided externally by fluorescent lamps or optic fibers. The main disadvantage of this type of reactor is the low surface area to volume ratio that leads to low light utilization efficiency [4]. Another type of column reactor is the bubble column. Bubble columns usually have height to diameter ratio that is greater than two. Mixing and mass transfer is achieved by bubbling gas mixture from the bottom [4]. Due to the absence of moving parts, in contrast with stirred tanks, mechanical shear stress will not damage the cells. Also, bubble columns have low capital cost, high surface area to volume ratio, satisfactory heat and mass transfer, relatively homogenous culture environment, and efficient O_2 and residual gas release [4]. The last type of column reactor is the airlift column where two interconnecting zones exist – the riser and the downcomer. Gas mixture is sparged at the riser region, which then disengages at the top of the riser region. The medium and cells are pulled down at the

downcomer region and the sparger recirculates them back to the riser region. Airlift PBRs can be configured into either internal loop or external loop reactor. Internal loop airlift PBRs can be further categorized as split reactor or concentric tube reactor. One major advantage of airlift reactors is the flashing light effect that results from the continuous passage of liquid through the light and dark phase [10]. This leads to better photosynthetic efficiency.

Development of a cost-effective and highly-efficient PBR is essential in lowering production cost. Thus, from these photobioreactors, airlift column was selected since it is simple and cost-effective. It does not contain moving parts that can potentially damage the cells. Airlift PBRs offer high mass transfer rates, large surface area to volume ratio, ease of control, and safe sterile operation [8]. It also has high biomass productivity. Oncel and Sukan (2008) [49] compared bubble and airlift columns and obtained higher dry biomass weight and chlorophyll-a concentration in airlift PBR than in bubble column. Airlift columns can also achieve better CO_2 and O_2 gas exchange between the liquid medium and aeration gas [9]. Another major advantage of airlift reactors is the flashing light effect that results from the continuous passage of liquid through the light and dark phase that leads to better photosynthetic efficiency[10].

Hwang and Cheng (1997) [11] tested the effect of changing the ratio of the cross-sectional areas of the riser and downcomer region (A_r/A_d = 1.0 and 3.0) on gas holdup, liquid velocity, and mixing time. They found that both the gas holdup and liquid velocity in the riser increased but in the downcomer decreased with decreasing tube diameter leading to less bubble entrainment in the downcomer. Decreasing the tube diameter, which translates to a decrease in A_r/A_d, may be advantageous. Hwang and Cheng (1997) [11] also found that an A_r/A_d = 1.0 resulted to higher mixing time than A_r/A_d = 3.0. This means that the reactor with A_r/A_d =1.0 needs longer time to attain 95% homogeneity. Therefore, there is a trade-off between mixing time, gas holdup and

liquid velocity when using smaller A_r/A_d that needs further investigation. This study will design an airlift reactor with an $A_r/A_d = 0.42$ to investigate if the higher liquid velocity in the riser could lead to lower mixing time.

Hwang and Cheng (1997) [11] also tested the effect varying draft tube lengths (70, 110, and 150 cm) on the liquid velocity and gas holdup in an airlift photobioreactor with 19-cm internal diameter (H/D = 3.7, 5.8, 7.9). They found that gas holdup in the riser decreased but increased in the downcomer when the draft tube length was increased. This means that more gases are entrained in the downcomer region resulting to less liquid circulation. Typically, column reactors have height to diameter ratio that is greater than two [4]. But, in this study, the airlift reactor will be designed to have an effective H/D ratio less than two.

With the reactor in this study having a different design configuration, there is a need to determine its mass transfer and hydrodynamic characteristics. Characterization aid in optimizing operational conditions, operate design improvements, and perform scale-up [50]. Operating at conditions with high mass transfer coefficient would ensure that carbon limitation is avoided as there is sufficient dissolved inorganic carbon in the medium[51]. Oxygen accumulation will also be prevented since oxygen removal efficiency is high. Hydrodynamic characterization should also be done since hydrodynamic forces is one of the mechanisms that can damage the cells [8].

Contreras *et al.* [8] found that maximum growth rate occurred at the maximum gas interfacial area and holdup that are in turn related to the superficial gas velocity. This finding shows the relationship between cell growth and hydrodynamic characteristics. The superficial gas velocity at which maximum growth rate is observed may be different for different reactor geometries. The high dependency of hydrodynamics on reactor geometry necessitates the hydrodynamic characterization of the photobioreactor fabricated in this study.

The airlift reactor was also constructed with internal lighting installed at the center of the reactor. In this case, light will radiate from the center radially outwards. Internal illumination increases average irradiance and the depth to which the light reaches[52]. Most studies install the light source in internally illuminated reactor at the downcomer region. With light source installed at the center, it is ensured that all the irradiance is captured by the cells.

III.2. HYPOTHESIS AND OBJECTIVES

This study hypothesized that a concentric tube airlift photobioreactor with central internal lighting, riser to downcomer cross-sectional area (A_r/A_d) ratio less than 1.0, height to diameter ratio (H/D) less than 2.0, and with porous sparger can improve hydrodynamic and mass transfer characteristics of the reactor.

This study has the following objectives:

Objective 1. To design and fabricate a concentric tube airlift photobioreactor with central internal lighting, riser to downcomer cross-sectional area ratio less than 1.0, height to diameter ratio less than 2.0, and with porous sparger;

Objective 2. To determine the liquid-phase physical and hydrodynamic characteristics such as viscosity, conductivity, mixing time (t_m), circulation time (t_c), and liquid circulation velocity (v_l) of the internally-illuminated concentric-tube airlift photobioreactor at superficial gas velocities (U_{GR}) varying from 0.0017 m s-1 to 0.0124 m s^{-1};

Objective 3. To determine the gas-phase hydrodynamic characteristics such as overall gas holdup (ε), Sauter (d_{32}) bubble diameter, and overall interfacial area (a_L) of the internally-illuminated concentric-tube airlift photobioreactor at superficial gas velocities (U_{GR}) varying from 0.0017 m s-1 to 0.0124 m s^{-1}; and

Objective 4. To determine the overall volumetric mass transfer coefficient of O_2 ($K_La_{(O2)}$) of the internally-illuminated concentric- tube airlift photobioreactor at superficial gas velocities (U_{GR}) varying from 0.0017 m s-1 to 0.0124 m s^{-1}.

III.3. LITERATURE REVIEW

III.3.1. Externally-illuminated airlift columns

Airlift bioreactors have been around for decades for use in mass cultivation of animal cell cultures and other microorganisms. It has also found application in microalgae growth, where airlift reactors are usually equipped with external lighting. Airlift photobioreactors can be categorized into internal loop and external loop. Internal loop airlift reactors are further classified into concentric tube and split cylinder reactors. Marker, Tsavalos and Young used a 30-L airlift photobioreactor for the cultivation of *Haematococcus pluvialis* [53]. They determined that the airlift reactor showed relatively high growth rates and accumulated up to 2.7% astaxanthin, which is however lower than what was achieved at laboratory conditions (>5.5% astaxanthin). Barbosa *et al.* [10] tested the effect if medium-frequency cycle time (10-100 s) and light fraction (0.1 -1.0) on growth rate and biomass yield of *Dunaliella tertiolecta*. They found that light fraction majorly affected biomass yield and growth rate while cycle time had little effect. In the study by Vega-Estrada *et al.* [54], a split-cylinder internal-loop airlift photobioreactor was used and tested for the effects of superficial gas velocity and gas entrance velocity on the growth of *H. pluvialis*. They found that cell growth decreased when the superficial gas velocity and entrance velocity were increased above 0.012 m s^{-1} and 22.8 m s^{-1}, respectively. Cell damage was greater when superficial gas velocity was increased by increasing air flow rate rather than by reducing the sparger's internal diameter.

Garcia Camacho (1999) used a vertical concentric tube airlift photobioreactor in outdoor cultivation *Phaeodactylum tricornutum* and compared its performance with a horizontal-loop tubular photobioreactor [55]. They found that higher photosynthetic efficiency was achieved by this reactor compared to horizontal-loop tubular photobioreactor. They attributed their findings to photoinhibition in the tubular reactor and negative effects of inappropriate light-dark cycling. Kaewpintong *et al.* [56] then compared the performance of airlift and bubble columns operated at the same conditions in *H. pluvialis* cultivation. They found that the airlift photobioreactor gave better performance (79.5×10^4 cells ml^{-1} and $\mu = 0.45\ d^{-1}$) than the bubble column (42×10^4 cells ml^{-1} and $\mu = 0.36\ d^{-1}$). Airlift photobioreactors provide a well-defined flow pattern compared to random flow in bubble column such that cells in the airlift reactor are more exposed to light. Similar results were obtained by Krichnavaruk, Powtongsook and Pavasant (2007) [57]. They found that batch cultivation of *Chaetoceros calcitrans* in an airlift reactor is superior to bubble column as the airlift offered better light utilization. The performance of split-cylinder and concentric tube airlift column reactors were then compared to the performance of a bubble column in the outdoor cultivation of *P. tricornutum* [47]. They found, however, that the three reactors have the similar biomass versus time profiles and final concentration ($\cong 4\ kg\ m^{-3}$). Oxygen inhibition and photo-inhibition also did not occur in the reactors.

III.3.2. Use of airlift drives in other photobioreactor types

Airlift drives have been used in other types of photobioreactors. One application is in flat plate photobioreactors. In the study by Degen *et al.* (2001) [58], an airlift flat plate photobioreactor with baffles was tested for growing *Chlorella vulgaris*. This reactor produced increase in biomass productivity that is 1.7 times greater than bubble column of identical

dimension. Also, a reduction in light path from 30 mm to 15 mm increased the biomass productivity by 2.5-fold. The effect of ratio between downcomer and riser area (A_d/A_r) and superficial gas velocity on the growth of *H. pluvialis* was also tested in 17-L and 90-L airlift flat plate photobioreactor [59]. An $A_d/A_r = 0.4$ and superficial gas velocity = 0.4 cm s^{-1} gave the best performance. Both airlift flat panel reactors have the same cell density ($\cong 4.0 \times 10^5$ cell ml^{-1}) but the 90-L reactor has lower specific growth rate (0.39 d^{-1}) compared to the 17-L reactor (0.52 d^{-1}). The authors also compared the performance of the airlift flat plate photobioreactor to a conventional cylindrical airlift photobioreactor. Both the 17-L cylindrical and flat plate airlift photobioreactor have the same performance (($\cong 3.5 \times 10^5$ cell ml^{-1}). But the best growth rate was observed using the 3-L cylindrical conventional airlift photobioreactor. Airlift flat plate photobioreactor also performed better against stirred tank reactor in growing *C. vulgaris* and *Scenedesmus sp.* [60].

Airlift drives has also been used in tubular photobioreactors. Acián Fernéndez *et al.* added a compact airlift section on horizontal tubular reactor for the outdoor cultivation of *P. tricornutum* to promote oxygen removal and elimination of dead zones and dark zones [61]. They obtained a biomass productivity of 1.20 g L^{-1} d^{-1} was obtained at a dilution rate of 0.05 h^{-1}. They also observed adverse effect of high dissolved oxygen on productivity. This was lessened by increasing the liquid velocity that also led to increased biomass yield. Sobczuk *et al.* [62] also used an airlift tubular reactor to study the influence of solar irradiance and CO_2 molar fraction in inject gas mixture on the behavior of continuous cultures of *P. tricornutum*. They found that the oxygen production rate and CO_2 consumption rate increased hyperbolically with increased solar irradiance. They also observed that the maximum CO_2 uptake efficiency occurred at 60% v/v CO_2 and that carbon losses of more than 100% occurred during the night when the cells are

respiring; while, carbon loss decreased to 10-20% during midday hours. Decreasing the CO2 in the inlet gas led to increase in biomass productivity and decrease by 60% in carbon losses during the day. Lastly, increasing the liquid flow rate led to increase in carbon loss. Airlift drives was also applied to helical tubular reactor. Lee and Bazin tested a 0.315-L airlift helical PBR in growing *Porphyridium cruentum* and compared its performance with a 0.625-L stirred reactor [63]. There was a three-fold increase in biomass concentration (4.6 g L^{-1}) in the airlift helical PBR compared to the stirred reactor (1.7 g L^{-1}). This improvement was attributed to the three-fold increase in surface area to volume ratio in the airlift reactor.

In general, airlift-driven photobioreactor performed better than other types of photobioreactors.

III.3.3. Internally-illuminated airlift photobioreactors

Although there have been a number of studies in photobioreactors that were externally illuminated, there are just a few on reactors with internal lighting especially on airlift reactors. In 1996, Ogbonna *et al.* [64] installed four units of 4-W lamps inside a stirred tank reactor with ring sparger for aeration. The reactor was tested in growing *C. pyrenoidosa*. Both linear growth rates and the final cell concentration increased linearly with light intensity. The cell yield in this reactor is also highest when compared with commercially available photobioreactors with external and internal lighting. In 2001, internal illumination in airlift reactor was used and tested in growing *Synechoccus* PCC 6301. A model-based light control was employed to maintain light condition at appropriate level during cultivation. Regulation of light intensity (30, 60, and 90 μmol m^{-2} s^{-1}) was achieved by increasing the number of light radiators. This method of light control enabled harvesting high cell density without photoinhibition. The cultivation time and

irradiating power consumption were also reduced. In 2011, Choi *et al.* [65] used an internally illuminated airlift photobioreactor in *H. pluvialis* cultivation. The growth was highly affected by light intensity resulting varied cell growth rates. Shading effect was also observed at high cell density even under internal illumination. As response, they employed a multistage mode of growing *H. pluvialis* by gradually increasing internal illumination, which showed better results.

III.3.4. Use of airlift photobioreactors in growing *Spirulina*

In the study by Oncel and Sukan (2008) [49], internal loop airlift and bubble column photobioreactors were compared in cultivating *Spirulina platensis*. Both reactors (1.5 L working volume) are operated at the same conditions. The culture temperature was maintained at 25 ± 1 °C. Light intensity of 5200 lx was provided externally by 18W daylight fluorescent lamps. There is also no CO_2 supplementation. Air flowrate at the 3-cm disk sparger was maintained at 1.5 L min^{-1} (1.0 vvm). Oncel and Sukan's results show that the airlift photobioreactor performed better than the bubble column. Higher dry biomass weight and chlorophyll-a concentration was obtained in airlift PBR than in the bubble column. The maximum growth rate of 0.45 d^{-1} was obtained in the airlift PBR compared to 0.33 d^{-1} in the bubble column.

Yuan *et al.* [66] then tested the effect of ammonia concentration in synthetic wastewater on the growth of *Spirulina* in an airlift photobioreactor. The working volume of 1.5 L was inoculated with *Spirulina* at an initial biomass concentration of 3.5 g L^{-1}. Light intensity was provided externally by twelve 9000-lx Philips F30T12/CW/RS fluorescent lamps. The photobioreactor was operated continuously for five months. Results show that high average biomass concentration (3.5 – 3.8 g L^{-1}) and productivity (5.1 g m^{-1} d^{-1}) were obtained when the ammonia level is 50% of the total nitrogen. Furthermore, high ammonia concentration and

mutual self-shading inhibited cell growth. This study showed the potential of *Spirulina* cultivation in high strength wastewater.

The effect of electromagnetic field on batch cultivation and composition of *Spirulina* in an airlift photobioreactor was also tested by Li *et al.* (2007) [67]. A 3.5-L novel external-loop magnetic airlift photobioreactor was constructed where the electromagnetic field (0 - 0.55 T) was fixed around the return tube. The authors found that 0.25 T electromagnetic stress increased the maximum cell dry weight by 22% two days earlier than the control. Nutritional composition of *Spirulina* was also improved in terms of amino acids and trace metals.

III.3.5. Mass transfer and hydrodynamic characterization of airlift reactors

Contreras *et al.* (1998) [8] performed a detailed characterization of an externally-illuminated 12-L concentric tube airlift PBR. It was found that circulation time generally decreases as superficial gas velocity increases then it becomes independent of superficial gas velocity at the heterogeneous flow regime. Also, the bubble mean diameter generally increases with increasing superficial gas velocity, but a maximum was observed for the interfacial area. The maximum interfacial area corresponds with the maximum holdup that occurred at 0.05-0.06 m s^{-1}. In bubbly flow (low superficial gas velocities), the oxygen volumetric mass transfer coefficient is highly sensitive to superficial gas velocity but becomes independent at the heterogeneous flow regime. Furthermore, it was found that the oxygen volumetric mass transfer coefficient, mixing time and mass transfer time are not affected by biomass concentration (0 – 4 g L^{-1}) in all flow regimes. The volumetric mass transfer coefficient was also found to be less sensitive to changes in bubble diameter than holdup and interfacial area. Maximum value of

specific growth rate was obtained at maximum interfacial area and holdup. This indicated the presence of growth inhibition in culture outside of the optimal gas velocity.

Hydrodynamic and mass transfer characterization were also done on bubble column and two split cylinder airlift photobioreactor – SCAPBR 50 (riser area to downcomer area ratio, $A_r/A_d = 1.0$) and SCAPBR 70 ($A_r/A_d = 3.0$) [50]. The working volume for all reactors is 3.5 liters. Mixing and circulation time, liquid circulation velocity, gas holdup, bubble characteristics and mass transfer coefficient were determined at superficial gas velocities from 0.001 m s^{-1} to 0.009 m s^{-1}. Results showed that bubble column has the smallest mixing time, followed by SCAPBR 70 then by SCAPBR 50. Bubble columns have more chaotic flow pattern compared to airlift PBRs with more organized cyclic flow resulting to the former having less mixing time. Low mixing time values can be interpreted physically that a reactor can achieve homogeneity in less time. SCAPBR 50 had faster liquid circulation velocity and lesser circulation time than SCAPBR 70 owing to the former's lesser A_r/A_d ratio. Similar to the results of Contreras *et al.* [8], the circulation time is dependent at low superficial gas velocities but becomes more flow-independent at higher gas velocities.

On the other hand, gas holdup increased almost linearly with superficial gas velocity as opposed to the result of Contreras *et al.* (1998) [8] where a maximum gas holdup was observed. It must be noted, however, that Contreras *et al.* (1998) [8] considered higher superficial gas velocities (U_{GR} = 0.01 – 0.25 m s^{-1}) than Fernandes *et al.* (2014) (U_{GR} = 0.001 – 0.009 m s^{-1}) [50]. Furthermore, SCAPBR 50 have lower gas holdup than SCAPBR 70, which have almost similar gas holdup with the bubble column. This difference can be explained by the difference in the geometry and circulation velocity of the two airlift reactors. Bubble diameter and elongation generally increases with superficial gas velocity. Bubble complexity degree also generally

increases with superficial gas velocity except for bubble column where the bubble complexity degree curve flattened starting from 0.007 m s^{-1} superficial gas velocity. The bubble velocity in the bubble column is also lower than in the airlift reactors, which means that bubble column is expected to have better mass transfer due to higher residence time of bubbles in the reactor. The mass transfer coefficient, on the other hand, increases with superficial gas velocity and are in close agreement with mixing time, gas holdup, and gas bubble velocity. Gas holdup influenced K_La the most. Although high K_La values were obtained in the three PBRs, the highest K_La values were obtained in the bubble column, followed by SCAPBR 70 then by SCAPBR 50.

The three reactors were then tested for C. vulgaris cultivation at superficial gas velocities 0.0011, 0.0044, and 0.0077 m s^{-1}. Contrary to the suggested results of hydrodynamic and mass transfer characterization, SCAPBR 50 has the highest biomass productivity (0.60 – 0.72 g L^{-1} d^{-1}) across all superficial gas velocities. The highest biomass productivity in all PBRs were observed at 0.0044 m s^{-1} superficial gas velocity and the lowest at 0.0077 m s^{-1}. Fernandes *et al.* (2014) [50] offered the explanation that the hydrodynamics and mass transfer do not limit cell growth at the superficial gas velocities considered. The major limiting factor would be light and the light/dark cycles. SCAPBR 50 has higher illumination area to volume ratio (78.3 m^2 m^{-3}) than SCAPBR 70 (71.6 m^2 m^{-3}) and bubble column (51.4 m^2 m^{-3}). So, the goal of this study is to design a reactor with high surface area to volume ratio.

In another study, Hwang and Cheng (1997) [11] measured the liquid velocity and gas holdup in three-phase airlift photobioreactor at varying draft tube lengths (70, 110, and 150 cm) and diameters (9, 12, and 14 cm that are equivalent to A_r/A_d = 0.69, 1.33, 3.22, respectively). The reactor's internal diameter is 19 cm. They found that gas holdup in the riser decreased but increased in the downcomer with increasing draft tube length. This may not good as the

difference in the gas holdup in the downcomer and riser decreases. This also means that more gases are entrained in the downcomer region resulting to less liquid circulation. Furthermore, both gas holdup and liquid velocity in the riser increased but in the downcomer decreased with decreasing tube diameter. There is less bubble entrained in the downcomer. Thus, decreasing the tube diameter and as a result decreasing A_r/A_d may be advantageous.

III.4. METHODOLOGY

III.4.1. Design of a short tank internally-illuminated concentric-tube airlift PBR

The concentric tube airlift photobioreactor had three major components – the main chamber, the light chamber, and the draft tube. The main chamber and the light chamber were made of glass and the draft tube was made of clear acrylic pipe. The reactor was designed in such a way that the working volume of the reactor was three liters. The main chamber had a round bottom to promote better circulation of cells and to eliminate corners where cells might concentrate. The light chamber, which was placed at the center of the reactor, also had a round bottom to promote smooth upward flow of liquid and cells along the light chamber.

The light source was placed at the center to minimize light limitation that light radiated radially outwards from the center. Cool white light-emitting diodes (LEDs) with 12V DC input (3 Watts per foot) and 164 lumens per foot output were used as light source. The reactor was covered with a mirrored acrylic plate.

The reactor was sized such that the liquid height is 80% of the total tank height to provide space for degassing and foam formation. The ratio of the cross-sectional area of the riser to the downcomer was 0.42 and the tank height to diameter ratio was 2.0. The effective liquid height to

diameter ratio was 1.6. The surface area to volume ratio was computed based on the reactor dimensions.

Three reactors of the same dimensions were constructed to be used for replicate runs.

III.4.2. Liquid-phase physical and hydrodynamic characterization

Determination of physical properties of Zarrouk's medium

Five gallons of Zarrouk's medium was prepared to be used both in characterization and in cultivation of *Spirulina* (Chapter IV). Twenty 100-ml samples were taken from the prepared medium and were used for viscosity, density, and conductivity measurements. All measurements were done at 25 °C. The viscosity and density were measured using a Cannon–Fenske viscometer and pycnometer, respectively. The conductivity was measured using conductivity meter (VWR® SB90M5 SympHony Meter).

Mixing time (t_m) and circulation time (t_c) determination

Fernandes *et al.* (2014) [50] found that hydrodynamic characteristics of tap water and growth medium are the same. Thus, hydrodynamic characterization was done in tap water. Mixing time and circulation time determination also followed the procedure of Fernandes *et al.* (2014) [50].

For determination of mixing time and circulation time, 5 mL saturated NaCl solution was injected using a syringe near the bottom of the riser area through a 1 mm stainless steel capillary. The conductivity of the liquid with the tracer was measured using a conductivity probe (VWR® SB90M5 SympHony Meter) placed near the top of the riser. Three replicates per reactor were made at each superficial gas velocity (U_{GR}), which varied from 0.0017 m s^{-1} to 0.0124 m s^{-1}.

This range of U_{GR} was equivalent to 0.13 to 1.0 vvm air flow rate. Mixing time was calculated as the time needed to reach 95% concentration homogeneity. The circulation time was computed as the average time spans between maximum consecutive peaks in conductivity probe response curve.

Liquid Circulation Velocity (v_l) Determination

This methodology also followed the procedure of Fernandes *et al.* (2014) [50]. The mean liquid circulation velocity in the riser was determined via thermal tracer method, which involved injecting a pulse of 5 ml of hot water in to the flowing liquid and plotting the time–temperature profile at two given points in the riser by means of two thermocouples. Two Type-K thermocouples were placed 13.7-cm apart in the riser area of the photobioreactor. Temperature were measured and logged every 0.5 sec using Campbell Scientific CR3000 Micrologger. The liquid linear velocity in the riser was obtained as the ratio of the distance between the two thermocouples and the differences in response times between the two sensors.

III.4.3. Gas-phase hydrodynamic characterization

Overall Gas Holdup Determination

The overall gas holdup was determined using volume expansion method [68]. First, the unaerated, static liquid height (h_L) was measured prior to each run. Then, the air compressor was switched on, and the rotameter was adjusted to a certain air flow rate corresponding to the experimental superficial gas velocity. Aeration was continued until a constant expanded liquid height was achieved. The aerated, expanded liquid height (h_D) was then measured. This

procedure was repeated three times for each superficial gas velocity for each reactor. The overall gas holdup was computed as follows:

$$\varepsilon = \frac{h_D - h_L}{h_D} \qquad \text{Eq. (III.1)}$$

III.4.4. Determination of overall volumetric mass transfer coefficient of oxygen ($K_La_{(O2)}$)

The overall volumetric mass transfer coefficient mass transfer coefficient (K_La) was determined using a modified general protocol of the American Society of Civil Engineers (ASCE) Standard 2-91 Measurement of Oxygen Transfer in Clean Water, presented in Babcock, Malda, and Radway [51]. The first step was sparging with nitrogen to deoxygenate the reactor contents. When the lowest or zero dissolved oxygen concentration was achieved, the nitrogen was turned off and air sparging at a certain superficial gas velocity was commenced. The oxygen concentration was measured by a dissolved oxygen meter (VWR® SB90M5 SympHony Meter) and logged every 10 s using HyperTerminal until a constant value was attained. The K_La was computed using the linearized form of the following equation:

$$C = C_\infty^* - (C_\infty^* - C_O)e^{K_L a \cdot t} \qquad \text{Eq. (III.2)}$$

where:

$C =$ dissolved oxygen concentration (mg L^{-1}) at time, t
$C_\infty^* =$ saturation dissolved oxygen concentration (mg L^{-1})
$C_O =$ initial dissolved oxygen concentration (mg L^{-1})
$K_L a =$ overall mass transfer coefficient ($time^{-1}$)
$t =$ time

Three trials per reactor per superficial gas velocity was made.

III.5. RESULTS AND DISCUSSION

III.5.1. Reactor specifications

The internally-illuminated concentric-tube airlift photobioreactor in this study was designed in such a way that the height to diameter ratio is less than 2.0, A_r/A_d is less than 1.0, and working volume capacity is 3 L. The dimensions of the reactor are shown in Table III-1 (refer to Appendix C for the design calculations). Three reactors were fabricated to comprise three replicates for subsequent experiments such as hydrodynamic and mass transfer characterization experiments and *Spirulina* cultivation experiments. Figure III-1 shows the actual experimental setup.

Table III-1. Actual dimensions and other specifications of the 3-L short tube internally-illuminated concentric-tube airlift photobioreactor.

	Main Chamber	Light Chamber	Draft Tube
D_o, cm (in.)	15.3 (6.02)	5.1 (2.01)	9.5 (3.74)
D_i, cm (in.)	14.6 (5.75)	4.7 (1.85)	8.8 (3.46)
H, cm (in.)	29.3 (11.54)	20.7 (8.15)	24.2 (9.53)
t, cm (in.)	0.35 (0.14)	0.2 (0.08)	0.35 (0.14)
A_o, m^2	0.0184	0.0020	0.0071
A_i, m^2	0.0167	0.0017	0.0061
A_r, m^2		0.0040	
A_d, m^2		0.0097	
A_r/A_d		0.42	
H_T/D		1.92	
H_L/D		1.53	
S/V (m^2 m^{-3})		67	
P/V (W m^{-3})		7,333.33	

The internally-illuminated concentric-tube airlift photobioreactor has a high surface-to-volume ratio (S/V = 67 m^2 m^{-3}). According to Tredici *et al.* (1991) [69], a reactor has a high

surface-to-volume ratio if its value ranges from 25 m^2 m^{-3} to 125 m^2 m^{-3}. Reactors with high S/V usually result to high biomass productivity.

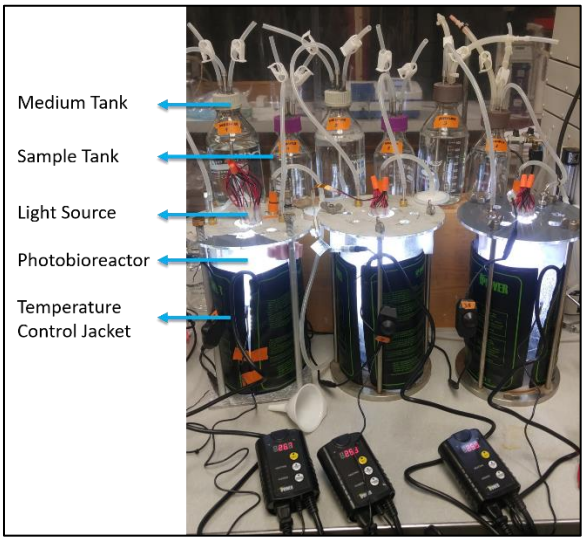

Figure III-1. Actual experimental setup showing the various components of the 3-L internally-illuminated airlift photobioreactor.

III.5.2. Liquid-phase physical and hydrodynamic characteristics

Zarrouk's medium was used in the *Spirulina* cultivation and reactor assessment experiments (Chapter IV). In this chapter, Zarrouk's medium physical characteristics were determined. Its density and viscosity were found to be similar to water ($\rho = 0.996 \pm 0.006$ g L^{-1} and $\mu = 0.997 \pm 0.007$ cP) as presented in Table III-2. Its conductivity, however, is found to be significantly higher than tap water ($\sigma = 22.4 \pm 0.333$ mS cm^{-1} for the medium compared to $\sigma = 1.03 \pm 0.046$ mS cm^{-1} for tap water) due to the former's higher ionic strength. But the medium's salt concentration is still dilute enough to make its density and viscosity equal to water.

Fernandes *et al.* (2014) [50] found that hydrodynamic characteristics of tap water and growth medium are the same indicating that liquid and gas phase characteristics as well as mass transfer do not change within a certain range of ionic strength. For this reason, hydrodynamic characterization of the three reactors were done using tap water. Figure III-1 shows the mixing and circulation times at different superficial gas velocities (0.0017 – 0.0124 m s^{-1}) corresponding to air flow rate 0.13 to 1.0 vvm. Mixing and circulation times shown are the average values obtained in the three reactors. The small deviation among values imply that the reactors have similar hydrodynamic characteristics in terms of mixing time and circulation time.

Table III-2. Physical properties of Zarrouk's medium at 25°C.

Physical Properties	Value
Density (g L^{-1})	0.996 ± 0.006
Viscosity (cP)	0.997 ± 0.007
Conductivity (mS cm^{-1})	22.4 ± 0.333

The mixing time was found to be highly dependent on superficial gas velocity at low values (Figure III-2). The mixing time decreased from 69.7 ± 8.92 s to 16.4 ± 2.62 s when the superficial gas velocity was increased from 0.0017 to 0.0037 m s^{-1}. Thus at 0.0037 m s^{-1}, it only takes about 16.4 s to homogenize and distribute the reactor contents. Sufficient mixing, as in this case, can improve biomass productivity since the frequency of cell exposure to light and dark zones of the reactor is increased as well as the mass transfer between cells and nutrients.

Mixing time and circulation time then become independent of superficial gas velocity at values more than 0.0037 m s^{-1}. This is in agreement with the results of Fernandes *et al.* (2014) [50] who found that mixing time was almost flow-independent for superficial gas velocities more than 0.003 m s^{-1}. Even though Fernandes *et al.* (2014) [50] found that reactor with higher Ar/Ad

has lower mixing time, the reactor in this study with lower A_r/A_d (equal to 0.42) was found to have lower mixing time. The mixing time of the concentric-tube airlift photobioreactor in this study was found to be equal to 11.74 s at U_{GR} = 0.0074 m s^{-1} compared to the mixing time of the split-cylinder airlift photobioreactor in Fernandes' study with A_r/A_d = 1 equal to approximately 38 s at U_{GR} = 0.0078 m s^{-1}. The lower mixing time of the reactor in this study may be due to the smaller working volume (3.0 L in this study vs. 3.7 L in Fernandes' study) as well as the lower H/D (1.53 vs. 6.67 in Fernandes' study).

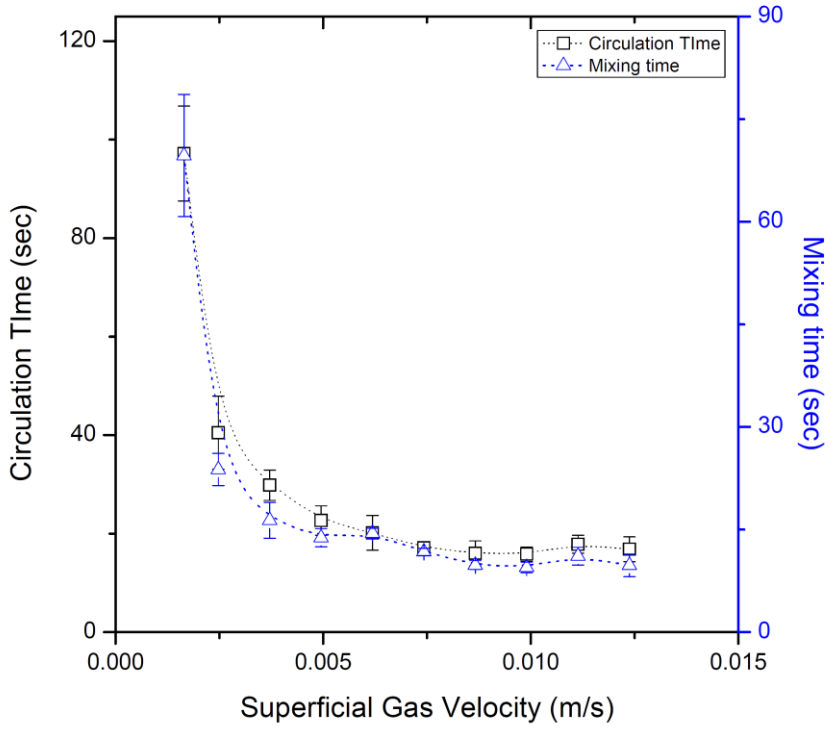

Figure III-2. Hydrodynamic properties of the liquid phase in the 3-L short tube internally-illuminated concentric-tube airlift photobioreactor at 0.0017 – 0.0124 m s^{-1} superficial gas velocity.

Figure III-2 also shows that the circulation time profile against superficial gas velocity is quite similar to the profile of mixing time. Circulation time measures the average time needed for particles to make one cycle in the bioreactor [50]. Circulation time decreased with increasing superficial gas velocity at values less than 0.005 m s^{-1}. Then circulation time becomes almost constant at superficial velocities above 0.005 m s^{-1}. This result was also found to be consistent with the result of Fernandes' study [50]. At the higher superficial gas velocity, micronization of gas bubbles occur; and the build-up of these micronized bubbles in the downcomer area leads to smaller difference in the gas hold-up between the riser and the downcomer area. This in turn leads to reduction in driving force for liquid circulation.

Figure III-2 also shows that larger deviations are observed at the lower superficial gas velocities. Variability in mixing and circulation time measurements then become smaller at higher superficial velocities. This shows that the effect of the differences in the total pore area of the sparger in the three photobioreactors, even if they have the same diameter, are more pronounced at the lower superficial gas velocities. It was observed that the sparger in one of the reactors have lesser total pore area than the other reactors.

At the higher range of superficial gas velocity, flow regime becomes more turbulent and can potentially damage the cells. Working in this range will not give additional benefits since there will be no significant decrease in mixing and circulation times; while, hydrodynamic stress will be more severe due to higher gas velocity. For this reason, 0.0037 m s^{-1} superficial gas velocity or 0.3 vvm air flow rate, which was the inflection point of the mixing time profile (Figure III-2), was chosen as the mid-level value of air flow rate in the *Spirulina* cultivation experiments in Chapter IV.

The mean liquid velocity was also measured by via thermal tracer method wherein liquid velocity is expressed as the ratio between the distance between two thermocouples and the difference between their response times after injecting a pulse input of hot water. Figure III-3 shows a sample time-temperature profile at 0.0017 m s^{-1} superficial gas velocity (0.13 vvm air flow rate), which is the lowest air flow rate. Table III-3 also shows data from all runs at this air flow rate. It shows that the difference in response times ranged between 0.5 to 1.5 s only. At higher air flow rate, the difference in response times will be shorter that the thermocouples may not be able to instantly and accurately respond to rise in temperature. Thus, liquid velocity at higher air flow rate was not obtained. Since the reactor can only fit a maximum distance of 13.7 cm between the two thermocouples, the tracer's exit velocity may have contributed to the short difference in response times even at the lowest superficial gas velocity. For this reason, the measurements cannot be regarded as accurate. Measurements may be more accurate for taller reactors and higher distance between the thermocouples.

The higher liquid velocity, or short difference in response times, may also be a result of the smaller riser area than most reactors. Fernandes *et al.* (2014) [50] found that a split-cylinder airlift photobioreactor with an $A_r/A_d = 1.0$ has a higher liquid velocity at all range of superficial gas velocity than a split-cylinder airlift photobioreactor with an $A_r/A_d = 3.0$. The A_r/A_d affects the liquid velocity as it modifies the resistance to flow by varying the fraction of the total volume contained in the downcomer and in the riser [50]. At lower A_r/A_d, resistance to flow at the riser area may also be lower as there is lesser liquid volume than in the downcomer. The reactor designed in this study has an $A_r/A_d = 0.42$, which explains why high liquid velocity was observed even at the lowest superficial gas velocity.

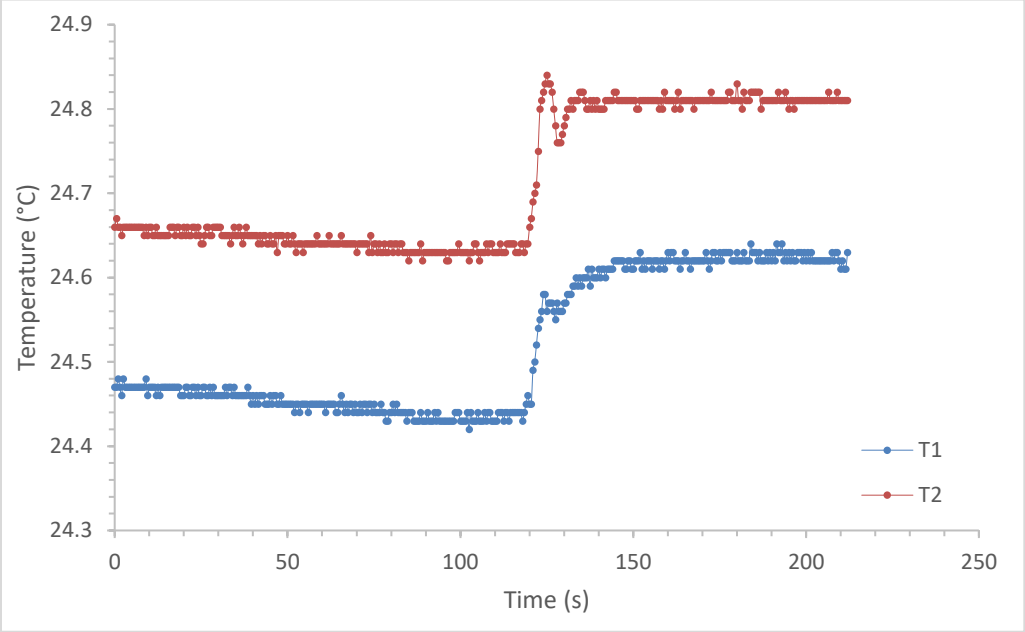

Figure III-3. A sample temperature response curve from two vertically-separated thermocouples to determine mean liquid circulation velocity at 0.0017 m s^{-1} superficial gas velocity (0.13 vvm air flow rate).

Table III-3. Data for mean liquid velocity determination at 0.0017 m s^{-1} superficial gas velocity (0.13 vvm air flow rate).

Reactor No.	Trial No.	Distance b/w thermocouples (cm)	Difference in response time (s)	Mean liquid velocity (cm/s)
I	1	13.7	0.50	27.4
	2	13.7	1.00	13.7
	3	13.7	1.00	13.7
II	1	13.7	1.50	9.1
	2	13.7	0.50	27.4
	3	13.7	1.00	13.7
III	1	13.7	0.50	27.4
	2	13.7	1.00	13.7
	3	13.7	0.50	27.4

III.5.3. Gas-phase hydrodynamic and mass transfer characteristics

Gas holdup indicates the volume fraction and mean residence time of gas phase in aerated vessels. In this study, air that is not supplemented with CO_2 was used to provide airlift in the photobioreactor. A high gas holdup would mean that the volume fraction and mean residence time of air — and thus O_2 — in the reactor is high. High gas holdup is not recommended for photosynthetic cultures since oxygen accumulation has been found to inhibit algal growth [70], [71].

Figure III-4 shows the gas hold up at various superficial gas velocities as well as the overall volumetric mass transfer coefficient of oxygen ($k_L a_{,O_2}$) that represents the rate at which oxygen is dissolved in a reactor's liquid phase. Figure III-4 also presents the relationship between gas holdup and $k_L a_{,O_2}$. Gas holdup is constant at $6.76 \times 10^{-3} \pm 1.01 \times 10^{-5}$ at superficial gas velocities 0.0017 m s^{-1} to 0.0025 m s^{-1}. Then, it rapidly increased to $3.40 \times 10^{-2} \pm 9.23 \times 10^{-4}$ at 0.0074 m s^{-1} superficial gas velocity. The gas holdup increased very slightly, thereafter. Similar relationship was observed between $k_L a_{,O_2}$ and superficial gas velocity. The $k_L a_{,O_2}$ increased very slightly from 0.057 ± 0.015 min^{-1} to 0.159 ± 0.020 min^{-1} from 0.0017 m s^{-1} to 0.0050 m s^{-1} superficial gas velocity. It then rapidly increased to 0.930 ± 0.065 min^{-1} at 0.0062 m s^{-1} superficial gas velocity. The $k_L a_{,O_2}$ increased very slightly, thereafter. Results from the gas-phase hydrodynamic characterization supported the decision to choose 0.3 vvm as the mid-level value of air flow rate in the *Spirulina* cultivation experiments in Chapter IV since it is the upper limit of gas velocity where gas holdup and $k_L a_{,O_2}$ were minimum. It is expected that at this gas velocity, oxygen accumulation can be prevented.

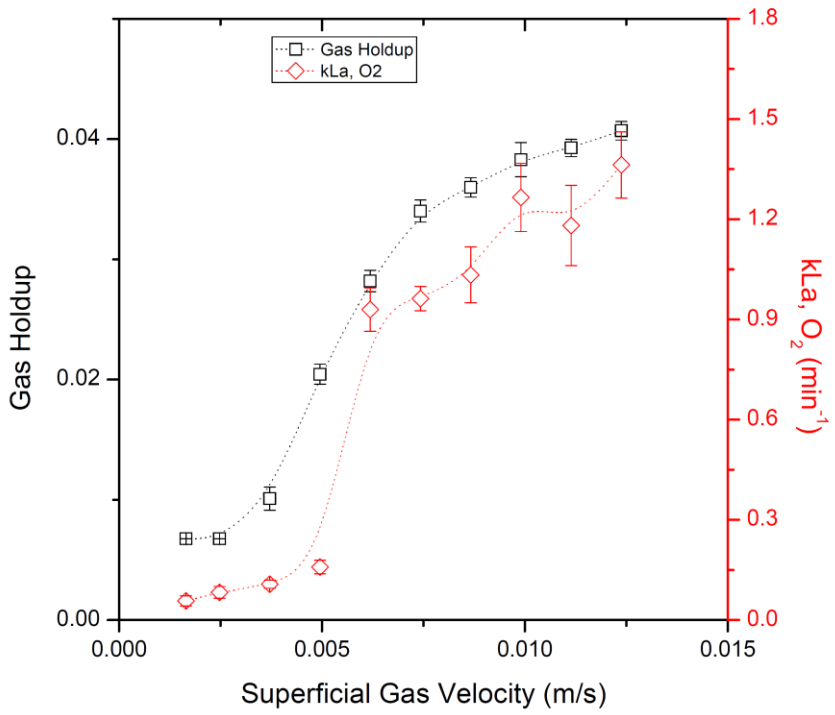

Figure III-4**.** Hydrodynamic and mass transfer characteristics of the gas phase in the 3-L short tube internally-illuminated concentric-tube airlift photobioreactor at 0.0017 – 0.0124 m s^{-1} superficial gas velocity.

III.6. SUMMARY AND CONCLUSION

A short tank internally-illuminated concentric-tube airlift photobioreactor was designed to have a capacity of 3 liters, height-to-diameter ratio of 2.0, and riser-to-downcomer area of 0.42. The liquid-phase and gas-phase hydrodynamic and mass transfer characteristics in the reactor were determined at various superficial gas velocities (0.0017 – 0.0124 m s^{-1}). From the results, a candidate superficial gas velocity was selected as the center point in a three-level experiment in assessing the effect of air flow rate on the growth of *Spirulina* (Chapter IV). Results show that mixing time and circulation time are inversely proportional with superficial gas velocities from 0.0017 – 0.0037 m s^{-1}. They are, however, almost constant at the higher

superficial gas velocities. Furthermore, gas holdup and overall volumetric mass transfer coefficient of oxygen increased very slightly at the lower superficial gas velocities. They then rapidly increased as the superficial gas velocity increased. A close relationship between gas holdup and overall volumetric mass transfer coefficient was also observed. From these results, 0.0037 m s^{-1} superficial gas velocity that is equivalent to 0.3 vvm air flow rate was chosen as the center point in a three-level experiment in testing the effect of air flow rate in *Spirulina* growth.

CHAPTER IV

ASSESSMENT OF GROWTH OF *Spirulina platensis* IN THE 3-L SHORT TANK INTERNALLY-ILLUMINATED CONCENTRIC-TUBE PHOTOBIOREACTOR

IV.1. INTRODUCTION

Cultivation of *Spirulina* has been around for centuries. In the 16th century, Spaniards discovered that the Aztecs living in the valley of Mexico gathered food from a lake [1]. This food was described as a blue-green cake. Although there was no clear evidence on its exact composition, the food must have contained a blue-green alga. *Spirulina* was rediscovered in the mid-1960s by Jean Léonard during a French-Belgian expedition to Africa [1]. He described a blue-green cake sold in the food market of Fort Lamy, Chad. This cake was found to contain *Spirulina* and was consumed by the Kanembu tribe living along the alkaline lakes of Chad and Niger. Around that same time in Mexico, Zarrouk was the first to perform a systematic and detailed study on the growth requirements and physiology of *Spirulina* in response to the request of a company called Sosa Texcoco to study an algal bloom in the evaporation ponds of their sodium bicarbonate production facility [1], [2].

Since then, researches on *Spirulina* have flourished. Researches spanned from outdoor cultivation in open ponds to outdoor cultivation in closed photobioreactors utilizing solar energy for growth. It then progressed to indoor cultivation in closed systems utilizing artificial lighting. Cultivation was performed not only in photoautotrophic cultures but in heterotrophic and mixotrophic cultures as well. Alternative growth media have also been proposed. Furthermore, photobioreactors today have a wide array of configurations — from flat panels to tubulars

reactors, either in helical or serpentine configurations, and then to bubble and airlift columns. Other technologies include hollow fiber, porous substrate biofilm, and microfluidic bioreactors.

In Chapter III, construction of a 3-L concentric-tube airlift photobioreactor is being proposed. As most photobioreactors are lighted from the outside, this photobioreactor will have internal lighting to be provided by light-emitting diodes. The light chamber will be installed at the center of the draft tube. The proposed photobioreactor will also have a height to diameter ratio of two, contrary to most reactors which have height to diameter ratio that is more than two. It is hypothesized that with this aspect ratio, the circulation time inside the reactor will be lesser leading to higher frequency of exposure of the cells to the lighted region of the reactor, ultimately leading to short light-dark cycles. Short light-dark cycles are said to be beneficial to the growth of cells due to the flashing light effect. The proposed photobioreactor a riser cross-sectional area to downcomer cross-sectional area ratio (A_r/A_d) equal to 0.42 contrary to most airlift reactors having A_r/A_d more than or equal to 1.0. It hypothesized that with $A_r/A_d < 1.0$, the liquid velocity will be higher leading to more cycles of the cells per time from the riser to the downcomer region.

The geometry of a reactor affects its performance. This is the reason why the determination of the mass transfer and hydrodynamic characteristics of the reactor has also been proposed in Chapter III to relate these characteristics to the performance of the reactor especially in growing algal cells. These characteristics are overall mass transfer coefficient, gas holdup, liquid velocity, mixing and circulation time, and bubble characteristics. Mass transfer characteristics relate to the delivery of nutrients and CO_2 to the cells as well as the removal of dissolved O_2 to prevent O_2 accumulation that inhibits cell growth. The hydrodynamic characteristics of the reactor relate to the residence time of the gas mixture provided by aeration,

the amount of time needed to attain homogeneous mixture, as well as the potential hydrodynamic stresses that the cells might experience.

The effects of environmental and operating conditions must also be investigated to gain a full grasp of the operation of the proposed photobioreactor. Environmental conditions include pH, temperature, CO2 supplementation, and light intensity levels. And, operating conditions include aeration/agitation rate and mode of operation whether in batch, fed-batch or continuous operation.

Thus, in this chapter the proposed airlift photobioreactor will be tested in growing *Spirulina*. The effects of aeration rate, CO2 supplementation, light intensity and initial cell density will be investigated. The results from this study will be related to the reactor's mass transfer and hydrodynamic characteristics. A preliminary techno-economic evaluation will also be conducted on a scaled-up (1 m^3) operation.

IV.2. HYPOTHESIS AND OBJECTIVES

The hypothesis of this study was that an internally-illuminated concentric-tube airlift photobioreactor with a different aspect ratio (lower height to diameter ratio) and riser to downcomer cross-sectional area ($A_r/A_d < 1.0$) will have different operating condition in maximizing biomass growth.

The following were the objectives of the study:

Objective 1. To test the effect of light intensity (69, 110, 166 μmol m^{-2} s^{-1}) on the specific growth rate, photosynthetic efficiency, algal composition and biomass and protein productivity of *Spirulina platensis* grown in a 3-L internally-illuminated concentric-tube airlift photobioreactors;

Objective 2. To test the effect of aeration rate (0.13, 0.3, 0.8 vvm) on the specific growth rate, photosynthetic efficiency, algal composition and biomass and protein productivity of *Spirulina platensis* grown in a 3-L internally-illuminated concentric-tube airlift photobioreactors;

Objective 3. To test the effect of initial biomass concentration (0.05, 0.10, 0.15 g L^{-1}) on the specific growth rate, photosynthetic efficiency, algal composition and biomass and protein productivity of *Spirulina platensis* grown in a 3-L internally-illuminated concentric-tube airlift photobioreactors; and

Objective 4. To conduct a preliminary techno-economic evaluation of the operation of a scaled-up (80 m^3) internally-illuminated concentric-tube airlift photobioreactor.

IV.3. LITERATURE REVIEW

IV.3.1. Effect of light intensity

Light intensity generally has a positive effect on the growth of *Spirulina platensis*. Light limitation usually occurs at low light intensities and growth rates increase as light intensity increase. However, inhibited growth may occur above a certain threshold of light intensity. The threshold level varies with culture volume, cell density and reactor configuration. In the study of Olaizola and Duerr [72], the threshold light intensity was found to be at 465 µmol m^{-2} s^{-1} (34.4 kilolux) where the growth of *Spirulina* in 100-ml culture tubes with 2.5 cm path length rapidly increased to 2.7 doublings/day. The growth then remained constant at 2.6 doublings/day at light intensities above this threshold. Also, the effect of light intensity on pigments production was tested in this study. While, the maximum total carotenoid productivity was observed at 500 µmol m^{-2} s^{-1} (37 kilolux). In the study by Chen, Zhang, and Guo [73] where photoheterotrophic growth of *Spirulina* was carried out on 100-ml Zarrouk medium

supplemented 2.5 g L^{-1} glucose, the specific growth rate was increased markedly with increasing light intensity until 2 kilolux. But, increasing the light intensity until 4 kilolux did not result to significant increase in specific growth rate. At a light intensity above 4 kilolux, photoinhibition occurred; although, phycocyanin production was favored. For light intensity below 2 kilolux, the optimal glucose supplementation should be 5.0 g L^{-1} to promote cell growth. In another study, Chojnacka and Noworyta [74] observed that photoinhibition occurred above 50 W m^{-2} (3 kilolux) in photoautotrophic culture of *Spirulina* grown in 1-L rectangular reactor with 5.25-cm path length.

Qiang, Zarmi and Richmond [75] also tested the effect of light intensity on the biomass output rate of high cell density cultures using flat plate photobioreactor with 14-mm light path. They found that for every light intensity and optical cell density, there was a maximum volumetric output rate, which generally increases with light intensity. The optical cell density also increases steadily with light intensity and did not exhibit full saturation even at 8000 µmol m^{-2} s^{-1}. Photoinhibition with respect to light intensity was not observed. Furthermore, the photosynthetic efficiency (≅15%) was not affected by light intensity until 2000 µmol m^{-2} s^{-1} and then started to decline from 2500 µmol m^{-2} s^{-1}. Similar to the effect on photosynthetic efficiency, the biomass areal production rate and the O_2 production rate increased linearly with light intensity up to 2000 µmol m^{-2} s^{-1}. Then, these parameters increased only very slightly above 2000 µmol m^{-2} s^{-1}. But in the study of Converti *et al.* (2006) [76] using a 5.5-L airlift driven horizontal tubular reactor, photolimitation occurred at 55 µmol photons m^{-2} s^{-1} (4 kilolux), producing only 6.6 g L^{-1} biomass in cultures. The reactor's illumination area and surface to volume ratio were 0.40 m^2 and 135 m^2 m^{-3}, respectively. Increasing the light intensity up to 80 and 120 µmol m^{-2} s^{-1} (5.9 and 8.9 kilolux) increased biomass production to a maximum

10.6 g L^{-1} after 19 and 15 days, respectively. No photoinhibition occurred at these light intensities. The maximum biomass concentration was the same for 80 and 120 µmol m^{-2} s^{-1} and did not increase further exhibiting self-shading effect.

IV.3.2. Effect of light quality

Olaizola and Duerr [72] also tested the effect of light quality (red, white, and blue light) on the growth and pigment production of *Spirulina platensis*. They found that growth of cultures in red light (133 µmol m^{-2} s^{-1}) decreased within the first two generations of exposure and did not change significantly thereafter (up to 8 generations). The growth rates under this condition were similar to cultures grown in white light of the same light intensity. The total pigment levels are also similar even though individual carotenoids responded differently. As for the effect of blue light (300 µmol m^{-2} s^{-1}), growth rate was less than half of growth rate of cultures grown under white light of the same light intensity. The total carotenoid levels decreased initially due to decrease in myxoxanthophyll content. But increased after 8 generations due to increase in β-carotene levels. Total carotenoid production under blue light is about one-third of cultures grown under white light.

IV.3.3. Effect of path length

Qiang, Zarmi and Richmond [75] also tested the effect of light path length on biomass output rate in a flat plate photobioreactor. They found that decreasing the light path length by 27-fold (200 mm to 7.5 mm) increased the biomass volumetric output rate by 50-fold. The areal output rate was also doubled. The specific growth rate remained constant at path lengths 100 mm to 200 mm, but it increased by 20% when path length was reduced from 50 mm to 7.5 mm.

IV.3.4. Effect of cell density

Vonshak *et al.* (1982) [2] studied the interrelations between solar irradiance and population density on the output rate of outdoor cultures of *Spirulina platensis* in fiberglass ponds. They found that the photosynthetic activity, specific respiration rate, biomass output rate, and specific growth rate are lower at higher cell density. In high cell density cultures (≥ 0.8 optical density at 540 nm), light limitation due to mutual shading was so extreme that most of the growth rate potential of the algae was limited by light. Cell densities below the optimal (0.4 – 0.5 g L^{-1}) resulted to lower biomass output rate, which indicates that high solar irradiance cannot be exploited by the cells at low cell density. Also, only about 20% of the cells (upper 2-3 cm depth) are exposed to the solar irradiance even at the optimal cell density. However, according to Qiang, Guterman and Richmond [77], ultrahigh cell densities reduces photoinhibition induced by high light intensity and low temperature. The extent of biomass loss is also minimal when operating at the optimal cell density (10-15 g L^{-1}). In their study, cultures were grown in 250-ml glass column with ID = 2.6 cm where illumination was provided by a series of 1500-W halogen lamps.

IV.3.5. Effect of growth medium

Chen, Zhang, and Guo [73] studied the effect of supplementing Zarrouk's medium either with glucose or sodium acetate in the photoheterotrophic growth of *Spirulina*. The highest specific growth rate (0.62 d^{-1}), cell concentration (2.66 g L^{-1}), and phycocyanin production (322 mg L^{-1}) was observed at 2.5 g L^{-1} glucose supplementation. These parameters were higher with that of non-supplemented Zarrouk's medium where *Spirulina*'s specific growth rate was found to be 0.35 d^{-1} and the cell dry concentration and phycocyanin production were 1.53 g L^{-1}

and 199 mg L^{-1}, respectively. For the acetate-supplemented medium the specific growth rate, cell concentration, and phycocyanin production were 0.52 d^{-1}, 1.81 g L^{-1}, and 246 mg L^{-1}, respectively. These values were also less than that found with glucose supplemented medium.

Similar results were found by Vonshak, Cheung and Chen [78]. They found that cells grown in mixotrophic cultures have higher photosynthetic rate, light saturation value, dark respiration rate and light compensation point than those grown in photoautotrophic conditions. Higher growth rates and biomass concentration were also observed. Photoautotrophic cultures were also more sensitive to high photon flux density resulting to a decline in light-dependent O_2 evolution rate and in the maximal efficiency of photosystem II. Mixotrophic cultures recovered faster and to a higher extent from high photon flux density stress than the photoautotrophic cultures.

These results were further supported by Chojnacka and Noworyta [74] who evaluated the growth of *Spirulina* sp. in photoautotrophic, heterotrophic, and mixotrophic cultures. Glucose concentration in heterotrophic and mixotrophic medium was varied from 0.1 g L^{-1} to 2.5 g L^{-1}. They found that although *Spirulina* was able to grow in all media, the highest specific growth rate (1.32 d^{-1}) was obtained in mixotrophic culture, above 30 W m^{-2} light intensity and initial glucose concentration 0.5 g L^{-1}. At 2.5 g L^{-1} initial glucose concentration, the specific growth rate increased with an increase in light intensity until 30 W m^{-2}. Photoinhibition occurred above 50 W m^{-2} in photoautotrophic culture.

A cheaper alternative medium was also tested by Madkour, Kamil and Nasr [79] in growing *Spirulina*. The components of Zarrouk's medium were substituted with cheaper and locally available fertilizers. The reduced cost medium includes single super phosphate (1.25 g L^{-1}), commercial sodium bicarbonate (16.8 g L^{-1}), Muriate of potassium (0.898 g L^{-1}),

and crude sea salt (1 g L^{-1}). Four levels of nitrogen concentrations (10%, 20%, 30% and 40% of Zarrouk's medium's nitrogen concentration) were tested and were sourced from ammonium nitrate (Treatments 1-4) and urea (Treatments 5-8). The results showed that *S. platensis* could grow well in ammonium nitrate with its growth increasing with increasing ammonium nitrate concentration, which resulted to a maximum biomass concentration of 0.813 g L^{-1}. However, growth parameters showed significant decrease with increasing urea concentrations. Growth parameters in Treatment 3 containing 0.353 g L^{-1} ammonium nitrate were comparable to that of Zarrouk's medium. But, the maximum biomass concentration in Treatment 3 was achieved after 27 days as compared to Zarrouk's medium, which achieved the maximum biomass in 15 days.

IV.3.6. Effect of culture system

Göksan, Zekeriyaoğlu, and Ak [80] compared the performance of growing *Spirulina* in 20-L transparent jar, in 300-L polyethylene bag, and in 2,500-L raceway pond, which were exposed outdoors in a greenhouse for 20 days. Aeration in the jars and the bags were maintained at 0.5 vvm. While, mixing was achieved by paddle wheels in the raceway pond. Liquid velocity in the pond was maintained at 30 cm/s. The highest cell density (0.99 g L^{-1}) was found in jar culture. But this culture produced the lowest protein content (33.4%). The biomass concentration in the bag and raceway pond cultures were found to be 0.5 g L^{-1}. Protein contents for the bag and pond cultures were 54.5 and 58.3%, respectively. The high cell density in the jar was attributed to higher temperature. But the lower protein content was attributed to nitrogen depletion due to faster growth.

IV.3.7. Effect of aeration mode and aeration rate

Qiang and Richmond [81] tested the effect of aeration rate on the biomass output rate and photosynthetic efficiency in a flat plate photobioreactor with 2.6 cm path length. A minimum of 0.6 vvm aeration rate was required to fully suspend the cells in the medium to prevent them from settling. An aeration rate of at least 6.3 vvm led to cell damage as indicated by the production of trichomes and yellowish-green foam and by significant decrease in biomass output rate. Dissolved oxygen also decreased linearly with aeration rate from 0.6 to 6.3 vvm. The maximum biomass productivity and O_2 production rate was observed at 4.2 vvm. It was also found that the biomass output rate was unaffected by aeration rate at low biomass concentration (< 5 g L^{-1}).

Ronda *et al.* [82] used a 20-L glass bubble column with aspect ratio 1:5, 0.5 cm thickness, and radius 12.5 cm to test the effect of aeration on the growth of *Spirulina* and on γ-linolenic acid (GLA) production. Illumination provided by three 18-W fluorescent lamps with average light intensity of 2000 lux. The reactor was operated under three operational conditions: static (unagitated), continuous (1.2 vvm for 24 h), and periodic aeration (1 h on and 1 h off at different aeration rates). Static, continuous, and periodic aeration resulted in 41.9%, 88.4%, and 108% air saturation of dissolved oxygen, which also correspond to 2.3, 6.5, and 7.5 mg GLA g^{-1} dry cell, respectively. Increasing the aeration rate under periodic aeration from 0.2 to 2.5 vvm improved the both the specific growth rate and GLA production.

IV.3.8. Effect of CO_2 and N_2 supply

Gordillo *et al.* [83] tested the effect of CO_2 enrichment under nitrogen-saturated and nitrogen-limited condition on biomass yield and cell and external medium composition. They found that CO_2 enrichment did not result to any change in maximum growth rate. It also did not

stimulate nitrogen assimilation, which could explain the lack of response in maximum growth rate. Increasing CO_2 levels also decreased the maximum biomass yield. Protein and pigments also decrease. The levels of phycocyanin, chlorophyll and carotenoids were reduced by about 50%. Although, carbohydrate content increased, the capability to store carbohydrate was saturated. C:N ratio remain unchanged while the amount of organic carbon released to the medium increased. This suggests an efficient mechanism by the cells to maintain their metabolic integrity, balancing C:N in response to CO_2 changes.

Soletto *et al.* [84] then investigated the combined effect of carbon dioxide feeding rate (0.44 – 1.03 g L^{-1} d^{-1}) and light intensity (80 – 250 µmol photons m^{-2} s^{-1}) on the growth of *Spirulina* in a fed-batch pulse feeding operation of a 4-L helical photobioreactor was investigated. The maximum cell concentration (12.8 g L^{-1}) was obtained at 166 µmol m^{-2} s^{-1} (12.3 kilolux) and 0.44 g CO_2 L^{-1} d^{-1}, which was the lowest CO_2 feeding rate considered. At this light intensity, the carbon utilization efficiency (≥ 90%) was maximum between 20 and 50 days of culture. The maximum photosynthetic efficiency (9.4%) was achieved at 125 µmol m^{-2} s^{-1} (9.25 kilolux). High CO_2 level inhibits biomass growth especially at low light intensity.

IV.3.9. Effect of O_2 accumulation

Torzillo *et al.* [70] found that increasing the O_2 partial pressure from 0.20 to 0.56 atmosphere did not affect biomass yield but the protein and phycocyanin content were significantly reduced; while, the Chlorophyll *a* content was slightly reduced. In environment containing 70% oxygen, the biomass yield was significantly reduced and almost completely hindered protein synthesis. Chlorophyll *a* content was scarcely affected while phycocyanin content was significantly reduced.

Marquez *et al.* [71] also tested the effect of dissolved oxygen on the growth of *S. platensis*. High oxygen accumulation, e.g. 1.25 mM dissolved oxygen, inhibited cell growth and resulted to 36% decrease in growth rate compared to cultures with 0.063 mM dissolved oxygen. It was also observed that growth inhibition was coupled with inhibition of photosynthetic activity. Contents of photosynthetic pigments also decreased.

IV.3.10. Effect of temperature

Oliveira *et al.* tested the effect of temperature (15-45 °C) on growth of *Spirulina platensis* and *Spirulina maxima* [85]. It was found that growth of both species generally increases with temperature from 20°C to 40°C. Reduction in metabolic activity was observed for temperatures below 17°C. At 15°C and 45°C, both species did not grow, which was attributed to the loss of green pigmentation. The highest cell concentration (2.4 g L^{-1}) was observed at 30°C and 35°C for *S. maxima* and at 25°C and 30°C for *S. platensis*.

IV.3.11. Repeated batch cultivation

Reinehr and Costa [86] tested the effect of cell concentration, renewal rate and strain on the specific growth rate and biomass productivity of *Spirulina platensis* grown via repeated batch cultivation in 2-L Erlenmeyer flasks for 2160 h at 30 °C and 2.5 kilolux light intensity under 12-h photoperiod. It was found that all factors significantly affect the growth of *Spirulina*. The highest specific growth rate and biomass productivity were 0.111 d^{-1} and 0.0423 g L^{-1} d^{-1}, respectively, when using Zarrouk's medium and 0.113 d^{-1} and 0.0467 g L^{-1} d^{-1}, respectively, when using Manguiera Lagoon water supplemented with 10% Zarrouk's medium. Repeated batch cultivation resulted to two to three times higher results than batch cultivation.

IV.4. METHODOLOGY

IV.4.1. Effect of light intensity

Spirulina was grown at different light intensities – 69, 110, and 166 μmol m^{-2} s^{-1} measured one inch from the reactor's light chamber. The light intensity was controlled by an LED dimmer. Initial biomass concentration (0.05 g L^{-1}) and air flow rate (0.3 vvm) were kept constant. Air is also not supplement with CO_2. The optical density of *Spirulina* stock culture was determined first and the volume of Zarrouk's medium and stock culture were computed to make 3 L of 0.05 g L^{-1} *Spirulina* aliquot. These amounts were poured into the reactor. The air compressor was then turned on and the air flow rate was adjusted to 0.9 L min^{-1} (0.3 vvm). The incoming air was filtered using a 0.2 μm air venting filter. The initial height of the expanded liquid, due to aeration, was marked. A 60-ml sample was taken after inoculation and after 5 h. Sample was taken every 24 h, thereafter. Then, fresh medium was injected to the reactor up to the initial liquid height to maintain culture volume. The sample's optical density was read at 680 nm using a UV-Vis spectrophotometer (VWR UV-Vis Scanning UV-3100). The remaining sample was then pipetted to three 15-ml centrifuge tubes and centrifuged at 1717 × g for 10 mins. The pellets were washed twice with deionized water to remove residual salts and precipitates. After washing, the pellets were resuspended by vortex in a given volume of deionized water to concentrate or dilute the sample to 1.5 absorbance. Five microliters from each mixture was pipetted to the FTIR (Shimadzu IRAffinity-1) ATR (MIRacle™ Single Reflectance Attenuated Total Reflectance) sample cell. The biomass was dried by nitrogen purge at 2.0 L min^{-1} for 5 mins. The sample was then scanned in the FTIR using Happ-Genzel apodization at 4000-600 cm^{-1} wavenumber range and 4 cm^{-1} resolution for 45 scans. Three

spectral measurements were obtained for each sample. The protein, carbohydrate, and lipid content of the sample were obtained using the PLS-regression model generated in Chapter 1.

Spirulina was grown for 8 days. The specific growth rate will be computed as:

$$\mu = slope\ of\ \ln\left({X}/{X_o}\right)\ versus\ time\ curve \quad \text{Eq. (IV.1)}$$

The doubling time will also be computed as:

$$doubling\ time = \frac{\ln 2}{\mu} \quad \text{Eq. (IV.2)}$$

The overall volumetric biomass productivity will be computed as:

$$Qx = \left(X_f - X_o\right)\left(t_f - t_o\right)^{-1} \quad \text{Eq. (IV.3)}$$

The daily volumetric biomass productivity will be computed as:

$$Qx = (X_2 - X_1)(t_2 - t_1)^{-1} \quad \text{Eq. (IV.4)}$$

The overall volumetric protein productivity will be computed as:

$$Qp = \left(P_f - P_o\right)\left(t_f - t_o\right)^{-1} \quad \text{Eq. (IV.5)}$$

And, the daily volumetric protein productivity will be computed as:

$$Qp = (P_2 - P_1)(t_2 - t_1)^{-1} \quad \text{Eq. (IV.6)}$$

where:

X = biomass concentration (g L^{-1}) at time, t
X_o = initial biomass concentration (g L^{-1})
X_f = final biomass concentration (g L^{-1})
μ = specific growth rate (d^{-1})
t = time (d)
t_o = initial time (d)
t_f = final time (d)
P_o = initial protein concentration (g L^{-1})
P_f = final protein concentration (g L^{-1})

The whole *Spirulina* culture was harvested after 8 days. Its final volume was measured. It was centrifuged and washed twice with deionized water in Beckman-Coulter Allegra™ 25R Centrifuge at 4633 × g and at 5 °C. The pellets were then dried at 60 °C in an oven until constant weight. And, the mass of the dried biomass will be obtained.

The heating value of the dried biomass was measured using Parr 6200 Calorimeter. The ash content was also measured. The heating value will then be corrected for the biomass' ash content. The photosynthetic efficiency was computed as:

$$PE = \frac{r_G H_G}{IPAR} \times 100\% \qquad \text{Eq. (IV.7)}$$

where:

r_G = maximum daily biomass production (g d^{-1})
H_G = corrected heating value of the biomass (kJ g^{-1})
$IPAR$ = input photosynthetically active radiation (kJ d^{-1})

The IPAR was computed as the product of PAR (kJ m^{-2} d^{-1}) and illuminated surface (m^2). The photosynthetic photon flux density (PPFD) was measured using a quantum PAR meter (Hydrofarm® LGBQM Quantum PAR Meter). The PPFD was then converted to PAR using the conversion factor 18.78 kJ s d^{-1} µmol^{-1}.

All culture runs were done in triplicate.

IV.4.2. Effect of aeration rate

This methodology followed the methodology in Section IV.4.1 except that *Spirulina* was grown at different aeration rates – 0.13, 0.30, and 0.80 vvm. The initial biomass concentration was 0.05 g L^{-1}. The light intensity was controlled and adjusted to the light intensity that gave the highest specific growth rate in Objective 1. The optical density of *Spirulina* stock culture was determined first and the volume of Zarrouk's medium and stock culture were computed to make 3 L of 0.05 g L^{-1} *Spirulina* aliquot. These amounts were poured into the reactor. The air compressor was then turned on and the air flow rate was adjusted to the test value of aeration rate. The incoming air was filtered using a 0.2 µm air venting filter. The initial height of the expanded liquid, due to aeration, was marked. A 60-ml sample was taken after inoculation and after 5 h. Sample was taken every 24 h, thereafter. Then, fresh medium was injected to the reactor up to the initial liquid height to maintain culture volume. The sample's optical density was read at 680 nm using a UV-Vis spectrophotometer (VWR UV-Vis Scanning UV-3100). The remaining sample was then pipetted to three 15-ml centrifuge tubes and centrifuged at 1717 × g for 10 min. The pellets were washed twice with deionized water to remove residual salts and precipitates. After washing, the pellets were resuspended by vortex in a given volume of deionized water to concentrate or dilute the sample to 1.5 absorbance. Five microliters from each mixture was pipetted to the FTIR (Shimadzu IRAffinity-1) ATR (MIRacle^{TM} Single Reflectance Attenuated Total Reflectance) sample cell. The biomass was dried by nitrogen purge at 2.0 L min^{-1} for 5 min. The sample was then scanned in the FTIR using Happ-Genzel apodization at 4000-600 cm^{-1} wavenumber range and 4 cm^{-1} resolution for 45 scans. Three spectral measurements were obtained for each sample. The protein, carbohydrate, and lipid content of the sample were obtained using the PLS-regression model generated in Chapter 1.

Spirulina was grown for 8 days. The specific growth rate, doubling time, overall and daily volumetric biomass productivity, overall and daily volumetric protein productivity, and photosynthetic efficiency were computed using Eq. IV.1 to IV.7.

All culture runs were done in triplicate.

IV.4.3. Effect of initial biomass concentration

Spirulina was grown at different initial biomass concentrations, which were 0.05, 0.10, and 0.20 g L^{-1}. The light intensity and aeration rate were adjusted to the level that gave the highest specific growth rate in Objectives 1 and 2, respectively. The optical density of *Spirulina* stock culture was determined first and the volume of Zarrouk's medium and stock culture were computed to make 3 L culture with the desired initial biomass concentration. These amounts were poured into the reactor. The air compressor was then turned on and the air flow rate was adjusted to the desired aeration rate. The incoming air was filtered using a 0.2 µm air venting filter. The initial height of the expanded liquid, due to aeration, was marked. A 60-ml sample was taken after inoculation and after 5 h. Sample was taken every 24 h, thereafter. Then, fresh medium was injected to the reactor up to the initial liquid height to maintain culture volume. The sample's optical density was read at 680 nm using a UV-Vis spectrophotometer (VWR UV-Vis Scanning UV-3100). The remaining sample was then pipetted to three 15-ml centrifuge tubes and centrifuged at 1717 × g for 10 min. The pellets were washed twice with deionized water to remove residual salts and precipitates. After washing, the pellets were resuspended by vortex in a given volume of deionized water to concentrate or dilute the sample to 1.5 absorbance. Five microliters from each mixture was pipetted to the FTIR (Shimadzu IRAffinity-1) ATR (MIRacle^{TM} Single Reflectance Attenuated Total Reflectance) sample cell. The biomass was

dried by nitrogen purge at 2.0 L min^{-1} for 5 min. The sample was then scanned in the FTIR using Happ-Genzel apodization at 4000-600 cm^{-1} wavenumber range and 4 cm^{-1} resolution for 45 scans. Three spectral measurements were obtained for each sample. The protein, carbohydrate, and lipid content of the sample were obtained using the PLS-regression model generated in Chapter 1.

Spirulina will be grown until the stationary phase. The specific growth rate, doubling time, overall and daily volumetric biomass productivity, overall and daily volumetric protein productivity, and photosynthetic efficiency will be computed using Eq. IV.1 to IV.7.

All culture runs will be done in triplicate.

IV.4.4. Preliminary techno-economic evaluation

The first step was to size a 20-m^3 internally-illuminated concentric-tube airlift photobioreactor. The aspect ratio = 2 and A_r/A_d = 0.42 were maintained. A total of four reactors was employed so that the total PBR capacity is 80 m^3. Then a process flow for biomass production was developed from inoculation to production and then to harvesting, drying, and packaging. The main product was the dried *Spirulina* biomass. Its selling price was taken from literature.

For the preliminary techno-economic evaluation, 300 days per year production and continuous operation was assumed. The power required by the lighting system was computed from the power to working volume ratio of the 3-L airlift photobioreactor. The power required by aeration was computed from the aeration rate. The equipment cost was computed using the six-tenth factor rule. The cost of materials was computed from the industrial cost of chemicals needed for the medium, and cost of reverse osmosis (RO) water. The amounts of these materials

were computed from material balance wherein the dilution rate will be equivalent to the highest specific growth rate attained in Objective 3. Other costs such as the cost of installation, instrumentation, piping, buildings and land were computed as percentage of the purchased equipment cost as provided by Peters, Timmerhaus and West (2003) [87]. The selling price of the *Spirulina* powder was based from the feasibility study report of Piccolo (2012) to the European Union[88]. The net profit and net profit margin were determined.

IV.5. RESULTS AND DISCUSSION

IV.5.1. Effect of light intensity

Light intensity is one of the major factors that affects growth of photosynthetic organism such as microalgae. Low light intensity may suppress growth due to insufficient source of energy needed for photosynthesis (photolimitation). On the other hand, severe light intensity may cause photo-oxidation and pigment bleaching (photoinhibition). Both cases result to low biomass yield. Optimal light intensity must be utilized for every culture grown at specific conditions and reactor geometry to obtain maximal biomass yield.

In this chapter, the effect of light intensity (69, 110, and 166 µmol photons m^{-2} s^{-1}) on growth of *Spirulina* was tested. Light intensity was measured one inch from the photobioreactor's light chamber. This is the distance of the inner surface of the draft tube from the outer surface of the light chamber. For this test, the air flow rate was maintained at 0.3 vvm and the initial biomass concentration was 0.05 g L^{-1}.

Figure IV-1(a) shows the time profile of biomass production of *Spirulina* grown at various light intensities in the 3-L short tank internally-illuminated concentric-tube airlift photobioreactor. Results show that biomass concentration generally increases with time.

Spirulina grown at 69 μmol m^{-2} s^{-1} has the lowest daily biomass concentration, followed by those grown at 110 μmol m^{-2} s^{-1}, and *Spirulina* grown at 166 μmol m^{-2} s^{-1} has the highest daily biomass concentration. The final biomass concentrations after 8 days were 0.777 ± 0.142 g L^{-1}, 0.989 ± 0.024 g L^{-1}, and 1.172 ± 0.056 g L^{-1}, respectively, for *Spirulina* grown at 69 μmol m^{-2} s^{-1}, 110 μmol m^{-2} s^{-1}, and 166 μmol m^{-2} s^{-1} light intensity (see Table IV-1) indicating that for the range of light intensities tested, biomass production increases with light intensity. *Spirulina* still has the potential to give better growth performance at higher light intensities since photo-oxidation has not yet been observed at the highest light intensity tested. Experiments at higher light intensities were not done since 166 μmol m^{-2} s^{-1} is the maximum light intensity that the light source can provide.

Figure IV-1(b) shows the various growth phases of *Spirulina* cultivated at various light intensities in the 3-L short tube internally-illuminated concentric-tube airlift photobioreactor. For all cultures, lag phase was almost negligible since the inoculum was acclimatized first in shake flasks at the same light intensity. For 69 μmol m^{-2} s^{-1}, the exponential phase was observed until the fifth day. The rate of growth then slowed down. For cultures grown at 110 μmol m^{-2} s^{-1} and 166 μmol m^{-2} s^{-1}, the exponential phase was observed until the fourth day. Figure IV-1(b) also indicates that cell growth would start to slow down when the biomass concentration reached 0.4 – 0.6 g L^{-1}.

Figure IV-1(c) shows the daily biomass productivity of cultures grown at various light intensities. It shows that biomass productivity increases with light intensity. It also shows that daily biomass productivity increases until a maximum is reached. These maxima were observed at the last day of the exponential phase.

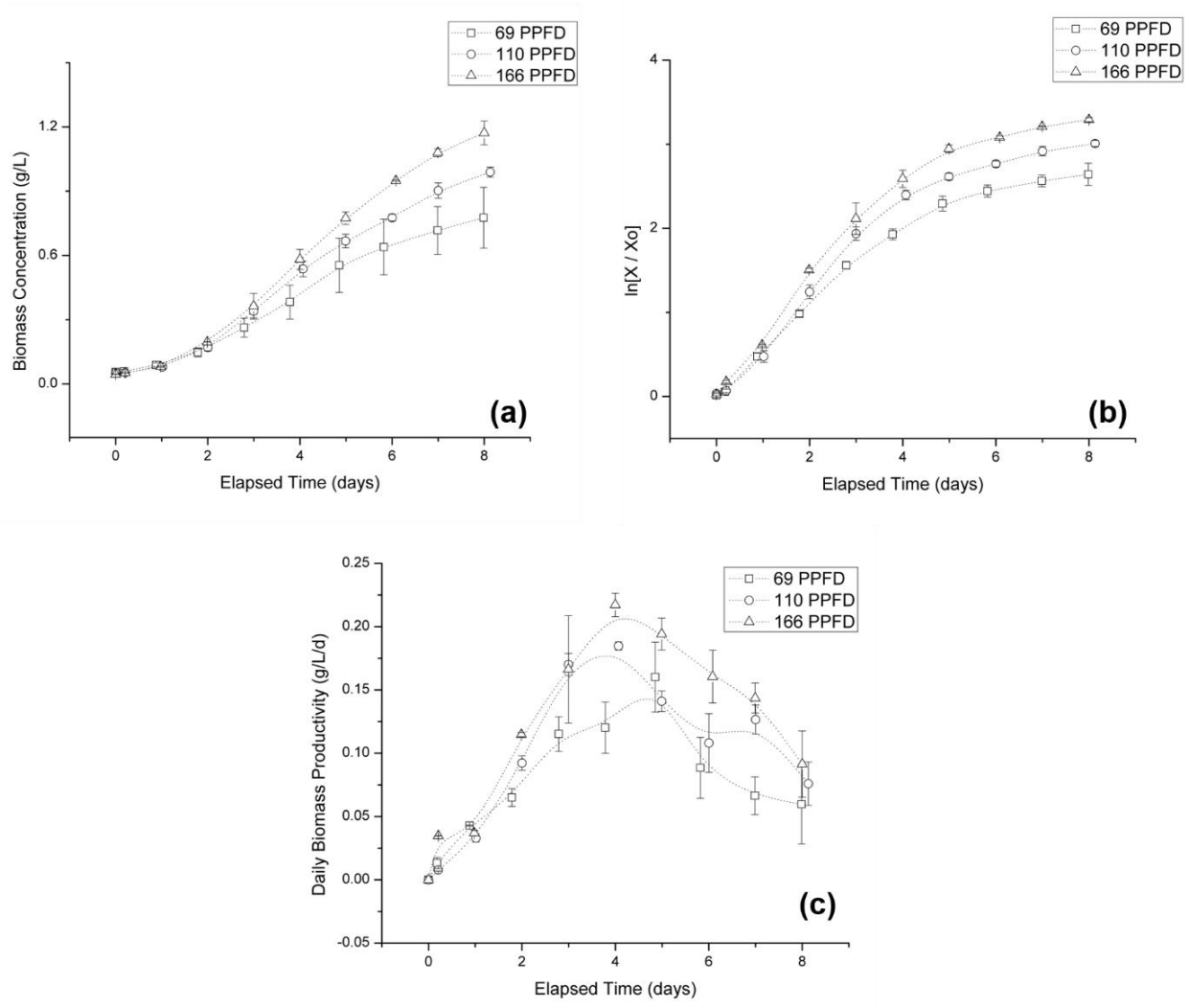

Figure IV-1. Growth curves as (a) biomass concentration vs. time plot, (b) logarithmic plot, and (c) daily biomass productivity time profile of *Spirulina platensis* cultivated at various light intensities in a 3-L short tube internally-illuminated concentric-tube airlift photobioreactor. Air flow rate was maintained at 0.3 vvm and the initial biomass concentration was 0.05 g L^{-1}. PPFD is photosynthetic photon flux density (µmol photons m^{-2} s^{-1})

The summary of the growth parameters for each culture were shown in Table IV-1. The specific growth rate was highest ($\mu = 0.664 \pm 0.035$ d^{-1}) at the highest light intensity tested. It also had the highest overall biomass productivity ($Q_x = 0.141 \pm 0.007$ g L^{-1} d^{-1}) and maximum

daily biomass productivity (0.217 ± 0.013 g L^{-1} d^{-1}). Culture grown at 110 μmol m^{-2} s^{-1} had the second highest growth performance. Its specific growth rate, overall biomass productivity, and maximum daily biomass productivity were 0.630 ± 0.008 d^{-1}, 0.115 ± 0.003 g L^{-1} d^{-1}, and 0.185 ± 0.006 g L^{-1} d^{-1}, respectively. Cultures grown at 69 μmol m^{-2} s^{-1} had the lowest growth performance among the light intensities tested. The specific growth rate, overall biomass productivity, and maximum daily biomass productivity were 0.485 ± 0.021 d^{-1}, 0.090 ± 0.017 g L^{-1} d^{-1}, and 0.160 ± 0.048 g L^{-1} d^{-1}, respectively.

The specific growth rates observed in this study were significantly higher than those observed by Converti *et al.* (2006) [76] who utilized a 5.5-L 0.5-in. diameter combined airlift-tubular photobioreactor in growing *Spirulina*. Converti *et al.* (2006) obtained $\mu = 0.17$ d^{-1} for cultures grown at 120 μmol m^{-2} s^{-1} compared to $\mu = 0.63$ d^{-1} obtained in this study for the 110 μmol m^{-2} s^{-1} culture. The reason may be due to the higher initial biomass concentration in Converti's study (0.15 g L^{-1} compared to 0.05 g L^{-1} in this study), wherein there would be less photon dose per cell mass at higher biomass concentration. It could also be due to the effect of internal lighting in this study where cells can utilize light irradiance more efficiently than when light is provided externally. This is supported by the fact that photosynthetic efficiency observed in this study was also higher than those observed by Converti *et al.* (2006). The difference in the type of reactors used may also have contributed to the different specific growth rates observed.

However, Converti *et al.* (2006) [76] reported better biomass productivity, which may be due to the shorter light path of their reactor (about 0.5 in.); whereas, the light path from the light chamber to the inner diameter of the draft tube of the reactor in this study is 1.0 in. The shorter light path may have prevented shading effect enabling the reactor to support higher biomass

concentrations. In this study, shading effect might have become significant just after a few days of growth since it was observed that growth slowed down just after 4-5 days.

It was also observed that there is only slight increase in the final biomass concentration, specific growth rate and biomass productivity from 110 to 166 μmol m^{-2} s^{-1} compared to the increase in these parameters from 69 to 110 μmol m^{-2} s^{-1}. According to Soletto *et al*. (2008) [84], biomass can grow rapidly at higher light intensity if supplied with sufficient amount of carbon. Since cultures were grown on same growth medium containing the same amount of carbon source, cultures grown at higher light intensity that have higher growth rate may have less carbon available per cell mass. Also, since cell density tend to become higher at higher light intensity, mutual shading may have prevented the cells to obtain higher increase in growth.

Table IV-1. Summary of growth parameters of *Spirulina platensis* cultivated at various light intensities in a 3-L short tube internally-illuminated concentric-tube airlift photobioreactor. Air flow rate was maintained at 0.3 vvm and the initial biomass concentration was 0.05 g L^{-1}.

Growth Parameters	**Light Intensity (μmol m^{-2} s^{-1})**		
	69	**110**	**166**
Specific growth rate, μ (d^{-1})	0.485 ± 0.021	0.630 ± 0.008	0.664 ± 0.035
Overall biomass productivity, Qx (g L^{-1} d^{-1})	0.090 ± 0.017	0.115 ± 0.003	0.141 ±0.007
Max. daily biomass productivity, (g L^{-1} d^{-1})	0.160 ± 0.048	0.185 ± 0.006	0.217 ± 0.013
Final biomass concentration, (g L^{-1})	0.777 ± 0.142	0.989 ± 0.024	1.172 ± 0.056
Final biomolecule content (% w/w)			
Protein	60.4 ± 0.87	56.2 ± 1.94	57.3 ± 0.777
Carbohydrate	36.1 ± 0.53	39.8 ± 2.20	38.8 ± 1.69
Lipid	3.4 ± 0.54	3.96 ± 0.550	3.91 ± 0.910
Overall product productivity (g L^{-1} d^{-1})			
Protein	0.050 ± 0.008	0.061 ± 0.002	0.075 ± 0.004
Carbohydrate	0.031 ± 0.005	0.044 ± 0.005	$0.051 \pm 6.02 \times 10^{-7}$
Lipid	0.0021 ± 0.0006	0.0041 ± 0.0006	0.0050 ± 0.0014
Max. daily product productivity (g L^{-1} d^{-1})			
Protein	0.117 ± 0.022	0.178 ± 0.040	0.185 ± 0.013
Carbohydrate	0.078 ± 0.021	0.109 ± 0.008	0.108 ± 0.005
Lipid	0.0081 ± 0.0017	0.0159 ± 0.0006	0.0146 ± 0.0001
Photosynthetic Efficiency (%)	18.6 ± 5.50	15.1 ± 0.186	10.6 ± 0.121

Table IV-1 also shows that the photosynthetic efficiency decreases with light intensity. This result is consistent with Qiang *et al.* (1998) as cited by Soletto *et al.* (2008) [84], who said that maximum photosynthetic efficiency is readily achieved at low light irradiance when there is small gap between the light saturation of the single cell and the energy absorbed by the culture. Even though the maximum daily biomass productivity increases with light intensity, the energy from the light source that was eventually stored in the biomass was not enough to compensate for the increase in the amount of energy provided to the culture. As cell density increases with light intensity, mutual shading may have prevented the efficient utilization of light resulting to less photosynthetic efficiency at higher light intensity. Mutual shading may be prevented by increasing the circulation rate; but the air flow rate was maintained at the same level for all cultures.

The time profiles of protein, carbohydrate, and lipid production of *Spirulina* were also obtained and were shown in Figure IV-2. The protein, carbohydrate and lipid concentration were measured using the method developed in Chapter II. Similar with biomass concentration, the biomolecule concentration of *Spirulina* generally increases with time. They increase only slightly during the first two days of growth; then increase rapidly, thereafter. The biomolecule production then slowed down during the last three days of cultivation.

Figure IV-2 also shows that biomolecule production increase with light intensity. *Spirulina* cultures grown at 166 μmol m^{-2} s^{-1} have the highest protein, carbohydrate and lipid production rate among the light intensities tested. At this light intensity, the overall protein, carbohydrate and lipid productivity were 0.075 ± 0.004 g L^{-1} d^{-1}, 0.051 ± 6.02 × 10^{-7} g L^{-1} d^{-1}, and 0.0050 ± 0.0014 g L^{-1} d^{-1}, respectively (Table IV-1). The maximum daily protein, carbohydrate, and lipid productivity were 0.185 ± 0.013 g L^{-1} d^{-1}, 0.108 ± 0.005 g L^{-1} d^{-1}, and

0.0146 ± 0.0001 g L^{-1} d^{-1}, respectively (Table IV-1). The final protein, carbohydrate and lipid concentration were 0.608 ± 0.033 g L^{-1}, 0.411 ± 0.001 g L^{-1}, and 0.042 ± 0.011 g L^{-1}, respectively. The next highest biomolecule production rate was observed for cultures grown at 110 μmol m^{-2} s^{-1} with final protein, carbohydrate and lipid concentration were 0.510 ± 0.012 g L^{-1}, 0.362 ± 0.041 g L^{-1}, and 0.036 ± 0.005 g L^{-1}, respectively. While, cultures grown at the lowest light intensity (69 μmol m^{-2} s^{-1}) have the lowest biomolecule production rate among the light intensities tested having final protein, carbohydrate and lipid concentration were 0.411 ± 0.065 g L^{-1}, 0.246 ± 0.043 g L^{-1}, and 0.023 ± 0.004 g L^{-1}, respectively.

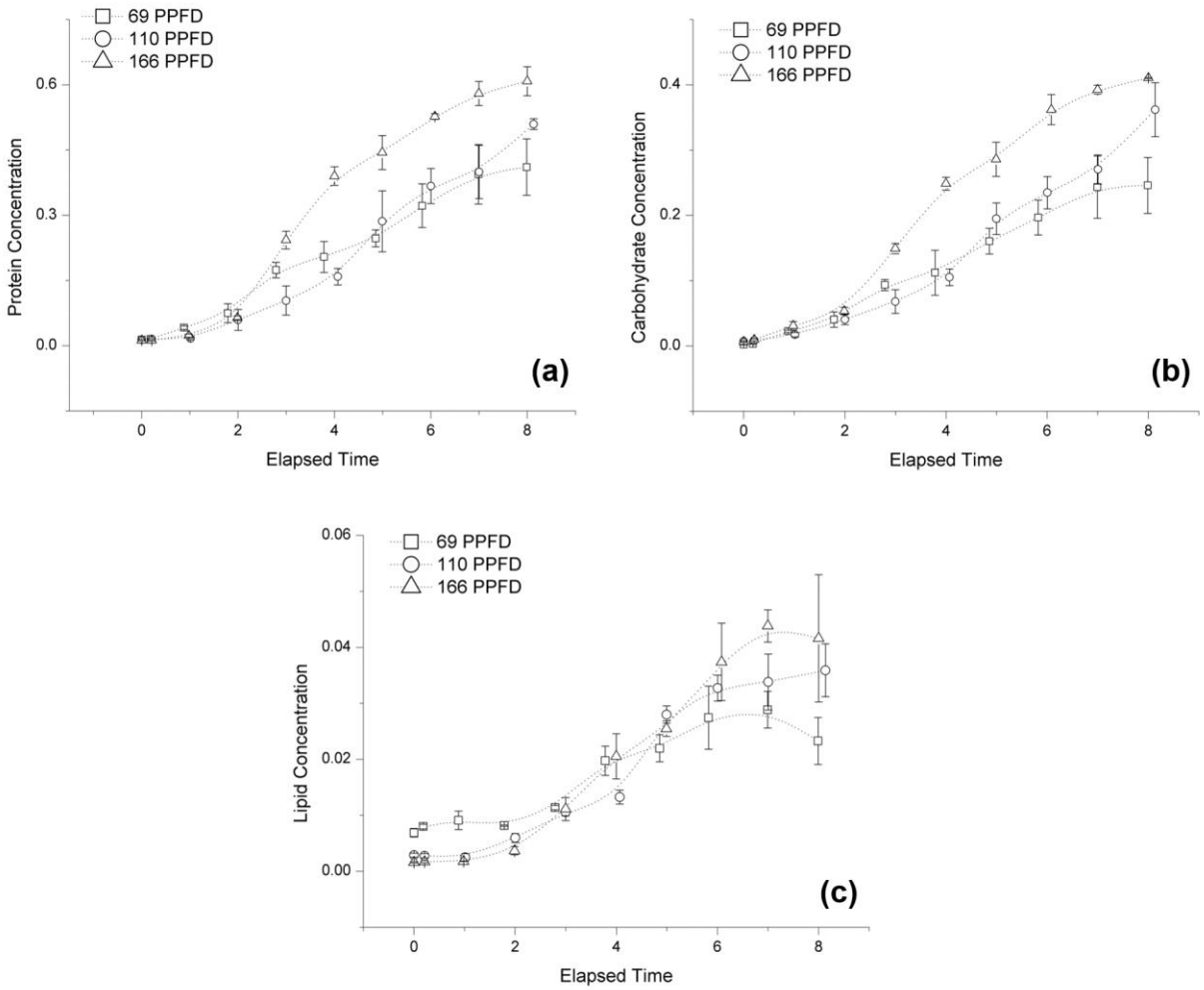

Figure IV-2. Time profile of (a) protein concentration, (b) carbohydrate concentration, and (c) lipid concentration of *Spirulina platensis* cultivated at various light intensities in a 3-L short tube internally-illuminated concentric-tube airlift photobioreactor. Air flow rate was maintained at 0.3 vvm and the initial biomass concentration was 0.05 g L^{-1}. PPFD is photosynthetic photon flux density (µmol photons m^{-2} s^{-1})

The time profile of *Spirulina*'s protein, carbohydrate and lipid content (% w/w of total organic material) were also presented in Figure IV-3 in order to determine how the biomolecule content changes as cells grow. The percent by weight is expressed in terms of the total organic material only so that its value is not influenced by the medium's inorganic components. It was

observed that the protein content of the biomass decreased initially, which was compensated by an increase in the carbohydrate content. This shows biomass production was driven by production of carbohydrates by the expense of protein and lipids in order for the cells to perform various cellular activities for photosynthesis. Biomolecule content remained constant as the cells become more acclimatized to culture environment.

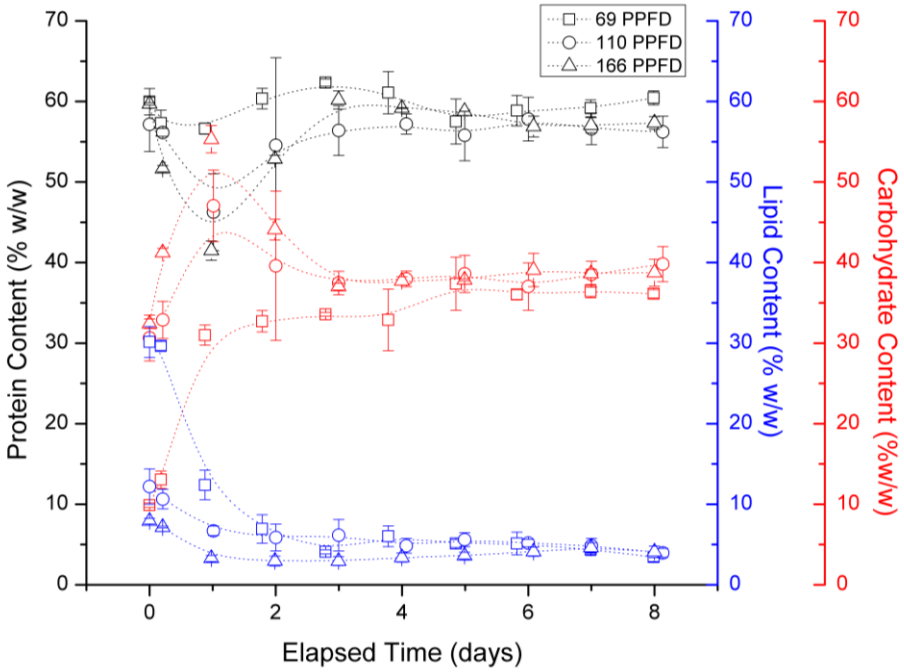

Figure IV-3. Time profile of biomolecule content (black – protein content, red – carbohydrate content, and blue – lipid content) of *Spirulina platensis* cultivated at various light intensities (open square - 69 μmol m^{-2} s^{-1}, open circle - 110 μmol m^{-2} s^{-1}, and open triangle - 166 μmol m^{-2} s^{-1}) in a 3-L short tube internally-illuminated concentric-tube airlift photobioreactor. Air flow rate was maintained at 0.3 vvm and the initial biomass concentration was 0.05 g L^{-1}. PPFD is photosynthetic photon flux density (μmol photons m^{-2} s^{-1}). The biomolecule contents are expressed in terms of %w/w of total organic material.

The final ash content of the biomass was 12.2 ± 2.1 %w/w, 14.1 ± 1.7 % w/w, and 9.5 ± 0.6 %w/w for cultures at 69 μmol photons m^{-2} s^{-1}, 110 μmol photons m^{-2} s^{-1}, and 166 μmol photons m^{-2} s^{-1}, respectively.

IV.5.2. Effect of aeration rate

Aeration rate is another important factor to consider in cultivating microalgae in photobioreactors especially in airlift photobioreactors as air is primarily used to provide liquid circulation. An aeration rate that is enough to completely suspend or lift algal cells through the riser area without damaging the cells should be chosen. If aeration rate is too low, algal cells will settle and concentrate at the bottom of the photobioreactor. In such case, the cells are not exposed to the photic zone of the reactor resulting to lower growth performance. On the other hand, extremely high aeration rate causes hydrodynamic stress the cells leading to trichome breakage and cell death.

In this section, the effect of air flow rate on the growth of *Spirulina* in the 3-L short tank internally-illuminated concentric-tube airlift photobioreactor was tested. Three levels of air flow rate were tested. They were 0.13 vvm, 0.3 vvm, and 0.8 vvm. From Chapter III, 0.3 vvm air flow rate was selected as the mid-level air flow rate to be tested since it corresponds to the highest superficial gas velocity (0.0037 m s^{-1}) at which mixing time, circulation time, gas holdup, and oxygen mass transfer coefficient were minimum. It was desired that mixing time and circulation time were minimum to ensure sufficient mixing and circulation in the reactor. Minimum gas holdup was also desired to promote better circulation of cells. While, minimum k_La was desired to prevent dissolved oxygen accumulation that could be detrimental to the cells. All these

parameters were selected at the highest possible air flow rate to prevent settling of cells. Light intensity was kept at 166 μmol m^{-2} s^{-1} and the initial biomass concentration was 0.05 g L^{-1}.

Figure IV-4(a) shows the biomass production of *Spirulina* at various air flow rates in the 3-L short tank internally-illuminated concentric-tube airlift photobioreactor. Replicate runs for the 0.13 vvm air flow rate were presented separately since they have different results. Possible reasons for such difference were discussed.

According to Figure IV-4(a), biomass concentration generally increases with time. *Spirulina* grown at the highest air flow rate tested (0.8 vvm) has a lower daily biomass concentration than those grown at 0.3 vvm. Lag phase was also observed for the first two days of growth (Figure IV-4(b)), which may be due to hydrodynamic stress resulting from the high air flow rate. Furthermore, intense frothing resulting from high gas holdup ($\varepsilon = 0.038 \pm 0.001$) was observed. This can slow down cell circulation in the reactor. On the other hand, lag phase was not observed for *Spirulina* grown at 0.3 vvm (Figure IV-4(b)). Frothing was also not observed. At this air flow rate, gas holdup was low ($\varepsilon = 0.010 \pm 0.003$) while still providing adequate mixing and circulation (mixing time = 16.4 ± 2.62 s and circulation time = 29.8 ± 3.06 s). Oxygen accumulation was also prevented since the oxygen mass transfer coefficient was low ($k_La,_{O2} = 0.107 \pm 0.012$ min^{-1}). Low oxygen mass transfer coefficient would mean that oxygen is slowly dissolved in the medium preventing oxygen accumulation. Daily measurement of dissolved oxygen indicated that the dO_2 concentration are way below saturation. These factors — adequate mixing and low dO_2 — led to better growth performance of the cell. The final biomass concentrations after 8 days were 1.172 ± 0.056 g L^{-1} and 1.096 ± 0.056 g L^{-1} for *Spirulina* grown at 0.3 vvm and 0.8 vvm, respectively (see Table IV-2). For both air flow rates, growth started to slow down when biomass concentration reached 0.6 g L^{-1}.

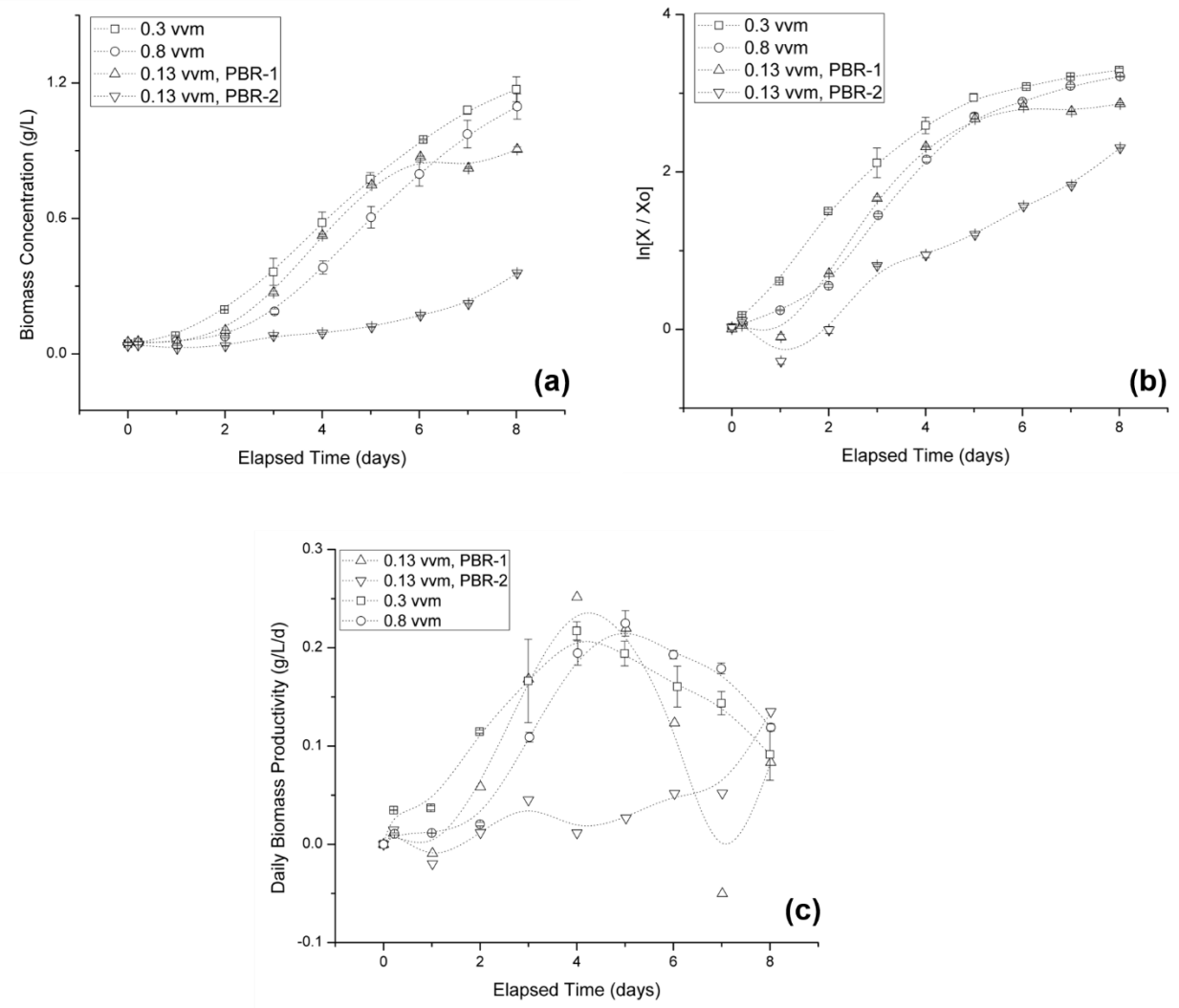

Figure IV-4. Growth curves as (a) time profile of biomass concentration, (b) logarithmic plot, and (c) daily biomass productivity time profile of *Spirulina platensis* cultivated at various air flow rates in a 3-L short tube internally-illuminated concentric-tube airlift photobioreactor. Light intensity was maintained at 166 μmol photons m^{-2} s^{-1} and the initial biomass concentration was 0.05 g L^{-1}. Where, vvm is volume flow rate of air per volume of growth medium (L L^{-1} m^{-1})

Spirulina grown at the lowest air flow rate (0.13 vvm) has the lowest daily biomass concentration and productivity, which was mainly due to settling of cells at the bottom of the reactor. The low air flow rate was insufficient to lift the cells and to promote circulation. As a

result, cells remained at the region of the reactor with poor illumination. There are, however, some cells that were able to circulate the reactor and were exposed to the photic zone that resulted in some growth. It was observed that after the first day of growth, cells have settled and formed a biofilm at the bottom of the reactor. Biofilm was also observed under the disk sparger as well as on the surface of the draft tube. The air flow rate was increased for a short period of time to resuspend the cells in the medium and break the biofilm. The air flow rate was brought back to 0.13 vvm (0.4 L min^{-1}) after. This explains why increase in biomass concentration was observed in PBR-1 until the air flow rate cannot lift the cells anymore due to increase in cell density. This was observed from Day 6. On the other hand, resuspending the cells in PBR-2 did not result in cell growth. After resuspension, most of the cells settled back again resulting to lagging growth. This demonstrates the difference between the spargers in the two PBRs. It was observed that at the low air flow rate, air came out only at a small portion of the sparger in PBR-2; while, air came out at almost the whole area of the sparger in PBR-1. This difference was more pronounced at the low air flow rates. This explains why large variability in mixing time and circulation time measurements were observed at the lower superficial gas velocity in Figure III-1 in Chapter III.

Table IV-2 shows that the specific growth rate of *Spirulina* grown ($\mu = 0.688 \pm 0.006\ d^{-1}$) at 0.8 vvm was higher than those grown at 0.3 vvm ($\mu = 0.664 \pm 0.035\ d^{-1}$). The higher growth rate can be attributed to shorter circulation time wherein the cells are exposed to shorter light/dark cycles. However, the 0.8 vvm cultures have a 2-day lag phase resulting in lower final biomass concentration ($1.096 \pm 0.056\ gL^{-1}$) than those grown at 0.3 vvm ($1.139 \pm 0.102\ g\ L^{-1}$). The cultures grown at 0.3 vvm also performed better in terms of overall biomass productivity — $0.141 \pm 0.007\ g\ L^{-1}\ d^{-1}$ compared to $0.131 \pm 0.007\ g\ L^{-1}\ d^{-1}$ for those grown at 0.8 vvm.

However, the maximum daily biomass productivity of cultures grown at 0.8 vvm is higher (0.225 ± 0.018 g L^{-1} d^{-1}) than those grown at 0.3 vvm (0.217 ± 0.013 g L^{-1} d^{-1}) due to the higher specific growth rate of the 0.8 vvm cultures. Culture grown at 0.13 vvm in PBR-1 has the highest specific growth rate. But, this may be a result of resuspension of the cells in the medium after it was observed that the cells settled at the bottom of the reactor after a day of growth. Culture grown at 0.13 vvm in PBR-2 has the lowest specific growth rate even after the cells were resuspended in the mixture due to settling. The air coming out of its sparger was not enough to promote cell circulation and growth. It was observed that air only came out at a small portion of the sparger in PBR-2.

Table IV-2**.** Summary of growth parameters of *Spirulina platensis* cultivated at various air flow rates in a 3-L short tube internally-illuminated concentric-tube airlift photobioreactor. Light intensity was maintained at 166 μmol photons m^{-2} s^{-1} and the initial biomass concentration was 0.05 g L^{-1}.

Growth Parameters	Air Flow Rate (vvm*)			
	0.13 (PBR-1)	0.13 (PBR-2)	0.3	0.8
Specific growth rate, μ (d^{-1})	0.823	0.364	0.664 ± 0.035	0.688 ± 0.006
Overall biomass productivity, Qx (g L^{-1} d^{-1})	0.107	0.04	0.141 ±0.007	0.131 ± 0.007
Max. daily biomass productivity, (g L^{-1} d^{-1})	0.252	0.135	0.217 ± 0.013	0.225 ± 0.018
Final biomass concentration, (g L^{-1})	0.906 ± 0.010	0.358 ± 0.002	1.172 ± 0.056	1.096 ± 0.056
Final biomolecule content (% w/w)				
Protein	59.70	58.5	57.3 ± 0.777	57.0 ± 0.156
Carbohydrate	36.20	38.2	38.8 ± 1.69	38.6 ± 1.47
Lipid	4.10	3.34	3.91 ± 0.910	4.42 ± 1.32
Overall product productivity (g L^{-1} d^{-1})				
Protein	0.059	0.022	0.075 ± 0.004	0.0674 ± 0.0006
Carbohydrate	0.036	0.014	$0.051 \pm 6.02 \times 10^{-7}$	0.0459 ± 0.002
Lipid	0.0039	0.0011	0.0050 ± 0.0014	0.005 ± 0.002
Max. daily product productivity (g L^{-1} d^{-1})				
Protein	0.11	0.041	0.185 ± 0.013	0.156 ± 0.033
Carbohydrate	0.066	0.029	0.108 ± 0.005	0.0934 ± 0.0177
Lipid	0.014	0.004	0.0146 ± 0.0001	0.0189 ± 0.0039
Photosynthetic Efficiency (%)	11.6	3.3	10.6 ± 0.121	11.0 ± 1.28

***** Where, vvm is volume flow rate of air per volume of growth medium (L L^{-1} m^{-1})

Figure IV-5 shows the time profiles of protein, carbohydrate, and lipid production by *Spirulina*. It shows similar trend with biomass concentration time profile. For the 0.3 vvm cultures, biomolecule concentration increases only slightly during the first two days of growth and increase rapidly until the sixth day. Biomolecule production rate then slowed down during the last two days of cultivation. For the 0.8 vvm cultures, biomolecule concentration did not change for the first two days, which was an indication of growth inhibition that may have resulted from hydrodynamic stress brought about by high air flow rate. During this time, the cells were still adjusting to the harsh growth environment. Biomolecule concentration started to increase on the third day. During the last two days of growth, biomolecule concentration increased only very slightly.

Figure IV-5 also shows that cultures grown at 0.3 vvm have higher daily biomolecule concentration than those grown at 0.8 vvm. The final protein, carbohydrate and lipid concentration were 0.608 ± 0.033 g L^{-1}, 0.411 ± 0.001 g L^{-1}, and 0.042 ± 0.011 g L^{-1}, respectively, for cultures grown at 0.3 vvm. While for those grown at 0.8 vvm, the final protein, carbohydrate and lipid concentration were 0.562 ± 0.006 g L^{-1}, 0.381 ± 0.020 g L^{-1}, and 0.044 ± 0.012 g L^{-1}, respectively.

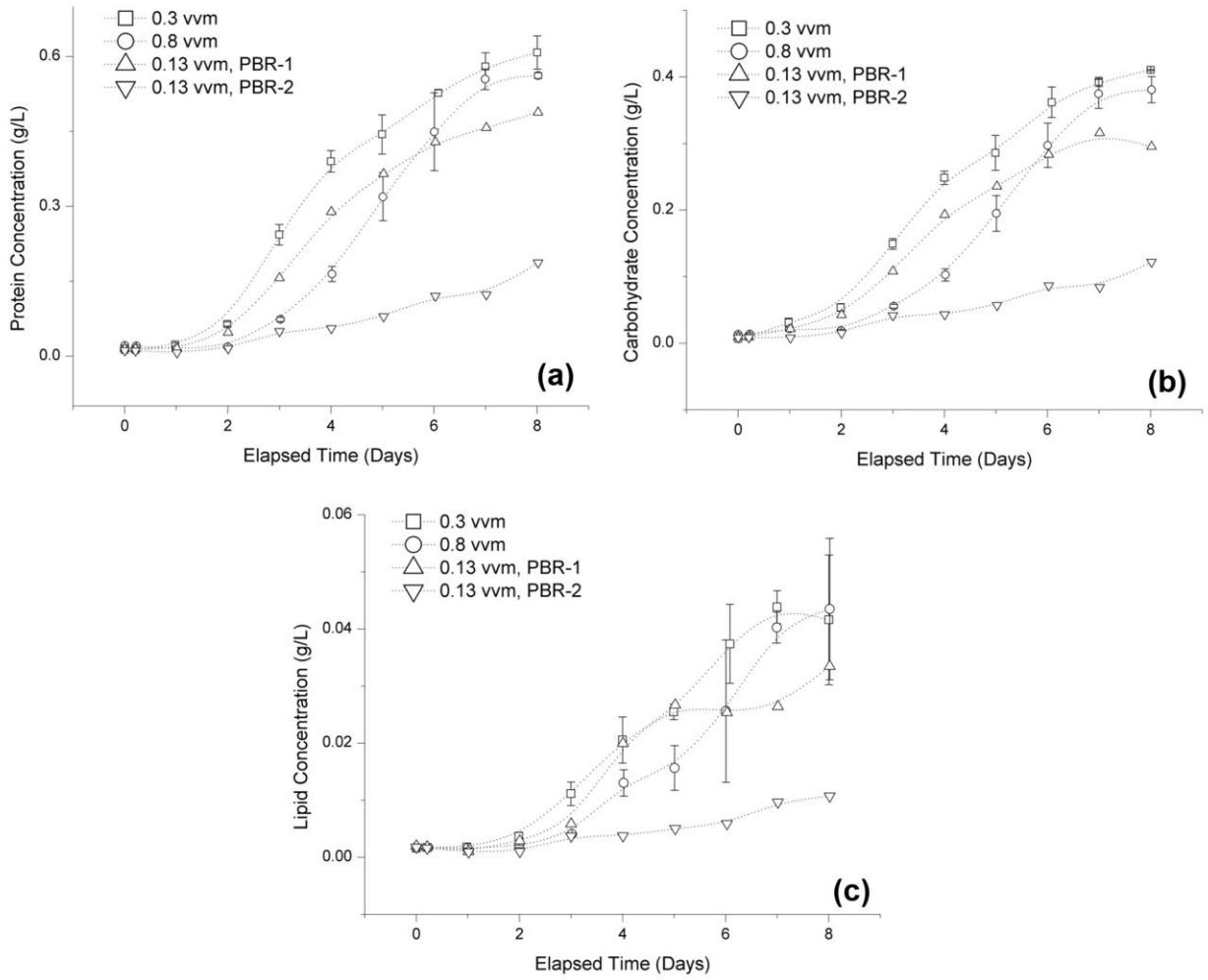

Figure IV-5. Time profile of (a) protein concentration, (b) carbohydrate concentration, and (c) lipid concentration of *Spirulina platensis* cultivated at various air flow rates in a 3-L short tube internally-illuminated concentric-tube airlift photobioreactor. Light intensity was maintained at 166 μmol photons m^{-2} s^{-1} and the initial biomass concentration was 0.05 g L^{-1}. Where, vvm is volume flow rate of air per volume of growth medium (L L^{-1} m^{-1})

The time profile of *Spirulina*'s protein, carbohydrate and lipid content (% w/w of total organic material) were also presented in Figure IV-6. The percent by weight is expressed in terms of the total organic material only so that its value is not influenced by the medium's inorganic components. It was observed that the protein content of the biomass decreased

initially, which was compensated by an increase in the carbohydrate content. This shows that biomass production at the early stage of growth was driven by production of carbohydrates by the expense of protein and lipids in order for the cells to perform various cellular activities for photosynthesis. Biomolecule content then remained constant as the cells become more acclimatized to culture environment. There was an abrupt decrease in the protein content of *Spirulina* grown at 0.8 vvm. The decrease in protein content continued until the second day of growth where the carbohydrate content also started to decrease. This could be due to the effect of hydrodynamic stress brought about by high air flow rate on the cells.

Results from this study indicates that the best aeration rate is 0.3 vvm as it is the lowest rate wherein settling of cells is prevented. At this rate, hydrodynamic stress on the cells is also not observed. This rate is lower than the minimum air flow rate (0.6 vvm) necessary to suspend cells in a flat plate photobioreactor, as reported by Qiang and Richmond (1996) [81]. This can be attributed to the lower height-to-diameter ratio and riser area-to-downcomer area of the airlift reactor that promoted better circulation of cells.

The final ash content of the biomass was 9.8 %w/w, 10.4 %w/w, 9.5 ± 0.6 %w/w, and 9.9 ± 3.4 %w/w for cultures grown at 0.13 vvm (PBR-1), 0.13 vvm (PBR-2), 0.3 vvm, and 0.8 vvm, respectively.

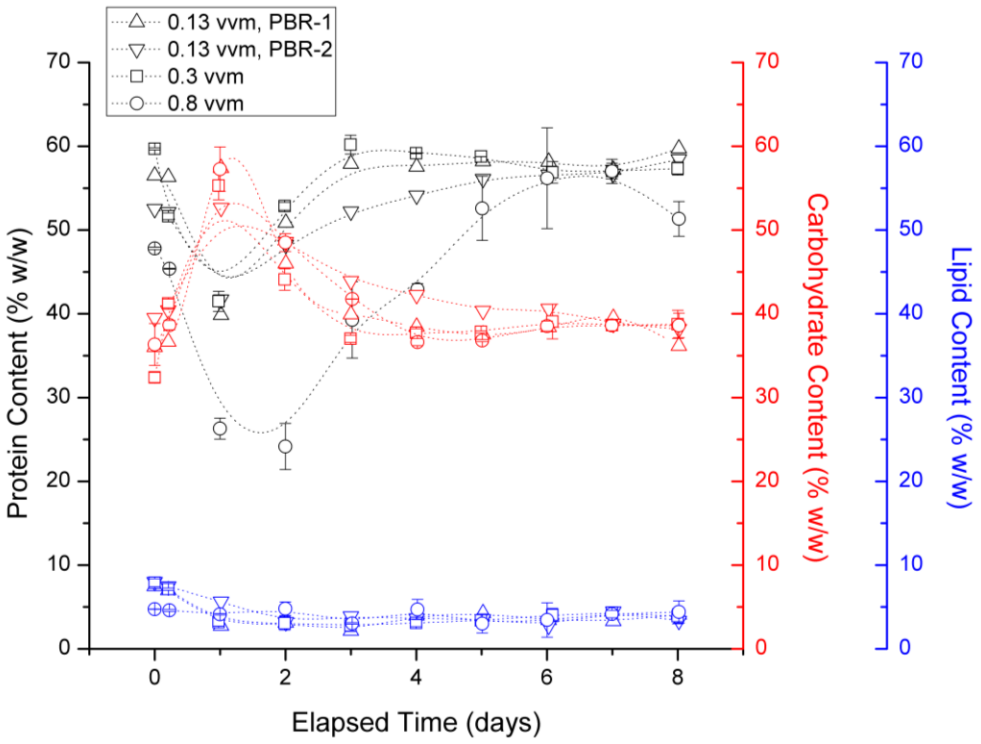

Figure IV-6. Time profile of biomolecule content (black – protein content, red – carbohydrate content, and blue – lipid content) of *Spirulina platensis* cultivated at various air flow rates (open triangle – 0.13 vvm (PBR-1), open inverted triangle – 0.13 vvm (PBR-2), open square – 0.3 vvm, and open circle – 0.8 vvm) in a 3-L short tube internally-illuminated concentric-tube airlift photobioreactor. Light intensity was maintained at 166 μmol m^{-2} s^{-1} and the initial biomass concentration was 0.05 g L^{-1}. Where, vvm is volume flow rate of air per volume of growth medium (L L^{-1} m^{-1}). The biomolecule contents are expressed in terms of %w/w of total organic material.

IV.5.3. Effect of initial biomass concentration

Population density was found to be a major factor in the production of *Spirulina* biomass [2]. Photoinhibition may result at very low biomass concentration since light may be intense enough to bleach the photosynthetic components of the cells. In another case, photolimitation may result at very high biomass concentration since light may not be enough to promote efficient photosynthesis due to mutual shading of the cells. For each reactor configuration and operating

conditions, the best working initial biomass concentration must therefore be selected to obtain the highest biomass and product productivity.

In this section, the performance of the 3-L internally-illuminated concentric-tube airlift photobioreactor was assessed in terms of the effect of initial biomass concentration. The light intensity and the air flow rate were maintained at 166 μmol photons m^{-2} s^{-1} and 0.3 vvm, respectively.

Figure IV-7 shows the growth curves of *Spirulina* at various initial biomass concentrations. The specific growth rate generally decreases with initial biomass concentration. The highest specific growth rate (0.664 ± 0.035 d^{-1}) was observed at the lowest initial biomass concentration (0.05 g L^{-1}) studied (see Table IV-3). At this case, growth is not photo-limited as all cells are exposed to light. This is followed by those grown at 0.10 g L^{-1} initial biomass concentration where the specific growth rate is 0.570 ± 0.021 d^{-1} (see Table IV-3). The lowest specific growth rate was observed at 0.20 g L^{-1} initial biomass concentration where the specific growth rate is 0.526 ± 0.027 d^{-1} (see Table IV-3). These results suggest that photolimitation due to mutual shading of the cells increases with biomass concentration due to the decrease in photon dose per cell mass. This is further supported by the fact that the onset of stationary phase is earlier for cultures grown at higher initial biomass concentration.

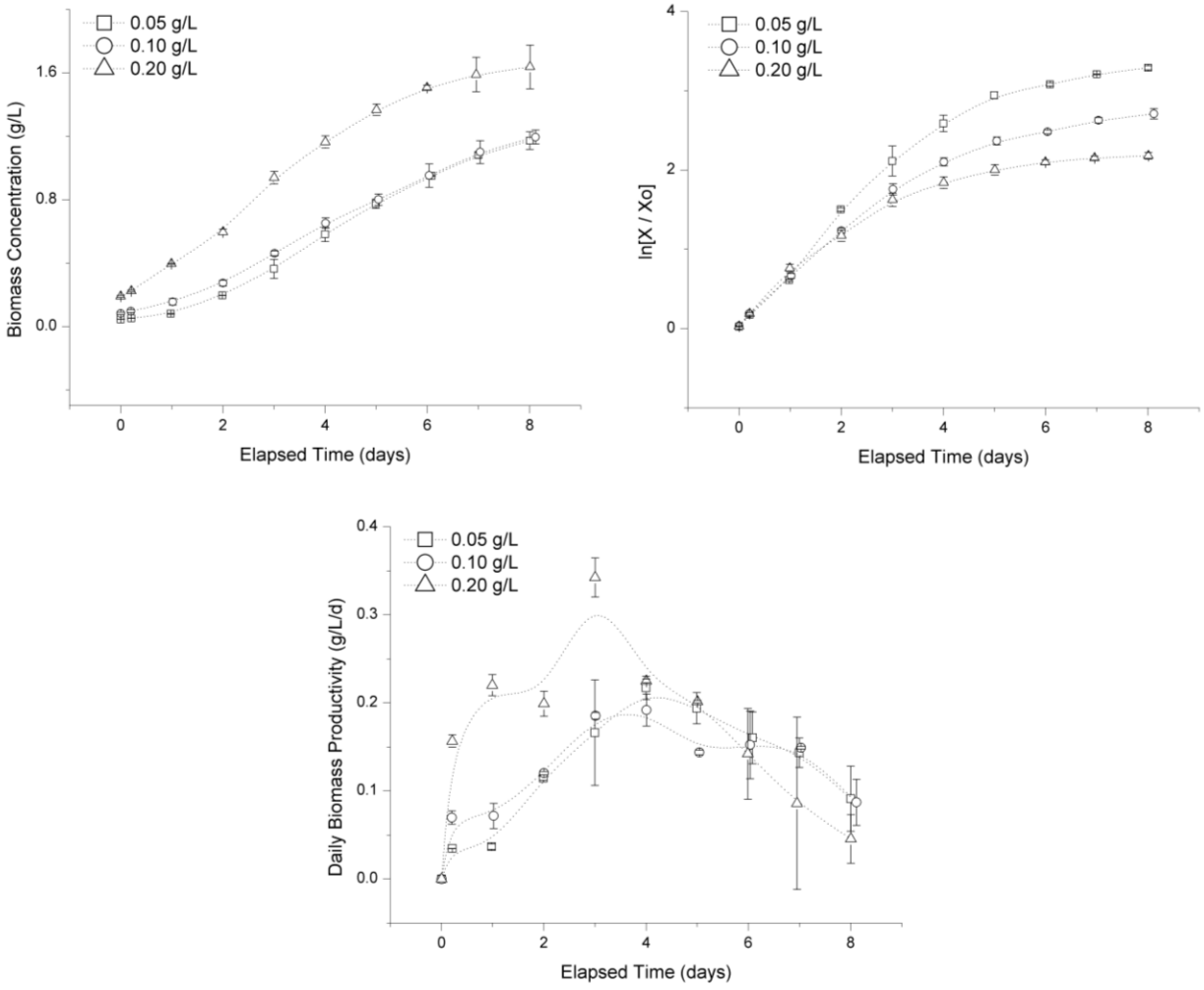

Figure IV-7. Growth curves as (a) time profile of biomass concentration, (b) logarithmic plot, and (c) daily biomass productivity time profile of *Spirulina platensis* cultivated at various initial biomass concentrations in a 3-L short tube internally-illuminated concentric-tube airlift photobioreactor. Light intensity was maintained at 166 µmol photons m^{-2} s^{-1} and the air flow rate was at 0.3 vvm. Where, vvm is volume flow rate of air per volume of growth medium (L L^{-1} m^{-1})

However, the opposite was observed in terms of overall biomass productivity. It generally increases with initial biomass concentration. The possible explanation is that photoinhibition, although not severe, may have occurred during the early days of growth of cultures grown at the lower initial biomass concentrations (0.05 g L^{-1} and 0.10 g L^{-1}) as shown in Figure IV-7 (a) and (b). This resulted to lower daily biomass productivity as shown in

Figure IV-7 (c). Photoinhibition during the first day of growth was not observed at the 0.20 g L^{-1} initial biomass concentration, which resulted to a higher daily biomass productivity. Mutual shading then dominates as the biomass concentration increases with time, which explains why 0.20 g L^{-1} initial biomass concentration has the lowest specific growth rate and the lowest daily biomass productivity during the latter days of cultivation.

In Figure IV-7(c), the daily biomass productivity increases from the day of inoculation until a maximum is reached from where the daily biomass productivity then decreases. It was also observed that the maximum daily biomass productivity was observed at the last day of the exponential phase.

Table IV-3. Summary of growth parameters of *Spirulina platensis* cultivated at various initial biomass concentrations in a 3-L short tube internally-illuminated concentric-tube airlift photobioreactor. Light intensity was maintained at 166 μmol photons m^{-2} s^{-1} and the air flow rate was at 0.3 vvm.

Growth Parameters	Initial Biomass Concentration, g L^{-1}		
	0.05	0.1	0.2
Specific growth rate, μ (d^{-1})	0.664 ± 0.035	0.570 ± 0.021	0.526 ± 0.027
Overall biomass productivity, Q_x (g L^{-1} d^{-1})	0.141 ±0.007	0.137 ± 0.004	0.181 ±0.016
Max. daily biomass productivity, (g L^{-1} d^{-1})	0.217 ± 0.013	0.196 ± 0.012	0.343 ± 0.022
Final biomass concentration, (g L^{-1})	1.172 ± 0.056	1.195 ± 0.044	1.637 ± 0.137
Final biomolecule content (% w/w)			
Protein	57.3 ± 0.777	54.2 ± 2.52	59.7 ± 2.34
Carbohydrate	38.8 ± 1.69	41.16 ± 2.65	36.6 ± 2.43
Lipid	3.91 ± 0.910	4.68 ± 0.122	3.72 ± 0.09
Overall product productivity (g L^{-1} d^{-1})			
Protein	0.075 ± 0.004	0.070 ± 0.001	0.105 ± 0.014
Carbohydrate	0.051 ± 6.02 × 10^{-7}	0.053 ± 0.007	0.063 ± 0.002
Lipid	0.0050 ± 0.0014	0.0060 ± 0.0002	0.0065 ± 0.0006
Max. daily product productivity (g L^{-1} d^{-1})			
Protein	0.185 ± 0.013	0.147 ± 0.014	0.290 ± 0.013
Carbohydrate	0.108 ± 0.005	0.098 ± 0.002	0.165 ± 0.030
Lipid	0.0146 ± 0.0001	0.012 ± 0.002	0.012 ± 0.001
Photosynthetic Efficiency (%)	10.6 ± 0.121	9.54 ± 0.914	17.6 ± 0.980

Since *Spirulina* grown at the initial biomass concentration of 0.20 g L^{-1} has the highest daily biomass productivity, its photosynthetic efficiency was also the highest at 17.6% (Table IV-3). This photosynthetic efficiency was higher than those reported in literature. Better liquid circulation, and efficient light utilization due to internal lighting and short light path may also have contributed to the high photosynthetic efficiency.

Figure IV-8 shows the time profile of the total biomolecule concentration in the cultures grown at different initial biomass concentration. This has the same trend with the time profile of biomass concentration (see Figure IV-7(a)) since these biomolecules primarily comprise the cell biomass. Cultures grown at 0.05 g L^{-1} and 0.10 g L^{-1} initial biomass concentration showed a slow increase in biomolecule concentration during the first day of growth; while, those grown at 0.20 g L^{-1} initial biomass concentration showed a steady increase. The highest final total proteins, total carbohydrates, and total lipids concentrations (0.916 ± 0.099 g L^{-1}, 0.559 ± 0.001 g L^{-1}, and 0.057 ± 0.005 g L^{-1}, respectively) were observed for cultures grown at 0.20 g L^{-1}. The lowest final biomolecule concentration was observed at the lowest initial biomass concentration tested.

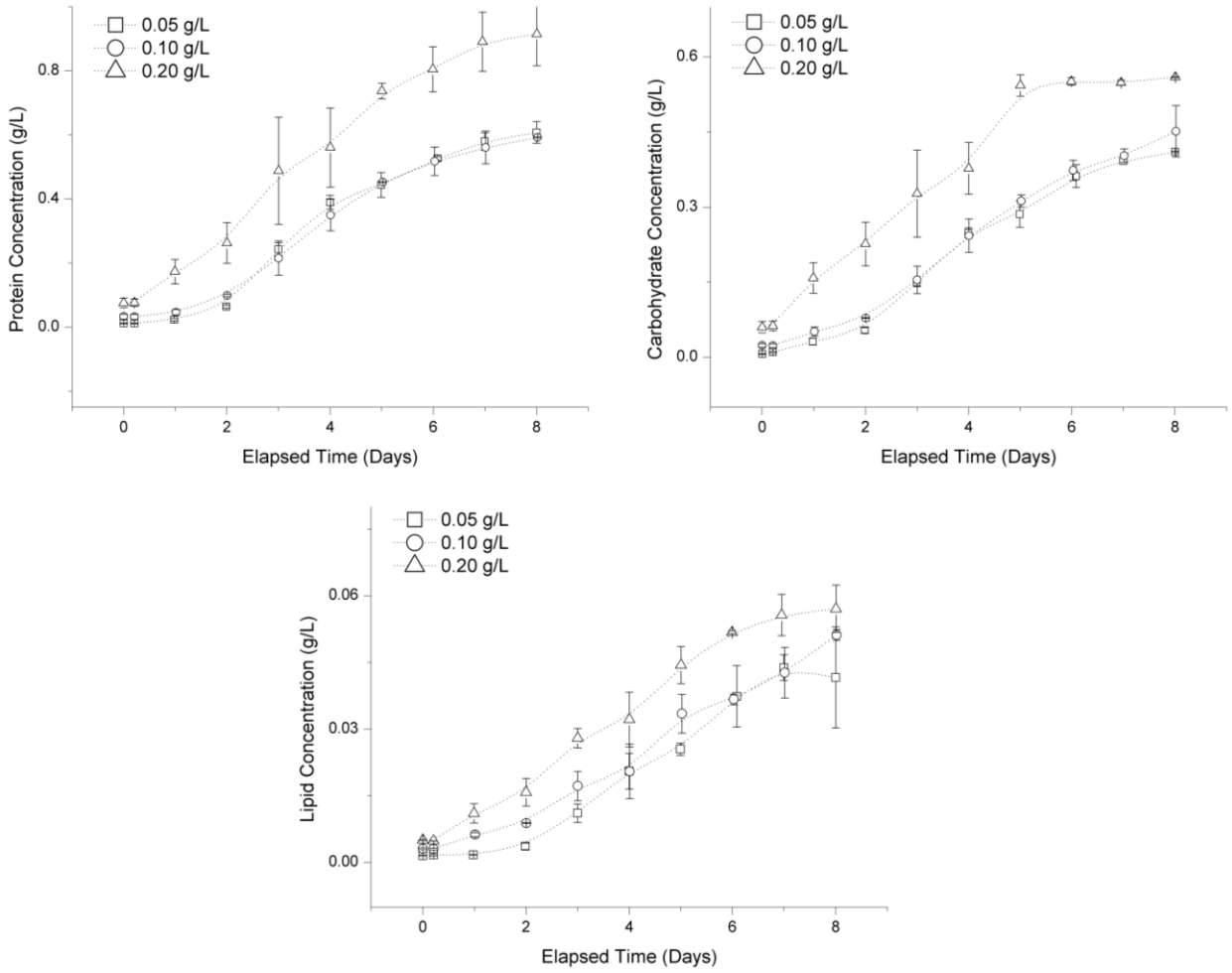

Figure IV-8. Time profile of (a) protein concentration, (b) carbohydrate concentration, and (c) lipid concentration of *Spirulina platensis* cultivated at various initial biomass concentrations in a 3-L short tube internally-illuminated concentric-tube airlift photobioreactor. Light intensity was maintained at 166 µmol photons m^{-2} s^{-1} and the air flow rate was at 0.3 vvm. Where, vvm is volume flow rate of air per volume of growth medium (L L^{-1} m^{-1})

The time profile of *Spirulina*'s protein, carbohydrate and lipid content (% w/w of total organic material) are presented in Figure IV-9 in order to determine how the biomolecule content changes as cells grow. The percent by weight is expressed in terms of the total organic material only so that its value is not influenced by the medium's inorganic components. It was observed

that the protein content of the biomass decreased initially, which was compensated by an increase in the carbohydrate content. This shows biomass production was driven by production of carbohydrates by the expense of protein and lipids in order for the cells to perform various cellular activities for photosynthesis. Biomolecule content remained constant as the cells become more acclimatized to culture environment.

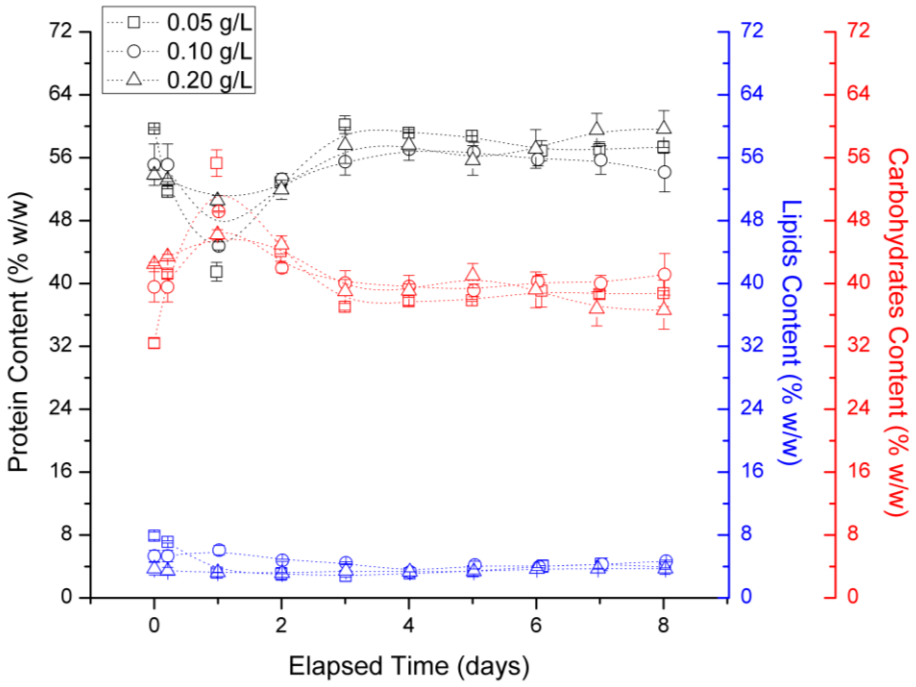

Figure IV-9. Time profile of biomolecule content (black – protein content, red – carbohydrate content, and blue – lipid content) of *Spirulina platensis* cultivated at various initial biomass concentrations (open square – 0.05 g L^{-1}, open circle – 0.10 g L^{-1}, and open triangle – 0.20 g L^{-1}) in a 3-L short tube internally-illuminated concentric-tube airlift photobioreactor. Light intensity was maintained at 166 µmol m^{-2} s^{-1} and the air flow rate was at 0.3 vvm. Where, vvm is volume flow rate of air per volume of growth medium (L L^{-1} m^{-1}). The biomolecule contents are expressed in terms of %w/w of total organic material.

The final ash content of the biomass was 9.5 ± 0.6 %w/w, 8.3 ± 1.2 %w/w, and 5.80 ± 0.01 %w/w for cultures grown at an initial biomass concentration of 0.05 g L^{-1}, 0.10 g L^{-1}, 0.20 g L^{-1}, respectively.

IV.5.4. Preliminary techno-economic evaluation

IV.5.4.1. Base case analysis

In this section, a preliminary techno-economic evaluation of *Spirulina* powder production was performed on a production plant that employed a scale-up of the 3-L short-tube internally-illuminated concentric-tube airlift photobioreactor. The photobioreactor was scaled-up to 20-m^3 capacity. The reactor size was limited to 20 m^3 since low S/V was obtained at higher reactor size even if the number of light chambers were increased. A total of four photobioreactors were employed (80-m^3 total reactor capacity) for the base case analysis.

The first step in the analysis was to devise a continuous process for the *Spirulina* powder production plant. The plant will be operated continuously for 300 days per year. The remaining days will be devoted to startup and maintenance. This process flow was presented in Figure IV-10. It consists of an upstream and a downstream process. The upstream process consists of biomass production using the scaled-up airlift photobioreactor. This photobioreactor maintains the dimension ratios of the bench-scale airlift photobioreactor. These dimension ratios were height-to-diameter (H/D) ratio, riser area-to-downcomer area (A_r/A_d) ratio, and illuminated surface area-to-volume ratio (S/V). High S/V was achieved by installing light chambers in both the riser and downcomer regions of the photobioreactors. The photobioreactors will be constructed using stainless steel 316 and will have a torispherical bottom, similar to the bench-

scale photobioreactor. Light chambers will be made of 3-in. cylindrical glass chambers. The photobioreactors will also be clean-in-place (CIP).

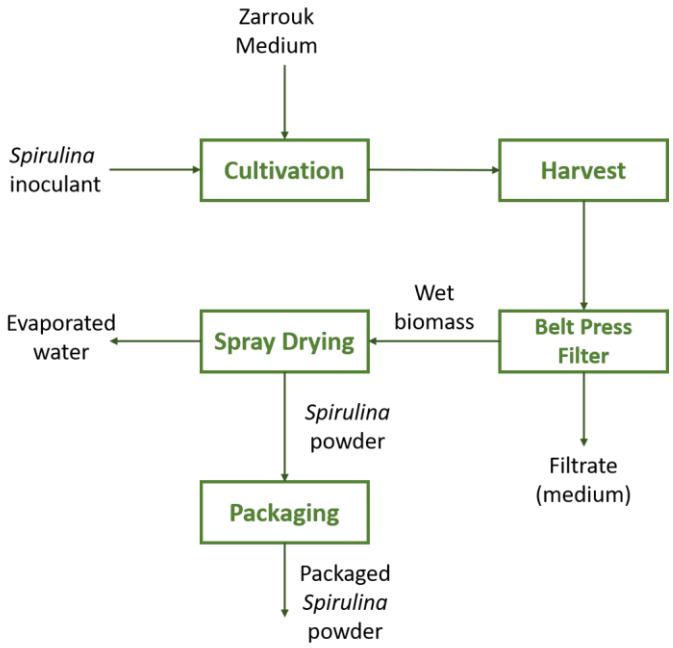

Figure IV-10. Process flow of *Spirulina* powder production.

The operating conditions selected from the bench-scale experiments were 166 μmol photons m^{-2} s^{-1} light intensity, 0.3 vvm air flow rate, and 0.20 g L^{-1} initial biomass concentration. These operating conditions were chosen to give the highest biomass throughput; thus, highest revenue for the plant. These conditions are expected to provide 14,500 kg yr^{-1} of *Spirulina* powder at 70% biomass recovery (see Appendix C for calculations).

The downstream process includes biomass harvesting, dewatering, drying and packaging. Harvesting will be achieved through three stages of filtration. Continuous belt filters with

decreasing mesh size will be used for this purpose. The mesh size will be selected according to the trichome size of the biomass. The final slurry was assumed to contain 20% solid content.

Freeze drying would be the best choice for drying the biomass. However, it was not chosen due to its cost. An alternative choice was the spray dryer. In the spray dryer, *Spirulina* droplets are sprayed into the drying chamber just long enough to flash evaporate the water. The powder is exposed to 60 °C heat for a few seconds as it falls to the bottom. No preservatives, additives, stabilizers nor irradiation are used in drying. The quick spray drying process guarantees preservation of heat sensitive nutrients, pigments and enzymes.

The powder exiting the dryer will be immediately vacuumed away to a collection hopper in the packaging drum and will be sealed under vacuum with special gas-barrier bags in order to minimize the oxidation of certain vital pigments like carotenoids. The sealed product can stay up to four years with little change in biochemical composition or nutritional properties.

A preliminary techno-economic evaluation was performed on this system. The summary of the results was presented in Table IV-4. It shows the capital investment requirement (equipment cost) as well as the production cost (raw material, utilities, labor, and supplies costs). Equipment costs were gathered from manufacturer's quotes except for the photobioreactor cost which was computed from the price of stainless steel. The cost of internal and auxiliary components of the photobioreactor was assumed to be 60% of the cost of the main chamber. The installation, instrumentation, and piping costs were also assumed to be 50%, 26%, and 31%, respectively, of the total purchased equipment cost. Buildings and land costs were also assumed to be 47% and 8% of the total purchased equipment cost. These percentages were based from typical values provided in Peters, Timmerhaus and West (2003) [87].

The amounts of chemicals and process water were determined by material balance. The cost of chemicals was determined from manufacturer's quotes. The cost of process water was also computed from Texas water and wastewater rates. The utilities cost was computed from each equipment's power rating except for the lighting requirements in the photobioreactor. Lighting power requirement was computed from actual measurement of voltage and resistance passing through the light chamber of the bench-scale reactor. This power requirement was scaled-up to the capacity needed by the 20-m^3 photobioreactor. For the labor cost, it was assumed that the plant will need three plant operators for each shift for a total of three shifts each day. The unit labor cost (19.60 \$ h^{-1}) was taken from Texas' May 2017 Occupational Employment and Wage Estimates for Plant and System Operators (Occupational Group 51-4011). The supplies cost was estimated from the yearly requirement of gas-barrier bags.

According to Table IV-4, the total fixed capital investment is $382,520. With a net income of $60,340 per year, this cost will be recovered in 6.34 years. Furthermore, the net income is 7.14% of the total revenue. Since the profit margin is positive, we can say that the venture is feasible.

Cost analysis revealed that labor cost is the major cost contributor. It consists 53.72% of the total production cost. This is followed by supplies cost (17.31%) then by raw material cost (14.94%). Utilities cost (14.03% of the total production cost) is the least among the cost components. This share in cost may change depending on the production capacity of the plant.

Table IV-4. Summary of preliminary techno-economic analysis of a continuous *Spirulina* powder production plant installed with 80-m^3 photobioreactor total capacity.

COMPONENT	AMOUNT (USD)
A. Equipment Cost	
Inoculation PBRs	11,500.00
Photobioreactor	54,200.00
RO Water system	7,000.00
Mixing tank	1,400.00
Medium Holding Tank	36,800.00
Compressor	12,500.00
Belt Filter	9,400.00
Spray Dryer	13,200.00
Installation Cost (50%)	73,000.00
Instrumentation (26%)	37,960.00
Piping (31%)	45,260.00
Sub-total	**302,220.00**
B. Buildings (47%)	**68,620.00**
C. Land (8%)	**11,680.00**
D. Fixed Capital Investment	**382,520.00**
E. Raw Material Cost	
Chemicals	83,700.00
Process Water	34,100.00
Sub-total	**117,800.00**
F. Utilities	
Lighting	12,200.00
Mixing tank	1,400.00
Compressor	82,000.00
Belt Filter	1,400.00
Spray Dryer	10,700.00
Sub-total	**107,700.00**
G. Labor	**423,360.00**
H. Supplies	**136,400.00**
I. Total Production Cost	**785,260.00**
J. Revenue	**845,600.00**
K. Net Income	**60,340.00**
L. Profit Margin	**7.14%**
M. Payback Period (years)	**6.34**

There are a few ways to reduce the cost of production. Water cost can be cut down by process optimization/integration. The filtrate/medium can be recycled back to the photobioreactor. However, organic matter that remained in the medium can accumulate that may result to autoinhibition and thus lower biomass yield. Pre-filters and UV system in the RO unit may also be needed to prevent contamination. Power cost can be cut down by utilizing solar

energy for the power requirement of the plant. But the additional capital investment requirement of the solar plant should be considered. Scaling up may also be beneficial due to economies of scale. But the PBR should be designed in such a way that light can still be efficiently utilized by a larger reactor since the S/V may decrease due to scale-up. Internal lighting also adds constraint in scaling up. A large number of large chambers will be needed for larger reactors.

IV.5.4.2. Sensitivity analysis

Sensitivity analysis based on some factors was performed. The effect of total photobioreactor capacity and of reactor operating conditions on the net income, profit margin, and payback period was tested. The minimum selling price to make the project feasible at different total photobioreactor capacities was also determined.

Effect of Total PBR Capacity

The effect of total photobioreactor capacity on net income, profit margin, and payback period was determined. Photobioreactor capacity is one of the major factors that affects project feasibility and profitability since as the working capacity is changed, equipment specifications and utilities, raw material, and supplies requirements will also change with or without change in the labor requirements. Other fixed capital requirements such land and buildings cost will also change accordingly.

For each photobioreactor capacity considered (40, 60, 80, 100, and 120 m^3), the reactor's dimensions and specifications were recalculated and the number of light chambers were increased or decreased depending on the capacity so that the surface-to-volume ratio of the photobioreactor is maintained. Other costs such as equipment, raw material, utilities and supplies

costs were recalculated based on the capacity. The *Spirulina* powder unit price of $58.3 per kilogram [88] was maintained for all cases. Figure IV-11 shows the results.

Figure IV-11 shows that profitability increases with photobioreactor capacity. The 120-m^3 photobioreactor capacity has the most attractive financial indicators. It has the highest net income ($307,940), highest profit margin (24.28%), and shortest payback period (1.48 years). This is followed by the case that employed 100-m^3 total photobioreactor capacity ($182,740 net income, 17.29% profit margin, and 2.17 years payback period). The base case (80-m^3 photobioreactor capacity) is also feasible ($57,640 net income, 6.82% profit margin, and 5.83 years payback period). Whereas, the venture with 40-m^3 and 60-m3 photobioreactor capacity are not feasible. These cases have net losses and negative profit margins. The payback period also cannot be computed due to negative net income.

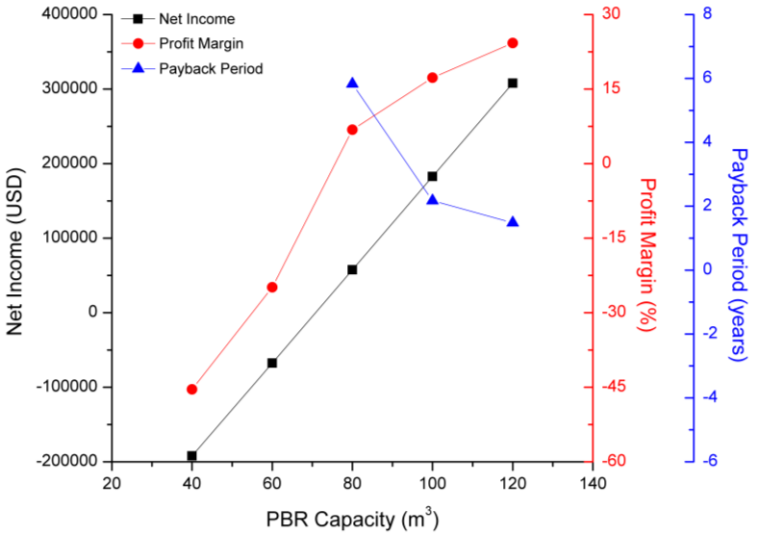

Figure IV-11. Effect of total photobioreactor capacity (40, 60, 80, 100, and 120 m^3) on the net income, profit margin and payback period of a *Spirulina* powder manufacturing plant.

It can be inferred from the results that increasing the photobioreactor capacity more than 100 m^3 may result to better profitability. The only challenge in scaling up is in maintaining high surface-to-volume ratio, which is equated to excellent growth performance. To do this, a large number of internal light chambers will be needed. This will lead to higher fabrication and maintenance cost.

Effect of PBR Operating Conditions

The conditions of operating the photobioreactor such as light intensity, aeration rate and initial biomass concentration also majorly affect project feasibility and profitability as these directly affect biomass yield, which is directly related to the revenue.

The sensitivity analysis was performed at the base case photobioreactor capacity (75 m^3). Also, the highest light intensity (166 μmol m^{-2} s^{-1}) and optimum aeration rate (0.3 vvm) were maintained since these conditions had the highest final biomass concentration and specific growth rate. Lower light intensity and aeration rate not equal to 0.3 vvm resulted to lower biomass yield; thus, lower profitability can be expected. Only the initial biomass concentration was changed since this factor had a positive effect on final biomass concentration but a negative effect on specific growth rate (see growth assessment results as function of initial biomass concentration in Section IV.5.3). Therefore, there is a trade-off in these growth parameters as the initial biomass concentration is changed. This trade-off was tested in this sensitivity analysis. The values of final biomass concentration and specific growth rate at different initial biomass concentration (0.05, 0.10, and 0.20 g L^{-1}) that were used in the analysis were taken from the results in “Section IV.5.3. Effect of Initial Biomass Concentration.”

Figure IV-12 shows that profitability increases with initial biomass concentration as a direct consequence of the increase in the final amount of *Spirulina* biomass produced. However, this result does not guarantee that further increase in initial biomass concentration will result to better profitability. The trade-off between the final biomass concentration and the specific growth rate must always be considered in working with higher initial biomass concentration at the same light intensity and aeration rate. For example, if a culture will be started at an initial biomass concentration higher than 0.20 g L^{-1} at constant light intensity (166 μmol m^{-2} s^{-1}) and aeration rate (0.3 vvm), the final biomass concentration may not be as high as a result of lower specific growth rate. The culture may be photolimited due to the lower photon dose per cell mass at higher initial biomass concentration and the aeration rate may not also be enough to suspend the cells due to the higher population density.

Figure IV-12 further shows that at 80 m^3 total photobioreactor capacity, the project is not feasible if the culture is to be grown at 0.05 g L^{-1} and 0.10 g L^{-1} initial biomass concentration, 166 μmol m^{-2} s^{-1} light intensity and 0.3 vvm aeration rate.

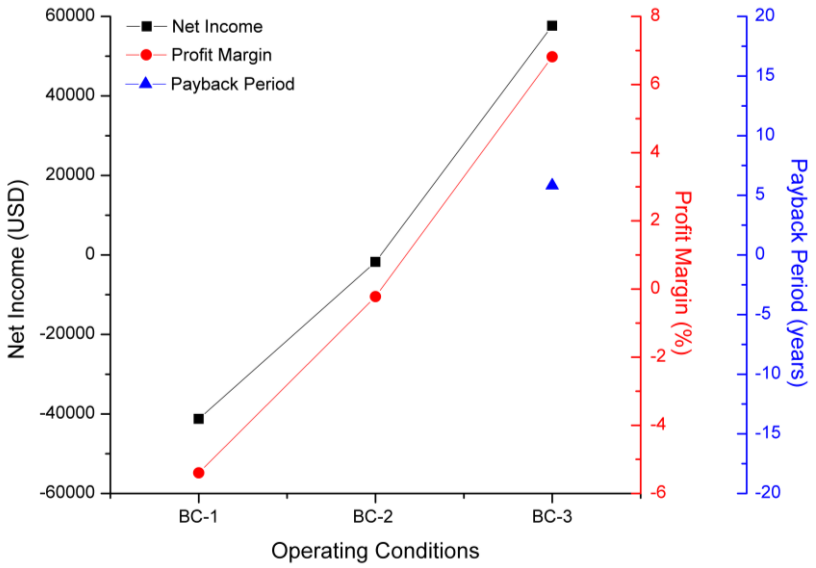

Figure IV-12. Effect of operating conditions on the net income, profit margin and payback period of a *Spirulina* powder manufacturing plant. Where, BC-1 = 166 μmol m^{-2} s^{-1} light intensity, 0.3 vvm aeration rate, 0.05 g L^{-1} initial biomass concentration; BC-2 = 166 μmol m^{-2} s^{-1} light intensity, 0.3 vvm aeration rate, 0.10 g L^{-1} initial biomass concentration, and; BC-3 = 166 μmol m^{-2} s^{-1} light intensity, 0.3 vvm aeration rate, 0.20 g L^{-1} initial biomass concentration.

Minimum Selling Price at Various Total PBR Capacity

The minimum selling price for each total photobioreactor capacity considered (40, 60, 80, 100, and 120 m^3) was also determined. In this analysis, the minimum selling price is defined as the selling price in US dollar per kilogram of *Spirulina* powder that will result to zero net income such that a selling price lower than the minimum selling price will render the project not profitable.

Figure IV-13 shows that the minimum selling price decreases with total photobioreactor capacity. In fact, the minimum selling prices when working at 40 m^3 and 60 m3 total PBR capacities are \$30.46 kg^{-1} and \$10.17 kg^{-1}, respectively, more expensive than the base case (\$54.34 kg^{-1} at 80 m^3 total PBR capacity). At 100 m^3 and 120 m^3 total PBR capacities, the minimum selling prices are \$6.12 kg^{-1} and \$10.20 kg^{-1}, respectively, cheaper than the base case.

It must be noted that these selling prices are only applicable for 166 μmol m^{-2} s^{-1} light intensity, 0.3 vvm aeration rate, and 0.20 g L^{-1} initial biomass concentration. Minimum selling price may be different for different operating conditions since the overall biomass yield will also be different.

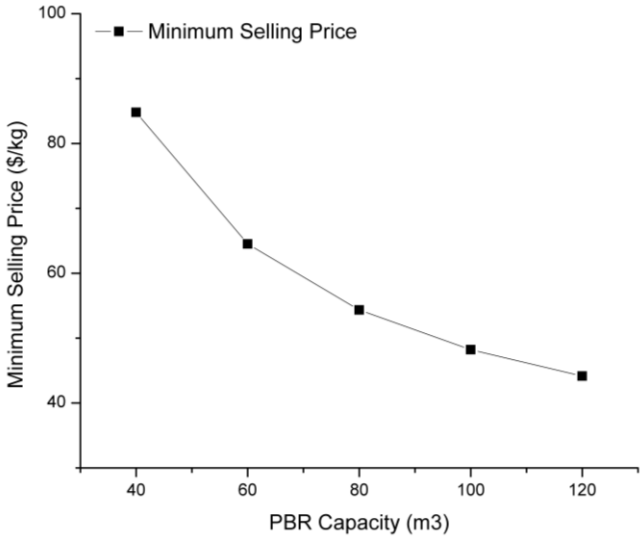

Figure IV-13**.** Minimum selling price of *Spirulina* powder at different total photobioreactor capacities. Analysis was done at 166 μmol m^{-2} s^{-1} light intensity, 0.3 vvm aeration rate, and 0.20 g L^{-1} initial biomass concentration.

IV.6. SUMMARY AND CONCLUSION

In this chapter, the performance of the 3-L short tank internally-illuminated concentric-tube airlift photobioreactor was assessed. The effect of light intensity, air flow rate, and initial biomass concentration on the growth of *Spirulina* was tested. A preliminary techno-economic evaluation was also performed.

For the effect of light intensity on *Spirulina* growth, it was found that growth performance increases with light intensity for the light intensities tested (69, 110, and

166 photons m^{-2} s^{-1}). This may have resulted due to the higher photon dose per cell mass at higher light intensity. Photoinhibition due to bleaching of the photosynthetic apparatus of the cells was also not observed even at the highest light intensity tested. This would mean that the reactor can still be operated at higher light intensity that may result to better growth performance. However, such experiment was not performed since the highest light intensity that the light source can provide is only 166 photons m^{-2} s^{-1}.

On the other hand, photosynthetic efficiency decreased with light intensity. At higher light intensity, there is a larger gap between the light saturation of the single cell and the energy provided to the culture. As cell density increases with light intensity, mutual shading may also have prevented the efficient utilization of light.

In the tests for the effect of aeration rate, it was found that the best aeration rate is 0.3 vvm as it is the lowest rate that can provide adequate cell circulation without hydrodynamic stress that can potentially damage the cells. This rate is lower than those reported in literature. This result is beneficial since lower aeration rate leads to lower operating cost. At 0.8 vvm, the cells may have experienced hydrodynamic stress as demonstrated by the lagging cell growth during the first two days of cultivation. At 0.13 vvm, cell settling was observed, which ultimately led to poor growth performance.

In the tests for the effect of initial biomass concentration, it was found that the specific growth rate decreases with initial biomass concentration but the overall biomass and product productivity increases with it. The lower specific growth rate may be attributed to the lower photon dose per cell mass at higher initial biomass concentration. On the other hand, the slow growth of cells during the early days of cultivation resulted to the lower overall biomass productivity of cultures grown at the lower initial biomass concentrations (0.05 g L^{-1} and

0.10 g L^{-1}). This slow growth may have resulted from photoinhibition, although not severe, during the first day of cultivation where the photon dose per cell mass is high.

From these results, it is recommended that the right combination of light intensity, air flow rate, and initial biomass concentration must be selected to produce the highest biomass throughput. At the beginning of the culture, a higher initial biomass concentration may be needed to prevent bleaching of the photosynthetic apparatus of the cells. The light intensity may need increasing as the cells grow to prevent photolimitation due to mutual shading. Also, aeration rate may also need increasing as the population density increases with time to maintain better circulation of the cells and prevent biomass settling. A smart control of these factors with respect to the instantaneous population density must be developed to attain better growth performance.

Lastly, the preliminary techno-economic evaluation on a *Spirulina* powder production plant with a total photobioreactor capacity of 80-m^3 revealed an attractive venture. The profit margin is positive and the payback period is only 6.34 years.

A few ways of reducing the cost of production were also discussed. Water cost can be cut down by recycling the medium back to the photobioreactor; but organic matter that remained in the medium should be removed first. This will add to the cost of equipment. Power cost can also be reduced by utilizing solar energy to power the plant. But the additional capital investment requirement of the solar plant should be considered. Scaling up may also be beneficial due to economies of scale. But the PBR should be designed in such a way that light can still be efficiently utilized by a larger reactor.

CHAPTER V

SUMMARY AND CONCLUSION

This research provided a comprehensive study on the bench-scale cultivation of *Spirulina* in a short-tank concentric-tube internally-illuminated airlift photobioreactor. There were three major sections in this study. The first was the development of a new analytical method for the rapid analysis of the biochemical composition of the *Spirulina* biomass. The use of FTIR-ATR spectroscopy and PLS-regression for this purpose was successfully demonstrated. PLS regression results was also compared to another regression technique, which is multipoint regression. PLS-regression was found to have better predictive power than multipoint regression as confirmed by higher R^2 and RPD and lower RMSEP and relative error. Comparison of PLS' predicted results with conventional biochemical methods such as Macro-Bradford assay for total proteins content and phenol-sulfuric acid method for total carbohydrates content revealed statistically similar results. However, both multipoint regression and PLS-regression were found to be inadequate in predicting lipid content in *Spirulina* possibly due to its low lipid content, small sample size and overlapping bands of amide I and C=O ester bond. Nevertheless, FTIR spectroscopy and PLS-regression was proven to precisely predict the major biomolecule contents of *Spirulina* biomass. This method reduced the time for sample preparation and eliminated the need to extract the target biomolecule for analysis especially that it usually requires long time and high temperature. The only sample preparation required by FTIR spectroscopy is centrifugation, washing, and drying of the biomass. Drying the biomass can be achieved in a few minutes since the sample mass used in the analysis was only in micro-quantity. With this, FTIR spectroscopy coupled with PLS-regression was proven to be a rapid and non-destructive method

in determining algal composition. This method has also been valuable in monitoring the growth and biochemical changes in *Spirulina* biomass over time.

The second was the design and construction of the bench-scale photobioreactor as well as the hydrodynamic and mass transfer characterization of the reactor. The reactor was designed to have a 3-L capacity, a H/D of approximately 2.0 and A_r/A_d of less than 1.0 as opposed to typical airlift reactors with higher H/D and A_r/A_d. It was hypothesized from the results of Hwang and Cheng (1997) [11] that a photobioreactor having such dimension ratios would have better hydrodynamic characteristics. The liquid-phase and gas-phase hydrodynamic and mass transfer characteristics in the reactor were determined at various superficial gas velocities (0.0017 – 0.0124 m s^{-1}). Results show that mixing time and circulation time are inversely proportional with superficial gas velocities from 0.0017 – 0.0037 m s^{-1}. They are, however, almost constant at the higher superficial gas velocities. Furthermore, gas holdup and overall volumetric mass transfer coefficient of oxygen increased very slightly at the lower superficial gas velocities. They then rapidly increased as the superficial gas velocity increased. A close relationship between gas holdup and overall volumetric mass transfer coefficient was also observed. From these results, 0.0037 m s^{-1} superficial gas velocity that is equivalent to 0.3 vvm air flow rate was chosen as the center point in a three-level experiment in testing the effect of air flow rate in *Spirulina* growth since it is the maximum air flow rate where the mixing time, circulation time, gas holdup and overall oxygen mass transfer coefficient is minimum. It was hypothesized that at this air flow rate, better growth performance can be achieved due to better liquid circulation (shorter light/dark cycle) and lesser accumulation of dissolved oxygen. This hypothesis was tested in Chapter IV – Effect of Aeration Rate.

The third was to assess the reactor's performance in cultivating *Spirulina*. The effects of light intensity, air flow rate, and initial biomass concentration on growth parameters such as specific growth rate, overall and daily biomass and product productivity, and photosynthetic efficiency were tested. For the effect of light intensity on *Spirulina* growth, it was found that growth performance increases with light intensity for the light intensities tested (69, 110, and 166 photons m^{-2} s^{-1}). This may have resulted due to the higher photon dose per cell mass at higher light intensity. Photoinhibition due to bleaching of the photosynthetic apparatus of the cells was also not observed even at the highest light intensity tested. This would mean that the reactor can still be operated at higher light intensity that may result to better growth performance. However, photosynthetic efficiency decreased with light intensity. This may be due to the larger gap between the light saturation of the single cell and the energy provided to the culture at higher light intensity. Mutual shading may also have prevented the efficient utilization of light at higher population density, which was observed at higher light intensity.

In the tests for the effect of aeration rate, it was found that the best aeration rate is 0.3 vvm, which proves the hypothesis made in Chapter III. This aeration rate is the lowest rate that can provide adequate cell circulation without providing hydrodynamic stress that can potentially damage the cells. This rate is also lower than those reported in literature. This result is beneficial since lower aeration rate leads to lower operating cost. At the higher aeration rate (0.8 vvm), the lagging cell growth may during the first two days of cultivation may have resulted from hydrodynamic stress experienced by the cells. At the lower aeration rate (0.13 vvm), cell settling was observed, which ultimately led to poor growth performance.

In the tests for the effect of initial biomass concentration, it was found that the specific growth rate decreases with initial biomass concentration but the overall biomass and product

productivity increases with it. The lower specific growth rate may be attributed to the lower photon dose per cell mass at higher initial biomass concentration. On the other hand, the slow growth of cells during the early days of cultivation resulted to the lower overall biomass productivity of cultures grown at the lower initial biomass concentrations (0.05 g L^{-1} and 0.10 g L^{-1}). This slow growth may have resulted from photoinhibition, although not severe, during the first day of cultivation where the photon dose per cell mass is high.

Thus, in the operation of an airlift photobioreactor, the right combination of light intensity, air flow rate, and initial biomass concentration must be selected to produce the highest biomass throughput. At the beginning of the culture, a higher initial biomass concentration may be needed to prevent bleaching of the photosynthetic apparatus of the cells. The light intensity may need increasing as the cells grow to prevent photolimitation due to mutual shading. Also, aeration rate may also need increasing as the population density increases with time to maintain better circulation of the cells and prevent biomass settling. A smart control of these factors with respect to the instantaneous population density must be developed to attain better growth performance.

A preliminary techno-economic analysis was also performed on a scaled-up *Spirulina* powder production plant with a total photobioreactor capacity of 80 m^3 to determine its possible commercial scale production. This evaluation revealed that this venture is attractive. The profit margin is positive and the payback period is only 6.34 years. Also, the sensitivity analysis showed that profitability increases with total PBR capacity and biomass yield.

A few ways of reducing the cost of production were also conceived. Water cost can be cut down by recycling the medium back to the photobioreactor; but organic matter that remained in the medium should be removed first. This will add to the cost of equipment. Power cost can

also be reduced by utilizing solar energy to power the plant. But the additional capital investment requirement of the solar plant should be considered. Scaling up may also be beneficial due to economies of scale. But the PBR should be designed in such a way that light can still be efficiently utilized by a larger reactor.

REFERENCES

[1] A. Vonshak, *Spirulina platensis (Arthispira): Physiology, cell biology and biotechnology*. London: Taylor & Francis, 1997.

[2] A. Vonshak, A. Abeliovich, S. Boussiba, S. Arad, and A. Richmond, "Production of *Spirulina* biomass: Effects of environmental factors and population density," *Biomass*, vol. 2, no. 3, pp. 175–185, 1982.

[3] C. U. Ugwu, H. Aoyagi, and H. Uchiyama, "Photobioreactors for mass cultivation of algae," *Bioresour. Technol.*, vol. 99, no. 10, pp. 4021–4028, 2008.

[4] R. N. Singh and S. Sharma, "Development of suitable photobioreactor for algae production - A review," *Renew. Sustain. Energy Rev.*, vol. 16, no. 4, pp. 2347–2353, 2012.

[5] I. S. Suh and C.-G. Lee, "Photobioreactor engineering: Design and performance," *Biotechnol. Bioprocess Eng.*, vol. 8, no. 6, pp. 313–321, 2003.

[6] M. Cuaresma, M. Janssen, C. Vílchez, and R. H. Wijffels, "Horizontal or vertical photobioreactors? How to improve microalgae photosynthetic efficiency," *Bioresour. Technol.*, vol. 102, no. 8, pp. 5129–5137, 2011.

[7] B. Wang, C. Q. Lan, and M. Horsman, "Closed photobioreactors for production of microalgal biomasses," *Biotechnol. Adv.*, vol. 30, no. 4, pp. 904–912, 2012.

[8] A. Contreras, F. García, E. Molina, and J. C. Merchuk, "Interaction between CO2-mass transfer, light availability, and hydrodynamic stress in the growth of *Phaeodactylum tricornutum* in a concentric tube airlift photobioreactor," *Biotechnol. Bioeng.*, vol. 60, no. 3, pp. 317–325, 1998.

[9] N. T. Eriksen, “The technology of microalgal culturing,” *Biotechnol. Lett.*, vol. 30, no. 9, pp. 1525–1536, 2008.

[10] M. J. Barbosa, M. Janssen, N. Ham, J. Tramper, and R. H. Wijffels, “Microalgae cultivation in air-lift reactors: Modeling biomass yield and growth rate as a function of mixing frequency,” *Biotechnol. Bioeng.*, vol. 82, no. 2, pp. 170–179, 2003.

[11] S. J. Hwang and Y.-L. Cheng, “Gas holdup and liquid velocity in in three-phase internal-loop airlift reactors,” *Chem. Eng. Sci.*, vol. 52, no. 21–22, pp. 3949–3960, 1997.

[12] H. Wagner, Z. Liu, U. Langner, K. Stehfest, and C. Wilhelm, “The use of FTIR spectroscopy to assess quantitative changes in the biochemical composition of microalgae,” *J. Biophotonics*, vol. 3, no. 8–9, pp. 557–566, 2010.

[13] H. Quiang and A. Richmond, *Handbook of Microalgal Culture : Applied Phycology and Biotechnology*, 2nd Ed., no. November. Somerset, NJ: John Wiley & Sons, 2013.

[14] J. N. Murdock and D. L. Wetzel, “FT-IR microspectroscopy enhances biological and ecological analysis of algae,” *Appl. Spectrosc. Rev.*, vol. 44, no. 4, pp. 335–361, 2009.

[15] K. Stehfest, J. Toepel, and C. Wilhelm, “The application of micro-FTIR spectroscopy to analyze nutrient stress-related changes in biomass composition of phytoplankton algae,” *Plant Physiol. Biochem.*, vol. 43, no. 7, pp. 717–726, 2005.

[16] D. Y. Duygu *et al.*, “Fourier transform infrared (FTIR) spectroscopy for identification of *Chlorella vulgaris* Beijerinck 1890 and *Scenedesmus obliquus* (Turpin) Kützing 1833,” *African J. Biotechnol.*, vol. 11, no. 16, pp. 3817–3824, 2012.

[17] J. Rüger, N. Unger, I. W. Schie, E. Brunner, J. Popp, and C. Krafft, “Assessment of growth phases of the diatom *Ditylum brightwellii* by FT-IR and Raman spectroscopy,” *Algal Res.*, vol. 19, pp. 246–252, 2016.

[18] K. Stehfest, M. Boese, G. Kerns, A. Piry, and C. Wilhelm, “Fourier transform infrared spectroscopy as a new tool to determine rosmarinic acid in situ.,” *J. Plant Physiol.*, vol. 161, no. 2, pp. 151–156, 2004.

[19] K. Sudhakar and M. Premalatha, “Characterization of micro algal biomass through FTIR/TGA/CHN analysis: Application to *Scenedesmus* sp.,” *Energy Sources, Part A Recover. Util. Environ. Eff.*, vol. 37, no. 21, pp. 2330–2337, 2015.

[20] A. Bartošová, L. Blinová, and K. Gerulová, “Characterisation of polysacharides and lipids from selected green algae species by FTIR-ATR spectroscopy,” *Res. Pap. Fac. Mater. Sci. Technol. Slovak Univ. Technol.*, vol. 23, no. 36, pp. 97–102, 2015.

[21] P. Heraud, B. R. Wood, M. J. Tobin, J. Beardall, and D. McNaughton, “Mapping of nutrient-induced biochemical changes in living algal cells using synchrotron infrared microspectroscopy,” *FEMS Microbiol. Lett.*, vol. 249, no. 2, pp. 219–225, 2005.

[22] A. Höskuldsson, “PLS regression methods,” *J. Chemom.*, vol. 2, no. 3, pp. 211–228, 1988.

[23] Y. Meng, C. Yao, S. Xue, and H. Yang, “Application of Fourier transform infrared (FT-IR) spectroscopy in determination of microalgal compositions,” *Bioresour. Technol.*, vol. 151, pp. 347–354, 2014.

[24] J. J. Mayers, K. J. Flynn, and R. J. Shields, “Rapid determination of bulk microalgal biochemical composition by Fourier-transform infrared spectroscopy,” *Bioresour. Technol.*, vol. 148, pp. 215–220, 2013.

[25] L. M. L. Laurens and E. J. Wolfrum, “High-throughput quantitative biochemical characterization of algal biomass by NIR spectroscopy; Multiple linear regression and multivariate linear regression analysis,” *J. Agric. Food Chem.*, vol. 61, no. 50, pp. 12307–12314, 2013.

[26] V. Challagulla, K. B. Walsh, and P. Subedi, “Biomass and total lipid content assessment of microalgal cultures using near and short wave infrared spectroscopy,” *Bioenergy Res.*, vol. 7, no. 1, pp. 306–318, 2014.

[27] V. Challagulla, K. B. Walsh, and P. Subedi, “Microalgal fatty acid composition: Rapid assessment using near-infrared spectroscopy,” *J. Appl. Phycol.*, vol. 28, no. 1, pp. 85–94, 2016.

[28] A. Robic, D. Bertrand, J. F. Sassi, Y. Lerat, and M. Lahaye, “Determination of the chemical composition of ulvan, a cell wall polysaccharide from *Ulva* spp. (*Ulvales, Chlorophyta*) by FT-IR and chemometrics,” *J. Appl. Phycol.*, vol. 21, no. 4, pp. 451–456, 2009.

[29] W. Mulbry, J. Reeves, Y. Liu, Z. Ruan, and W. Liao, “Near- and mid-infrared spectroscopic determination of algal composition,” *J. Appl. Phycol.*, vol. 24, no. 5, pp. 1261–1267, 2012.

[30] S. A. Patel, F. Currie, N. Thakker, and R. Goodacre, “Spatial metabolic fingerprinting using FT-IR spectroscopy: Investigating abiotic stresses on *Micrasterias hardyi*,” *Analyst*, vol. 133, no. 12, pp. 1629–1800, 2008.

[31] C. Jebsen, A. Norici, H. Wagner, M. Palmucci, M. Giordano, and C. Wilhelm, “FTIR spectra of algal species can be used as physiological fingerprints to assess their actual growth potential,” *Physiol. Plant.*, vol. 146, no. 4, pp. 427–438, 2012.

[32] L. M. L. Laurens and E. J. Wolfrum, “Feasibility of spectroscopic characterization of algal lipids: Chemometric correlation of NIR and FTIR Spectra with exogenous lipids in algal biomass,” *Bioenergy Res.*, vol. 4, no. 1, pp. 22–35, 2011.

[33] J. M. Girard, J. S. Deschênes, R. Tremblay, and J. Gagnon, “FT-IR/ATR univariate and multivariate calibration models for in situ monitoring of sugars in complex microalgal culture media,” *Bioresour. Technol.*, vol. 144, pp. 664–668, 2013.

[34] C. Zarrouk, *Contribution a l’etude d’une cyanobacterie: influence de divers facteurs physiques et chimiques sur la croissance et la photosynthese de Spirulina maxima (Setchell et Gardner) Geitler*. University of Paris, France, 1966.

[35] T. Rausch, “The estimation of micro-algal protein-content and its meaning to the evaluation of algal biomass.1. Comparison of methods for extracting protein,” *Hydrobiologia*, vol. 78, no. 3, pp. 237–251, 1981.

[36] M. M. Bradford, “A rapid and sensitive method for the quantitation of microgram quantities of protein utilizing the principle of protein-dye binding,” *Anal. Biochem.*, vol. 72, no. 1–2, pp. 248–254, 1976.

[37] C. Bigogno, I. Khozin-Goldberg, S. Boussiba, A. Vonshak, and Z. Cohen, “Lipid and fatty acid composition of the green oleaginous alga *Parietochloris incisa*, the richest plant source of arachidonic acid,” *Phytochemistry*, vol. 60, no. 5, pp. 497–503, 2002.

[38] M. Romeo, B. Mohlenhoff, and M. Diem, “Infrared micro-spectroscopy of human cells: Causes for the spectral variance of oral mucosa (buccal) cells,” *Vib. Spectrosc.*, vol. 42, no. 1, pp. 9–14, 2006.

[39] S. Wold, M. Sjostrom, and L. Eriksson, “PLS-regression: A basic tool of chemometrics,” *Chemom. Intell. Lab. Syst.*, vol. 58, pp. 109–130, 2001.

[40] B. M. Nicolaï *et al.*, “Nondestructive measurement of fruit and vegetable quality by means of NIR spectroscopy: A review,” *Postharvest Biol. Technol.*, vol. 46, no. 2, pp. 99–118, 2007.

[41] B. C. Smith, *Fundamentals of Fourier Transform Infrared Spectroscopy*, 2nd Ed. Roca Baton, FL: CRC Press Taylor and Francis Group, 2011.

[42] L. N. Tsoglin, B. V Gabel, T. N. Fal'kovich, and V. E. Semenenko, *Closed photobioreactors for microalgal cultivation*, vol. 43. 1996.

[43] Y. Chisti, "Microalgae as sustainable cell factories," *Environ. Eng. Manag. J.*, vol. 5, no. 3, pp. 261–274, 2006.

[44] A. S. Mirón, A. C. Gómez, F. G. Camacho, E. M. Grima, and Y. Chisti, "Comparative evaluation of compact photobioreactors for large-scale monoculture of microalgae," *Prog. Ind. Microbiol.*, vol. 35, no. C, pp. 249–270, 1999.

[45] C. Posten, "Design principles of photo-bioreactors for cultivation of microalgae," *Eng. Life Sci.*, vol. 9, no. 3, pp. 165–177, 2009.

[46] Q. Hu, N. Kurano, M. Kawachi, I. Iwasaki, and S. Miyachi, "Ultrahigh-cell-density culture of a marine green alga *Chlorococcum littorale* in a flat-plate photobioreactor," *Appl. Microbiol. Biotechnol.*, vol. 49, no. 6, pp. 655–662, 1998.

[47] A. S. Mirón, M.-C. C. Garcia, F. G. Camacho, E. M. Grima, and Y. Chisti, "Growth and characterization of microalgal biomass produced in bubble column and airlift photobioreactors: Studies in fed-batch culture," *Enzyme Microb. Technol.*, vol. 31, pp. 1015–1023, 2002.

[48] G. Chini Zittelli, L. Rodolfi, N. Biondi, and M. R. Tredici, "Productivity and photosynthetic efficiency of outdoor cultures of *Tetraselmis suecica* in annular columns," *Aquaculture*, vol. 261, no. 3, pp. 932–943, 2006.

[49] S. Oncel and F. V. Sukan, “Comparison of two different pneumatically mixed column photobioreactors for the cultivation of *Artrospira platensis* (*Spirulina platensis*),” *Bioresour. Technol.*, vol. 99, no. 11, pp. 4755–4760, 2008.

[50] B. D. Fernandes, A. Mota, A. Ferreira, G. Dragone, J. A. Teixeira, and A. A. Vicente, “Characterization of split cylinder airlift photobioreactors for efficient microalgae cultivation,” *Chem. Eng. Sci.*, vol. 117, pp. 445–454, 2014.

[51] R. W. Babcock, J. Malda, and J. A. C. Radway, “Hydrodynamics and mass transfer in a tubular airlift photobioreactor,” *J. Appl. Phycol.*, vol. 14, no. 3, pp. 169–184, 2002.

[52] M. Javanmardian and B. O. Palsson, “High-density photoautotrophic algal cultures: Design, construction, and operation of a novel photobioreactor system,” *Biotechnol. Bioeng.*, vol. 38, no. 10, pp. 1182–1189, 1991.

[53] M. Marker, A. J. Tsavalos, and A. J. Young, “Autotrophic growth and carotenoid production of *Haematococcus pluvialis* in a 30 liter air-lift photobioreactor,” *J. Ferment. Bioeng.*, vol. 82, no. 2, pp. 113–118, 1996.

[54] J. Vega-Estrada, M. C. Montes-Horcasitas, A. R. Dom??nguez-Bocanegra, and R. O. Ca??izares-Villanueva, “*Haematococcus pluvialis* cultivation in split-cylinder internal-loop airlift photobioreactor under aeration conditions avoiding cell damage,” *Appl. Microbiol. Biotechnol.*, vol. 68, no. 1, pp. 31–35, 2005.

[55] F. García Camacho, A. Contreras Gómez, F. G. Acién Fernández, J. Fernández Sevilla, and E. Molina Grima, “Use of concentric-tube airlift photobioreactors for microalgal outdoor mass cultures,” *Enzyme Microb. Technol.*, vol. 24, no. 3–4, pp. 164–172, 1999.

[56] K. Kaewpintong, A. Shotipruk, S. Powtongsook, and P. Pavasant, “Photoautotrophic high-density cultivation of vegetative cells of *Haematococcus pluvialis* in airlift bioreactor,” *Bioresour. Technol.*, vol. 98, no. 2, pp. 288–295, 2007.

[57] S. Krichnavaruk, S. Powtongsook, and P. Pavasant, “Enhanced productivity of *Chaetoceros calcitrans* in airlift photobioreactors,” *Bioresour. Technol.*, vol. 98, no. 11, pp. 2123–2130, 2007.

[58] J. Degen, A. Uebele, A. Retze, U. Schmid-staiger, and W. Tro, “A novel airlift photobioreactor with baffles for improved light utilization through the ashing light effect,” *J. Biotechnol.*, vol. 92, pp. 89–94, 2001.

[59] K. Issarapayup, S. Powtongsook, and P. Pavasant, “Flat panel airlift photobioreactors for cultivation of vegetative cells of microalga *Haematococcus pluvialis*,” *J. Biotechnol.*, vol. 142, no. 3–4, pp. 227–232, 2009.

[60] I. A. J. Ratchford and H. J. Fallowfield, “Performance of a flat plate, air-lift reactor for the growth of high biomass algal cultures,” *J. Appl. Phycol.*, vol. 4, no. 1, pp. 1–9, 1992.

[61] F. G. Acién Fernández, J. M. Fernández Sevilla, J. A. Sánchez Pérez, E. Molina Grima, and Y. Chisti, “Airlift-driven external-loop tubular photobioreactors for outdoor production of microalgae: Assessment of design and performance,” *Chem. Eng. Sci.*, vol. 56, no. 8, pp. 2721–2732, 2001.

[62] M. Sobczuk, G. Camacho, and R. Camacho, “Carbon dioxide uptake efficiency by outdoor microalgal cultures in tubular airlift photobioreactors,” *Biotechnol. Bioeng.*, vol. 67, no. 4, pp. 465–475, 2000.

[63] E. T. -. LEE and M. J. BAZIN, “A laboratory scale air-lift helical photobioreactor to increase biomass output rate of photosynthetic algal cultures,” *New Phytol.*, vol. 116, no. 2, pp. 331–335, 1990.

[64] J. C. Ogbonna, H. Yada, H. Masui, and H. Tanaka, “A novel internally illuminated stirred tank photobioreactor for large- scale cultivation of photosynthetic cells,” *J. Ferment. Bioeng.*, vol. 82, no. 1, pp. 61–67, 1996.

[65] Y. E. Choi, Y. S. Yun, J. M. Park, and J. W. Yang, “Multistage operation of airlift photobioreactor for increased production of astaxanthin from *Haematococcus pluvialis*,” *J. Microbiol. Biotechnol.*, vol. 21, no. 10, pp. 1081–1087, 2011.

[66] X. Yuan, A. Kumar, A. K. Sahu, and S. J. Ergas, “Impact of ammonia concentration on *Spirulina platensis* growth in an airlift photobioreactor,” *Bioresour. Technol.*, vol. 102, no. 3, pp. 3234–3239, 2011.

[67] Z. Y. Li, S. Y. Guo, L. Li, and M. Y. Cai, “Effects of electromagnetic field on the batch cultivation and nutritional composition of *Spirulina platensis* in an air-lift photobioreactor,” *Bioresour. Technol.*, vol. 98, no. 3, pp. 700–705, 2007.

[68] M. Y. Chisti, *Airlift Bioreactors*. Essex, England: Elsevier Science Publishers, Ltd., 1989.

[69] M. R. Tredici, P. Carlozzi, G. Chini Zittelli, and R. Materassi, “A vertical alveolar panel (VAP) for outdoor mass cultivation of microalgae and cyanobacteria,” *Bioresour. Technol.*, vol. 38, no. 2–3, pp. 153–159, 1991.

[70] G. Torzillo, L. Giovannetti, F. Bocci, and R. Materassi, “Effect of oxygen concentration on the protein content of *Spirulina* biomass,” *Biotechnol. Bioeng.*, vol. 26, no. 9, pp. 1134–1135, 1984.

[71] F. J. Marquez, K. Sasaki, N. Nishio, and S. Nagai, “Inhibitory effect of oxygen accumulation on the growth of *Spirulina platensis*,” *Biotechnol. Lett.*, vol. 17, no. 2, pp. 225–228, 1995.

[72] M. Olaizola and E. O. Duerr, “Effects of light intensity and quality on the growth rate and photosynthetic pigment content of *Spirulina platensis*,” *J. Appl. Phycol.*, vol. 2, no. 2, pp. 97–104, 1990.

[73] F. Chen, Y. Zhang, and S. Guo, “Growth and phycocyanin formation of *Spirulina platensis* in photoheterotrophic culture,” *Biotechnol. Lett.*, vol. 18, no. 5, pp. 603–608, 1996.

[74] K. Chojnacka and A. Noworyta, “Evaluation of *Spirulina* sp. growth in photoautotrophic, heterotrophic and mixotrophic cultures,” *Enzyme Microb. Technol.*, vol. 34, no. 5, pp. 461–465, 2004.

[75] H. Qiang, A. Richmond, and Y. Zarmi, “Combined effects of light intensity, light-path and culture density on output rate of *Spirulina platensis* (cyanobacteria),” *Eur. J. Phycol.*, vol. 33, no. 2, pp. 165–171, 1998.

[76] A. Converti, A. Lodi, A. Del Borghi, and C. Solisio, “Cultivation of *Spirulina platensis* in a combined airlift-tubular reactor system,” *Biochem. Eng. J.*, vol. 32, no. 1, pp. 13–18, 2006.

[77] H. Qiang, H. Guterman, and a Richmond, “Physiological characteristics of *Spirulina platensis* (Cyanobacteria) cultured at ultrahigh cell densities,” *J. Phycol.*, vol. 32, no. 6, pp. 1066–1073, 1996.

[78] A. Vonshak, S. M. Cheung, and F. Chen, “Mixotrophic growth modifies the response of *Spirulina* (*Arthrospira*) *platensis* (Cyanobacteria) cells to light,” *J. Phycol.*, vol. 36, no. 4, pp. 675–679, 2000.

[79] F. F. Madkour, A. E. W. Kamil, and H. S. Nasr, “Production and nutritive value of *Spirulina platensis* in reduced cost media,” *Egypt. J. Aquat. Res.*, vol. 38, no. 1, pp. 51–57, 2012.

[80] T. Göksan, A. Zekeriyaoğlu, and I. Ak, “The growth of *Spirulina platensis* in different culture systems under greenhouse condition,” *Turkish J. Biol.*, vol. 31, no. 1, pp. 47–52, 2007.

[81] H. Qiang and A. Richmond, “Productivity and photosynthetic efficiency of *Spirulina platensis* as affected by light intensity, algal density and rate of mixing in a flat plate photobioreactor,” *J. Appl. Phycol.*, vol. 8, no. 1986, pp. 139–145, 1996.

[82] S. R. Ronda, C. S. Bokka, C. Ketineni, B. Rijal, and P. R. Allu, “Aeration effect on *Spirulina platensis* growth and γ-linolenic acid production,” *Brazilian J. Microbiol.*, vol. 43, no. 1, pp. 12–20, 2012.

[83] F. J. L. Gordillo, C. Jiménez, F. L. Figueroa, and F. X. Niell, “Effects of increased atmospheric CO_2 and N supply on photosynthesis, growth and cell composition of the cyanobacterium *Spirulina platensis* (*Arthrospira*),” *J. Appl. Phycol.*, vol. 10, no. 5, pp. 461–469, 1998.

[84] D. Soletto *et al.*, “Effects of carbon dioxide feeding rate and light intensity on the fed-batch pulse-feeding cultivation of *Spirulina platensis* in helical photobioreactor,” *Biochem. Eng. J.*, vol. 39, no. 2, pp. 369–375, 2008.

[85] M. A. C. L. de* Oliveira, M. P. C. Monteiro, P. G. Robbs, and S. G. F. Leite, “Growth and chemical composition of *Spirulina maxima* and *Spirulina platensis* biomass at different temperatures,” *Aquac. Int.*, vol. 7, no. 5221, pp. 261–275, 1999.

[86] C. O. Reinehr and J. A. V Costa, “Repeated batch cultivation of the microalga *Spirulina platensis*,” *World J. Microbiol. Biotechnol.*, vol. 22, no. 9, pp. 937–943, 2006.

[87] M. S. Peters, K. D. Timmerhaus, and R. E. West, *Plant Design and Economics for Chemical Engineers*, 5th ed. New York: McGraw-Hill, 2003.

[88] A. Piccolo, “*Spirulina* a livelihood and a business venture,” 2012. [Online]. Available: http://www.fao.org/3/a-az386e.pdf.

APPENDIX A

FIGURES

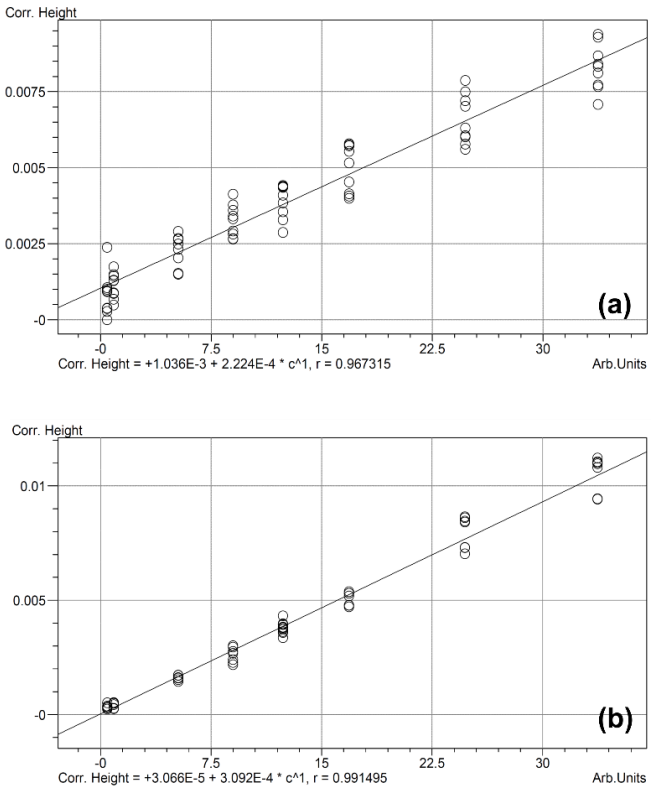

Appendix A-1. Results of multipoint regression on infrared spectra of aqueous samples of (a) protein and (b) carbohydrate standards (0.45 – 33.73 mg ml^{-1}).

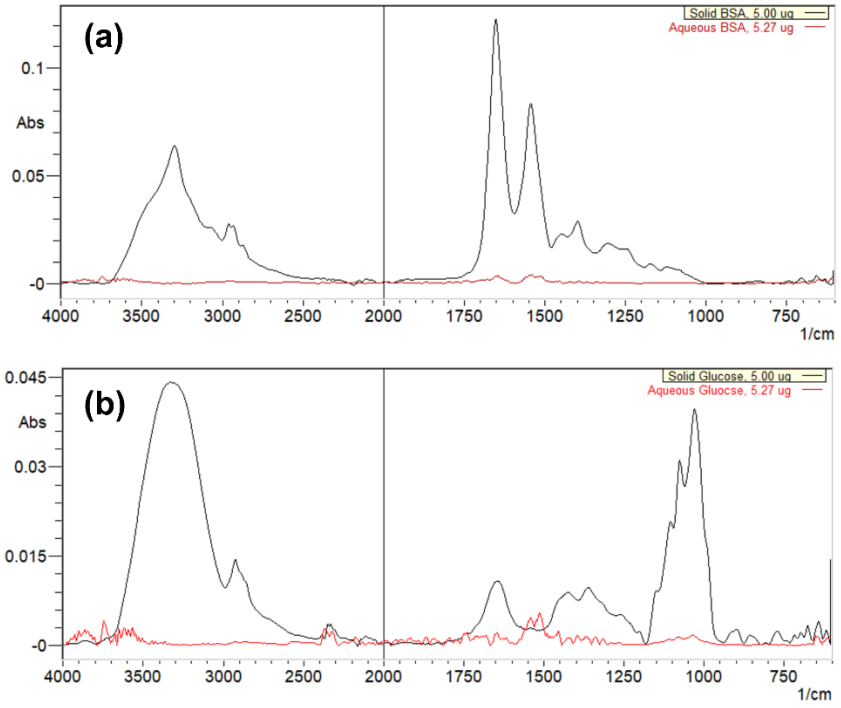

Appendix A- 2. Overlaid infrared spectra of dry (black) and aqueous (red) samples of (a) protein and (b) carbohydrate standards scanned using Happ-Genzel apodization, 45 scans, and 4 cm^{-1} resolution.

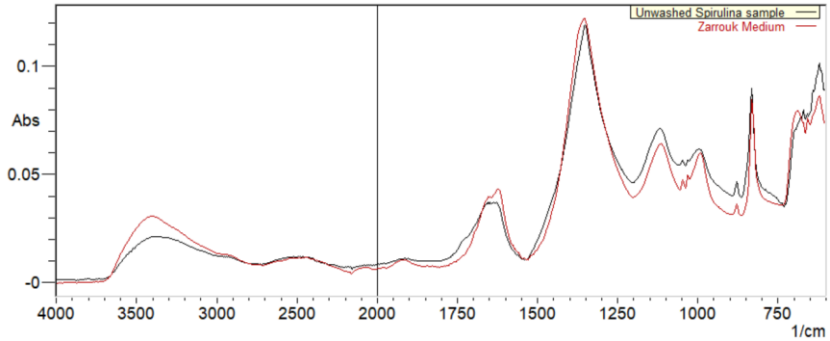

Appendix A-3. Overlaid infrared spectra of unwashed *Spirulina* sample (black) and of Zarrouk medium (red) scanned using Happ-Genzel apodization, 45 scans, and 4 cm^{-1} resolution.

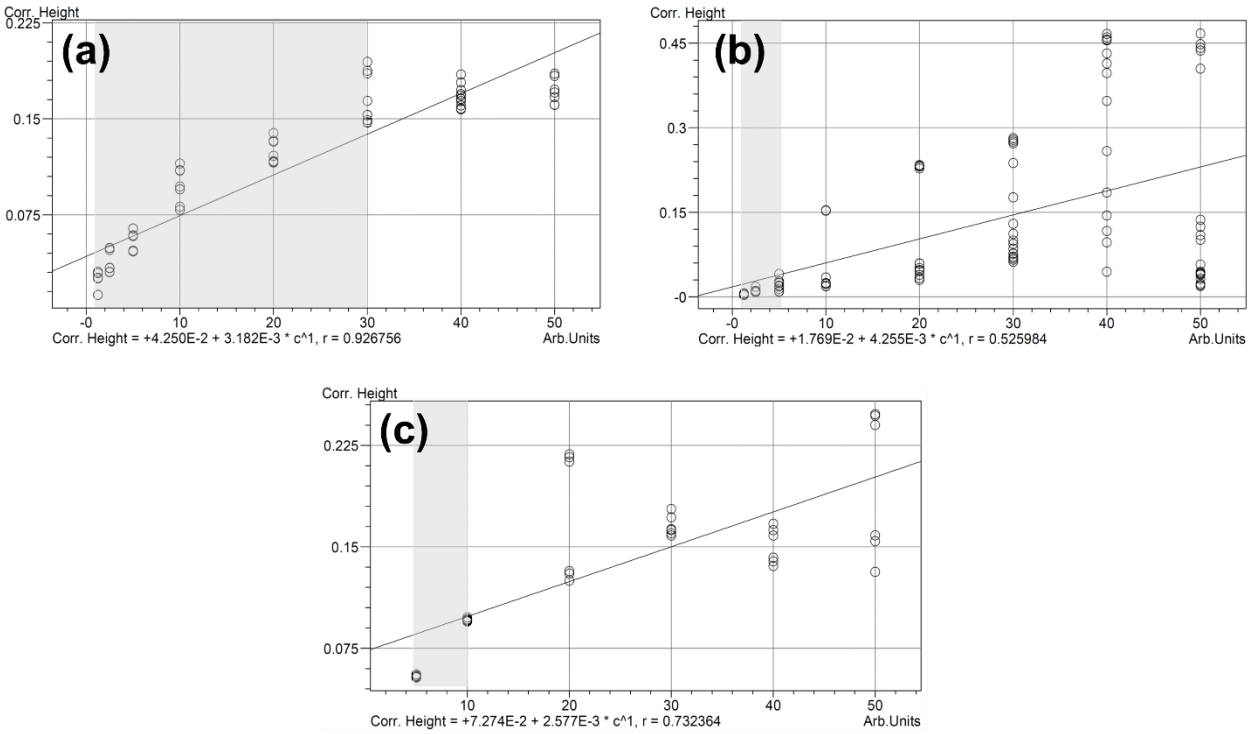

Appendix A-4. Results of multipoint regression on infrared spectra of dry samples of (a) protein, (b) carbohydrate, and (c) lipid standards (0.25 – 10 mg ml^{-1} equivalent to 1.25 – 50 µg for 5 µL sample size). Shaded portion shows limit of quantification.

APPENDIX B

TABLES

Appendix B-1. Algal composition of *Spirulina* predicted by PLS-regression model that was built over 0.25 -1.00 mg ml^{-1} concentration (equivalent to 1.25 – 5.00 µg for 5 µL sample size) of protein, carbohydrate and lipid standards.

Sample No.	**PLS Predicted Values, % w/w**		
	Protein	**Carbohydrate**	**Lipid**
1	-18.45	5.62	-4.90
2	-19.00	5.51	-5.20
3	-18.91	5.28	-6.25
4	-32.64	11.31	-5.52
5	-17.66	7.32	-6.44
6	-17.76	7.11	-6.07
7	-19.55	7.14	-5.10
8	-17.44	7.19	-4.48
9	-18.94	7.60	-3.67
10	-19.35	2.20	-5.74
11	-17.62	2.19	-6.05
12	-11.39	1.96	-5.03
Mean	-19.06	5.87	-5.37
Standard Deviation	4.79	2.74	0.81

APPENDIX C

CALCULATIONS

Appendix C.1. Sizing the 3-L short tank concentric-tube internally-illuminated airlift photobioreactor

Assumptions:

Height – to – diameter ratio (H/D) = 2.0
Riser area – to – downcomer area ratio (A_r/A_d) = 0.5
Effective capacity is 85% of total tank volume (H_L/H = 0.85)
Effective capacity (V_L) = 3.0 L

1. Main Chamber Sizing:

$$V_L = Main\ Chamber\ Volume - Light\ Chamber\ Volume$$
$$V_L = \left[\frac{\pi}{4}D^2H_L + \frac{\pi}{6}D^3\right] - \left[\frac{\pi}{4}d^2h + \frac{\pi}{6}d^3\right]$$

where: $d = \frac{1}{3}D$

$h = 0.7H$ (to provide clearance from tank bottom and space for the sparger)

$$3000\ cm^3 = \left[\frac{\pi}{4}D^2(2D)(0.85) + \frac{\pi}{6}D^3\right] - \left[\frac{\pi}{4}\left(\frac{1}{3}D\right)^2(0.7)(2D)(0.85) + \frac{\pi}{6}\left(\frac{1}{3}D\right)^3\right]$$

Solving for D:

$D = 12\ cm = 4.72\ in.$
$H = 24\ cm = 9.45\ in.$

Note: *The main chamber diameter and height were modified based on the diameter of the old fermenter available in our laboratory (Biomass Energy Testing and Analysis Lab (BETALab), BAEN Dep't., TAMU)*

Dimensions of the Old Fermenter in BETALab, BAEN Dep't., TAMU:

$D_o = 6.02\ in.$
$D_i = 5.75\ in.$
$H = 11.54\ in.$
$t = 0.14\ in.$

2. Light Chamber Sizing

$d_o = \frac{1}{3} D_o = \frac{1}{3}(6.02\ in.) = 2.01\ in.$
$h = 0.7H = 0.7(11.54\ in.) = 8.08\ in.$
$t = 2\ mm = 0.08\ in.$

Note: Thickness of the light chamber is the thinkness of the glass cylinder used to make the glass chamber

3. Draft Tube Sizing

${A_r}/{A_d} = 0.5$
$A_r = \frac{1}{4}\left[{D_{d_i}}^2 - {d_o}^2\right]$
$A_d = \frac{1}{4}\left[{D_i}^2 - {D_{d_o}}^2\right]$
$D_{d_o} = D_{d_i} + 2t$
$t = 0.14\ in.$ (thickness of commercially available clear acrylic tube)

$${A_r}/{A_d} = \frac{{D_{d_i}}^2 - {d_o}^2}{{D_i}^2 - {D_{d_o}}^2} = \frac{\left(D_{d_o} + 2t\right)^2 - {d_o}^2}{{D_i}^2 - {D_{d_o}}^2}$$

Substitute ${A_r}/{A_d} = 0.5$, $d_o = 2.01\ in.$, $D_i = 5.75\ in.$, and $t = 0.14\ in.$,
Then, solve for D_{d_o}:

$D_{d_o} = 3.8875\ in.$

Note: Choose $D_{d_o} = 3.75\ in.$, which is commercially available

$D_{d_i} = D_{d_o} - 2t$
$D_{d_i} = 3.75\ in. - 2(0.14\ in.)$
$D_{d_i} = 3.47\ in.$

$h_d = 0.825H$
$h_d = 9.52\ in.$

4. Calculating the actual ${A_r}/{A_d}$

$$A_r = \frac{1}{4}\left[{D_{d_i}}^2 - {d_o}^2\right]$$
$$A_r = \frac{1}{4}[(3.47\ in.)^2 - (2.01\ in.)^2]$$
$$A_r = 6.28\ in.^2$$

$$A_d = \frac{1}{4}\left[{D_i}^2 - {D_{d_o}}^2\right]$$
$$A_d = \frac{1}{4}[(5.75\ in.)^2 - (3.75\ in.)^2]$$

$$A_d = 14.92\ in.^2$$

$${A_r}/{A_d} = {6.28\ in.^2}/{14.92\ in.^2}$$
$${A_r}/{A_d} = 0.42$$

Appendix C.2. Preliminary techno-economic evaluation calculations

1. Sizing of 15-m^3 short tank concentric-tube internally-illuminated airlift photobioreactor

Assumptions:

Height – to – diameter ratio (${}^{H}/_{D}$) = 2.0
Riser area – to – downcomer area ratio (A_r/A_d) = 0.5
Effective capacity is 85% of total tank volume (${}^{H_L}/_{H}$= 0.85)
Effective capacity (V_L) = 15 m^3
${}^{h}/_{H}$= 0.7

1.1. Main chamber sizing

$$V_L = Main\ Chamber\ Volume - Light\ Chamber\ Volume$$
$$V_L = \frac{\pi}{4} D^2 H_L - (n_d + n_r)\frac{\pi}{4} d^2 h$$

Substitute $H = 2D$, $H_L = 0.85H$, $h = 0.7H$,

Substitute $n_d = 288$ and $n_r = 288$, which were to be interpolated to obtain $S/V > 40$,

Then solve for D (Excel™ was used in solving for D since the equation is cubic):

$$D = 2.337\ m$$

Since $H = 2D$:

$$H = 4.674\ m$$

Since effective capacity is 85% of total tank volume (${}^{H_L}/_{H}$= 0.85):

$$H_L = 0.85H = 3.973\ m$$

Thickness was calculated using the following formula:

$$t = \frac{2.6D(H_L - 1)G}{S} + CA$$
$$t = \frac{2.6\left(2.337\ m\ \times \frac{3.28\ ft}{1\ m}\right)\left(\left(3.973\ m\ \times \frac{3.28\ ft}{1\ m}\right) - 1\ ft\right)(1.00)}{10{,}500\ psi} + 0.125\ in.$$

$t = 0.148\ in.$

But, according to API-650 Standard, the minimum thickness of tanks with <50 ft diameter should be 0.1875 in.

Therefore, choose $t = 0.1875\ in.$

1.2. Draft Tube Sizing

$A_r/A_d = 0.5$

$A_r = \frac{1}{4}\left[{D_{d_i}}^2 - n_r {d_o}^2\right]$

$A_d = \frac{1}{4}\left[{D_i}^2 - {D_{d_o}}^2 - n_d {d_o}^2\right]$

$D_{d_o} = D_{d_i} + 2t$

$t = 0.1875\ in.$ (thickness of commercially available clear acrylic tube)

$$A_r/A_d = \frac{{D_{d_i}}^2 - n_r {d_o}^2}{{D_i}^2 - {D_{d_o}}^2 - n_d {d_o}^2} = \frac{\left(D_{d_o} + 2t\right)^2 - n_r {d_o}^2}{{D_i}^2 - {D_{d_o}}^2 - n_d {d_o}^2}$$

Substitute $A_r/A_d = 0.5$, $d_o = 3\ in.$, $D_i = 2.327\ m$, $t = 0.1875\ in.$, and $n_d = n_r = 288$ (n_d and n_r were to be interpolated to obtain $S/V > 40$

Then, solve for D_{d_o}:

$D_{d_o} = 1.544\ m$

$D_{d_i} = D_{d_o} - 2t$

$D_{d_i} = 1.544\ m - 2\left(0.1875\ in. \times \frac{0.0254\ m}{1\ in.}\right)$

$D_{d_i} = 1.534\ m$

$h_d = 0.9H$

$h_d = 4.21\ m$

1.3. Light Chamber Sizing

$n_d = n_r = 288$ (n_d and n_r were to be interpolated to obtain $S/V > 40$

$d_o = 3\ in.$ (diameter of internal light chamber of bench-scale reactor was maintained)

$h = 0.85H$
$h = 3.973\ m$

1.4. Determine S/V

$$\frac{S}{V} = \frac{S_{main\ chamber} + S_{light\ chamber} + S_{draft\ tube}}{Working\ Volume}$$

$S_{main\ chamber} = \pi D_i H$
$S_{main\ chamber} = \pi(2.327\ m)(4.674\ m)$
$S_{main\ chamber} = 34.17\ m^2$

$S_{light\ chamber} = \pi(n_r + n_d)d_i h$
$S_{light\ chamber} = \pi(288 + 288)\left(3\ in.\ \times \frac{0.0254\ m}{1\ in.}\right)(3.973\ m)$
$S_{light\ chamber} = 547.78\ m^2$

$S_{draft\ tube} = \pi\left(D_{d_o} + D_{d_i}\right)h_d$
$S_{draft\ tube} = \pi(1.544\ m + 1.534\ m)(4.21\ m)$
$S_{draft\ tube} = 40.67\ m^2$

$$\frac{S}{V} = \frac{34.17\ m^2 + 547.78\ m^2 + 40.67\ m^2}{20\ m^3}$$
$$\frac{S}{V} = 40.96\ \frac{m^2}{m^3}$$

Note: The calculation procedure for the inoculation PBRs follow the methods in 1.1 through 1.4. The only difference is the effective capacity, which are 20 L, 200 L, and 2 m^3.

2. Sizing of mixing tank for the growth medium

$\mu = 0.526\ d^{-1}$
$F = \mu V_L$
$F = (0.526\ d^{-1})(20\ m^3)$
$F = 42.19\ m^3\ d^{-1}$

$\tau = 1\ hr$

$V = \tau F$
$V = (1\ hr)\left(\frac{1\ day}{24\ hr}\right)(42.19\ m^3\ d^{-1})$
$V = 1.758\ m^3$
$V = \frac{\pi}{4} D^2 H_L$
$D = H_L$
$V = \frac{\pi}{4} D^3$
$D = \sqrt[3]{\frac{4V}{\pi}} = \sqrt[3]{\frac{4(1.758\ m^3)}{\pi}}$
$D = 1.31\ m$

From D, the following dimensions of a mixing tank with 6-flat blade turbine impeller were calculated:

Dimension	Formula	Value
Tank Diameter, D	D	1.308 m
Liquid Height, H_L	$D = H_L$	1.308 m
Impeller Diameter, D_I	$D = 3D_I$	0.436 m
Baffle Width, W	$D = 10W$	0.131 m
Height of Impeller from Tank Bottom, Z_I	$D_I = Z_I$	0.436 m
Impeller Disk Diameter, D_d	$3D_I = 4D_d$	0.327 m
Impeller Blade Length, I	$D_I = 4I$	0.109 m
Impeller Blade Width, b	$D_I = 5b$	0.087 m
Baffle Distance from Tank Bottom, m	$D = 5m$	0.262 m

Determination of mixing time, t_m:

$$t_m = \frac{5{N_{FR}}^{1/6}\left(\frac{H_L}{D_I}\right)^{0.5}}{N\left(\frac{D_I}{D}\right)^2}$$

$$where: N_{FR} = \frac{N^2 D_I}{g}$$

N was calculated from the blade tip speed, V_p.

The typical initial assumption for V_p is 4 m s^{-1}.

$$V_p = \pi N D_I$$
$$N = \frac{V_p}{\pi D_I}$$
$$N = \frac{4\ m\ s^{-1}\left(\frac{60\ s}{1\ min}\right)}{\pi(0.436\ m)}$$
$$N = 175.21\ rpm$$

$$N_{FR} = \frac{(175.21\ rpm)^2(0.436\ m)}{9.81\ m\ s^{-2}\left(\frac{60\ s}{1\ min}\right)^2}$$
$$N_{FR} = 0.379$$

$$t_m = \frac{5{N_{FR}}^{1/6}\left(\frac{H_L}{D}\right)^{0.5}}{N\left(\frac{D_I}{D}\right)^2}$$
$$t_m = \frac{5(0.379)^{1/6}(1)^{0.5}}{(175.21\ rpm)\left(\frac{1}{3}\right)^2}$$
$$t_m = 0.218\ min$$

Determination of power dissipation, P:

$$P = N_P \rho N^3 {D_I}^5$$

To get N_P, determine impeller Reynolds Number $\left(N_{RE_I}\right)$ first.

$$N_{RE_I} = \frac{\rho N {D_I}^2}{\mu}$$

$$N_{RE_I} = \frac{(1000\ kg\ m^{-3})(175.21\ rpm)\left(\frac{1\ min}{60\ s}\right)(0.436\ m)^2}{(0.001\ kg\ m^{-1}s^{-1})}$$

$$N_{RE_I} = 5.6 \times 10^5$$

From Figure 6-40 of the Perry's Chemical Engineers Handbook, 8th ed., the $N_P = 5$

Determine power dissipation:

$$P = N_P \rho N^3 {D_I}^5$$

$$P = (5)(1000\ kg\ m^{-3})(175.21\ rpm)^3\left(\frac{1\ min}{60\ s}\right)^3(0.436\ m)^5$$

$$P = 1962.06\ W$$

3. Sizing of the medium holding tank

$$F = 42.19\ m^3\ d^{-1}$$
$$\tau = 7\ days$$

$$V_L = \tau F$$
$$V_L = (7\ days)(42.19\ m^3\ d^{-1})$$
$$V_L = 295.31\ m^3$$

$$V_L = 0.9 V_T$$
$$V_T = \frac{V_L}{0.9}$$
$$V_T = 328.12\ m^3$$

From API-650, $H_T = 5.5\ m$

$$V_T = \frac{\pi}{4} D^2 H_T$$
$$D = \sqrt{\frac{4V_T}{\pi H_T}}$$
$$D = \sqrt{\frac{4(328.12\ m^3)}{\pi(5.5\ m)}}$$
$$D = 8.72\ m$$

$H_L = 0.9H_T$
$H_L = 4.95\ m$

Determine shell thickness, t:

$$t = \frac{2.6D(H_L - 1)G}{S} + CA$$

$$t = \frac{2.6\left(8.72\ m\ \times \frac{3.28\ ft}{1\ m}\right)\left[\left(4.95\ m\ \times \frac{3.28\ ft}{1\ m}\right) - 1\ ft\right](1.00)}{21{,}050\ psi} + 0.125\ in.$$

$t = 0.178\ in.$

But, according to API-650 Standard, the minimum thickness of tanks with <50 ft diameter should be 0.1875 in.

Therefore, choose $t = 0.1875\ in.$

4. Equipment Costing

4.1. Photobioreactor Cost

The unit price of stainless steel 316 is $4,004 per metric ton according to *http://www.meps.co.uk/Stainless%20Prices.htm* (March 2018 price)

To calculate for the price of steel needed to fabricate the main chamber of the photobioreactor, the mass of steel needed needs to be determined first. This can be done by determining the surface volume of steel and then multiply it by the density of steel, $\rho_{SS-316} = 8000\ kg\ m^{-3}$

$$Surface\ Volume = \pi D H_T t$$
$$Surface\ Volume = \pi(2.327\ m)(4.674\ m)(0.1875\ in.)(0.0254\ m\ in.^{-1})$$
$$Surface\ Volume = 0.16\ m^3$$

$$Weight_{SS-316} = (Surface\ Vol.)(\rho_{SS-316})$$
$$Weight_{SS-316} = (0.16\ m^3)(8000\ kg\ m^{-3})\left(\frac{1\ MT}{1000\ kg}\right)$$
$$Weight_{SS-316} = 1.30\ MT$$

$$Price_{SS-316} = (1.30\ MT)\left(\frac{\$4{,}000}{MT}\right)$$
$$Price_{SS-316} = \$5{,}212.95$$

Assume that the cost of internal and auxiliary parts is 80% of the price of steel and the fabrication cost is also 80% of price of steel.

$$Overall\ PBR\ Price = (Price_{SS-316})(1 + 0.8 + 0.8)$$
$$Overall\ PBR\ Price = (\$5{,}212.95)(1 + 0.8 + 0.8)$$
$$Overall\ PBR\ Price = \$13{,}553.66$$

Since four (4) PBRs will be employed:

$$Total\ PBR\ Price = (\$13{,}553.66)(4)$$
$Total\ PBR\ Price = \$54{,}214 \approx \$54{,}200$ (rounded off to the nearest hundreds to account for uncertainty)

Note: The price of the inoculation PBRs were determined using the method above and was found to be $11,500.

4.2. Medium Mixing Tank Cost

According to *https://www.alibaba.com/product-detail/Stainless-steel-Agitator-Mixer-Stirrer-Homogenizer_60228178551.html?s=p*, the price of 15-m^3 mixing tank is $5000.

Using the six-tenth factor rule to estimate the cost of 1.758-m^3 mixing tank:

$$Mixing\ Tank\ Price = \$5000\left(\frac{1.758\ m^3}{15\ m^3}\right)^{0.6}$$
$Mixing\ Tank\ Price = \$1{,}381.33 \approx \$1{,}400$ (rounded off to the nearest hundreds to account for uncertainty)

4.3. Medium Holding Tank Price

The unit price of stainless steel 316 is $4,004 per metric ton according to *http://www.meps.co.uk/Stainless%20Prices.htm* (March 2018 price)

To calculate for the price of steel needed to fabricate the medium holding tank, the mass of steel needed needs to be determined first. This can be done by determining the surface volume of steel and then multiply it by the density of steel, $\rho_{SS-316} = 8000\ kg\ m^{-3}$

$$Surface\ Volume = \pi D H_T t$$
$$Surface\ Volume = \pi(8.72\ m)(5.50\ m)(0.1875\ in.)(0.0254\ m\ in.^{-1})$$
$$Surface\ Volume = 0.72\ m^3$$

$$Weight_{SS-316} = (Surface\ Vol.)(\rho_{SS-316})$$
$$Weight_{SS-316} = (0.72\ m^3)(8000\ kg\ m^{-3})\left(\frac{1\ MT}{1000\ kg}\right)$$
$$Weight_{SS-316} = 5.74\ MT$$

$$Price_{SS-316} = (5.74\ MT)\left(\frac{\$4{,}000}{MT}\right)$$
$$Price_{SS-316} = \$22{,}973.33$$

Assume that the fabrication cost is 60% of price of steel.

$$Medium\ Tank\ Price = (Price_{SS-316})(1 + 0.6)$$
$$Medium\ Tank\ Price = (\$5{,}212.95)(1 + 0.6)$$
$$Medium\ Tank\ Price = \$36{,}757.33\ \approx \$36{,}800$$ (rounded off to the nearest hundreds to account for uncertainty)

4.4. Air Compressor Price

Air compressor will be used to provide air in the PBR.

From the bench-scale tests, it was found that aeration rate should be 0.3 vvm.

Find the compressor's air rate in cfm (cubic feet per minute):

$$CFM = \left(0.3\frac{L}{L-min}\right)(20\ m^3)\left(\frac{3.28\ ft}{1\ m}\right)^3\ (4\ PBRs)$$
$$CFM = 848.81\ cfm$$

According to *https://www.tractorsupply.com/tsc/product/ingersoll-rand-ss5l5-5-hp-60-gallon-high-capacity-air-compressor*, the price of 10.6 cfm air compressor is $900.

Using the six-tenth factor rule to estimate the cost of 848.81-cfm air compressor:

$$Compressor\ Price = \$900\left(\frac{848.81}{10.6\ cfm}\right)^{0.6}$$
$$Compressor\ Price = \$12{,}493.46\ \approx \$12{,}500$$ (rounded off to the nearest hundreds to account for uncertainty)

4.5.Belt Press Filter Cost

According to *https://www.alibaba.com/product-detail/Livestock-horizontal-vacuum-belt-filter-filters_60808128828.html?s=p*, the price of belt press filter at 12 m^3 h^{-1} filtration rate is $10,000.

Material balance around the filtration unit to get a slurry with 20% solids, the filtration rate was found to be 1.75 m^3 h^{-1}.

Using the six-tenth factor rule to estimate the cost of the belt press filter:

$$Belt\ Press\ Filter\ Price = \$10{,}000\left(\frac{1.75\ {}^{m^3}/_{h}}{12\ {}^{m^3}/_{h}}\right)^{0.6}$$

$$Belt\ Press\ Filter\ Price = \$3{,}146.02$$

Since three (3) belt press filters will be used, the total price is:

$$Total\ Belt\ Press\ Filter\ Price = (\$3{,}146.02)(3)$$

$Total\ Belt\ Press\ Filter\ Price = \$9{,}438.06 \approx \$9{,}400$ (rounded off to the nearest hundreds to account for uncertainty)

4.6.Spray Dryer Cost

According to *https://www.alibaba.com/product-detail/LPG-Model-High-Speed-Centrifugal-Atomizer_60191455859.html?s=p*, the cost of spray dryer with 5 kg h^{-1} evaporation rate is $8,000.

Material balance around the spray dryer revealed the evaporation rate is 11.51 kg h^{-1}.

Using the six-tenth factor rule to estimate the cost of the spray dryer:

$$Spray\ Dryer\ Price = \$8{,}000\left(\frac{11.51\ {}^{kg}/_{h}}{5\ {}^{kg}/_{h}}\right)^{0.6}$$

$Belt\ Press\ Filter\ Price = \$13{,}194.46 \approx \$13{,}200$ (rounded off to the nearest hundreds to account for uncertainty)

4.7.RO Water System Cost

According to https://reverseosmosis.com/collections/commercial-ro/products/proseries-300-gpd-water-system, the price of 300 GPD RO water system is $795.

From previous calculations, $F = 42.19\ m^3\ d^{-1} \approx 11{,}145.92\ gal\ d^{-1}$

Using the six-tenth factor rule to estimate the cost of the belt press filter:

$$RO\ Water\ System\ Price = \$795\left(\frac{11{,}145.92\ {}^{gal}/_{d}}{300\ {}^{gal}/_{d}}\right)^{0.6}$$

$RO\ Water\ System\ Price = \$6{,}956.07 \approx \$7{,}000$ (rounded off to the nearest hundreds to account for uncertainty)

4.8.Total Equipment Cost

$$Purchased\ Equipment\ Cost = Sum\ of\ all\ equipment\ costs$$
$$Purchased\ Equipment\ Cost = \$11{,}500 + \$54{,}200 + \$7{,}000 + \$1{,}400 + \$36{,}800 + \$12{,}500 + \$9{,}400 + \$13{,}200$$
$$Purchased\ Equipment\ Cost = \$146{,}000$$

From Peters, Timmerhaus and West (2003), the installation cost, instrumentation cost, and piping cost, are 50%, 26%, and 31% of the purchased equipment cost, respectively.

$$Total\ Equipment\ Cost = (Purchased\ Equipment\ Cost)(1 + 0.5 + 0.26 + 0.31)$$
$$Total\ Equipment\ Cost = (\$146{,}000)(1 + 0.5 + 0.26 + 0.31)$$
$$Total\ Equipment\ Cost = \$302{,}220$$

5. Fixed Capital Investment (FCI)

According to Peters, Timmerhaus and West (2003), the building cost and land cost are 47% and 8% of the purchased equipment cost, respectively.

$$Buildings\ Cost = 0.47(\$146{,}000)$$
$$Buildings\ Cost = \$68{,}620$$

$Land\ Cost = 0.08(\$146{,}000)$
$Land\ Cost = \$11{,}680$

$FCI = Total\ Equipment\ Cost + Building\ Cost + Land\ Cost$
$FCI = \$302{,}220 + \$68{,}620 + \$11{,}680$
$FCI = \$382{,}520$

6. Raw Material Cost

6.1. Process Water Cost

$F = 42.19\ m^3\ d^{-1}$

According to *https://efc.sog.unc.edu/resource/texas-water-and-wastewater-rates-dashboard-0*, the unit water price is \$0.0102 per gal

$$Process\ Water\ Cost = (42.19\ m^3\ d^{-1})\left(\frac{300\ d}{yr}\right)\left(\frac{1000\ L}{1\ m^3}\right)\left(\frac{1\ gal}{3.785\ L}\right)\left(\frac{\$0.0102}{gal}\right)$$

$Process\ Water\ Cost = \$34{,}106.52 \approx \$34{,}100$ (rounded off to the nearest hundreds to account for uncertainty)

6.2. Chemicals Cost

$F = 42.19\ m^3\ d^{-1}$

From F, the following were determined:

Zarrouk medium	g/L	kg/yr	Price per ton	Price
NaHCO3	16.8	212,624.061	250	53,156.02
NaNO3	2.5	31,640.485	400	12,656.19
K2So4	1	12,656.194	450	5,695.29
NaCl	1	12,656.194	50	632.81
MgSO4.7H20	0.2	2,531.239	110	278.44
K2HPO4	0.5	6,328.097	1500	9,492.15
CaCl2.2H20	0.04	506.248	350	177.19
FeSO4.7H2O	0.01	126.562	80	10.12
EDTA	0.08	1,012.496	1500	1,518.74
Trace Metal A5				
MnSO4.7H2O	2.5	31.640	500	15.82
ZnSO4.7H2O	0.222	2.810	850	2.39
CuSO4.5H2O	0.079	1.000	2000	2.00
Na2MoO4.2H2o	0.021	0.266	11000	2.92
H3BO3	2.86	36.197	750	27.15
TOTAL PRICE/YR				**83,667.22**

7. Utilities Cost

7.1. PBR Lighting Cost

From actual voltage and resistance measurement in the bench-scale reactor, the following values were obtained:

$Volts = 11.25\ V$
$Resistance = 6{,}108\ \Omega$

$I = {}^{V}/_{R}$
$I = {}^{11.25\ V}/_{6{,}108\ \Omega}$
$I = 0.0018\ A$

$P = IV$
$P = (0.0018\ A)(11.25V)$
$P = 0.021\ W$ (this is the power per 8 in. LED strip)

Recall: $h = 3.973\ m$, $n_r = n_d = 288$, and in a 3-in. diameter light chamber, 17 LED strips can fit.

$$Total\ P = \left(\frac{0.021\ W}{8\ in.}\right)(3.973\ m)\left(\frac{1\ in.}{0.0254\ m}\right)\left(\frac{17\ strips}{light\ chamber}\right)(288 + 288)(4\ PBRs)\left(\frac{1\ kW}{1000\ W}\right)$$

$Total\ P = 15.87\ kW$

$$Electric\ Energy\ Requirement = (15.87\ kW)\left(\frac{300\ d}{yr}\right)\left(\frac{24\ hr}{d}\right)$$

$Electric\ Energy\ Requirement = 114{,}241.59\ kWh$

The power unit price is \$0.1 per kWh

$$Lighting\ Power\ Cost = (114{,}241.59\ kWh)\left(\frac{\$0.1}{kWh}\right)$$

$Lighting\ Power\ Cost = \$11{,}424.16$

Note: The inoculation PBRs' power costs were determined using method above.

$Total\ Lighting\ Cost = Lighting\ Cost_{PBR} + Lighting\ Cost_{Inoc.PBRs}$
$Total\ Lighting\ Cost = \$12{,}193.60 \approx \$12{,}200$ (rounded off to the nearest hundreds to account for uncertainty)

7.2.Medium Mixing Tank Power Cost

From Appendix C.2. Section 2, $P = 1962.06\ W$

$$Power\ Cost_{Mixing\ Tank} = (1.962\ kW)\left(\frac{300\ d}{yr}\right)\left(\frac{24\ hr}{d}\right)\left(\frac{\$0.1}{kWh}\right)$$

$Power\ Cost_{Mixing\ Tank} = \$1{,}412.68 \approx \$1{,}400$ (rounded off to the nearest hundreds to account for uncertainty)

7.3.Compressor Power Cost

$$\frac{hp}{cfm} = 0.015P(R^{0.29} - 1)$$

$where$:
$P = gauge\ pressure\ of\ compressed\ air$
$$R = \frac{P_{compressed\ air}}{P_{ambient}} = \frac{90\ psig + 14.7}{14.7\ psia} = 7.12$$

$$\frac{hp}{cfm} = 0.015(90\ psig)((7.12)^{0.29} - 1)$$
$$\frac{hp}{cfm} = 0.169\ \frac{hp}{cfm}$$

Recall: $CFM = 848.81\ cfm$
$$hp = \left(0.169\frac{hp}{cfm}\right)(848.81\ cfm) = 143.57\ hp$$
$$kWh_{theo} = (143.57\ hp)\left(\frac{746\ W}{hp}\right)\left(\frac{1\ kW}{1000\ W}\right)\left(\frac{300\ d}{yr}\right)\left(\frac{24\ hr}{d}\right)$$
$$kWh_{theo} = 771{,}161.1\ kWh$$

Mechanical Efficiency (full load),η = 94%

$$kWh_{actual} = \frac{kWh_{theo}}{\eta}$$
$$kWh_{actual} = \frac{771{,}161.1\ kWh}{0.94} = 820{,}384.17\ kWh$$

$$Power\ Cost_{Compressor} = (820{,}384\ kWh)\left(\frac{\$0.1}{kWh}\right)$$

$Power\ Cost_{Compressor} = \$82{,}038.42 \approx \$82{,}000$ (rounded off to the nearest hundreds to account for uncertainty)

7.4. Belt Press Filter Power Cost

According to *https://www.alibaba.com/product-detail/Livestock-horizontal-vacuum-belt-filter-filters_60808128828.html?s=p*, the power requirement of belt press filter at 12 $m^3\ h^{-1}$ filtration rate is 2.05kW.

Material balance around the filtration unit to get a slurry with 20% solids, the filtration rate was found to be 1.75 $m^3\ h^{-1}$.

Using the six-tenth factor rule:

$$Power\ Cost_{\ Filter} = 2.05\ kW \left(\frac{1.75}{12}\right)^{0.6} \left(\frac{300\ d}{yr}\right)\left(\frac{24\ hr}{d}\right)\left(\frac{\$0.1}{kWh}\right)(3\ units)$$

$Power\ Cost_{\ Filter} = \$1{,}393.06 \approx \$1{,}400$ (rounded off to the nearest hundreds to account for uncertainty)

7.5. Spray Dryer Power Cost

According to *https://www.alibaba.com/product-detail/LPG-Model-High-Speed-Centrifugal-Atomizer_60191455859.html?s=p*, the power requirement of spray dryer with 5 kg h^{-1} evaporation rate is 9 kW.

Material balance around the spray dryer revealed the evaporation rate is 11.51 kg h^{-1}.

Using the six-tenth factor rule:

$$Power\ Cost_{Spray\ Dryer} = 9\ kW \left(\frac{11.51}{5}\right)^{0.6} \left(\frac{300\ d}{yr}\right)\left(\frac{24\ hr}{d}\right)\left(\frac{\$0.1}{kWh}\right)$$

$Power\ Cost_{\ Spray\ Dryer} = \$10{,}687.52 \approx \$10{,}700$ (rounded off to the nearest hundreds to account for uncertainty)

8. Labor Cost

No. of Operators: 3
No. of Shifts/day: 3
Hours per Shift: 8

Unit Labor Cost: \$19.6 h^{-1} (*from https://www.bls.gov/oes/current/oes_tx.htm#51-0000*, Occupational Group 51-4011)

$$Labor\ Cost = (3\ operators)(3\ shifts)\left(\frac{8\ hrs}{shift}\right)\left(\frac{300\ days}{yr}\right)\left(\frac{\$19.6}{yr}\right)$$

$$Labor\ Cost = \$423{,}360$$

9. Supplies

$$Biomass\ Production_{theo} = x_F F$$

$$Biomass\ Production_{theo} = \left(1.637\ \frac{kg}{m^3}\right)\left(42.187\ \frac{m^3}{d}\right)\left(\frac{300\ d}{yr}\right)$$

$$Biomass\ Production_{theo} = 20{,}721.07\ \frac{kg}{yr}$$

From *https://www.parchem.com/chemical-supplier-distributor/Spirulina-Powder-001803.aspx*, the bulk density of *Spirulina* powder is 0.4 kg L^{-1}

$$Volume_{Biomass} = \frac{20{,}721.07\ \frac{kg}{yr}}{0.4\ \frac{kg}{L}}$$

$$Volume_{Biomass} = 51{,}802.66\ L$$

The volume per bag of special gas-barrier bags is computed from its dimension (560mm × 485mm) assuming depth of filled bag is 10mm.

$$Volume\ per\ bag = 2.72\ L$$

$$No.of\ bags = \frac{51{,}802.66\ L}{2.72\ L/bag} = 19{,}073.15\ bags \approx 19{,}074\ bags$$

From *http://www.cxdglobal.com/category.aspx?id=261*, price per bag is £5.46 (exchange rate is \$1.31 per pound)

$$Supplies\ Cost = (19{,}074\ bags)\left(\frac{£5.46}{bag}\right)\left(\frac{\$1.31}{£1.00}\right)$$

$Supplies\ Cost = \$136{,}428.69 \approx \$136{,}400$ (rounded off to the nearest hundreds to account for uncertainty)

10. Total Production Cost (TPC)

$$TPC = Material\ Cost + Utilities\ Cost + Labor + Supplies$$
$$TPC = \$83{,}700 + \$34{,}100 + \$107{,}700 + \$423{,}360 + \$136{,}400$$
$$TPC = \$785{,}260$$

11. Revenue

$$Biomass\ Production_{theo} = 20{,}721.07\ \frac{kg}{yr}$$

Recovery = 70%

$$Biomass\ Production_{actual} = \left(20{,}721.07\ \frac{kg}{yr}\right)(0.70)$$
$$Biomass\ Production_{actual} = 14{,}504.75\ \frac{kg}{yr}$$

From *http://www.fao.org/3/a-az386e.pdf*, the price per kg of *Spirulina* powder is $58.3 per kg

$$Revenue = \left(14{,}504.75\ \frac{kg}{yr}\right)\left(\frac{\$58.3}{kg}\right)$$
$Revenue = \$845{,}626.70 \approx \$845{,}600$ (rounded off to the nearest hundreds to account for uncertainty)

12. Net Income

$$Net\ Income = Revenue - TPC$$
$$Net\ Income = \$845{,}600 - \$785{,}260$$
$$Net\ Income = \$60{,}340$$

13. Profit Margin

$$Profit\ Margin = \frac{Net\ Income}{Revenue} \times 100\%$$
$$Profit\ Margin = \frac{\$60{,}340}{\$845{,}600} \times 100\%$$
$$Profit\ Margin = 7.14\%$$

14. Payback Period

$$Payback\ Period = \frac{FCI}{Net\ Income}$$
$$Payback\ Period = \frac{\$382{,}520}{\$60{,}340/yr}$$
$$Payback\ Period = 6.34\ years$$